

NEUROPSYCHIATRIC CORRELATES OF
BLOOD-BRAIN BARRIER LEAKAGE

by

Lyna Kamintsky

Submitted in partial fulfilment of the requirements
for the degree of Doctor of Philosophy

at

Dalhousie University
Halifax, Nova Scotia
April 2021

© Copyright by Lyna Kamintsky, 2021

Dedication

This thesis is dedicated to:

My **mom**, who survived the impossible for me and my brother. To **grandma Sara** who taught me curiosity, perseverance, and generosity. To my **brother**, for always having my back and for weekly asking me when I will finish my PhD and what do I intend to do with my life.

To **Tristan Cleveland**, who during my PhD went from being a guy I kept running into, to the husband dreams are made of. To my **auntie Olga**, who taught me who dad was, and who I can become. To **Alon Friedman**, who does not cease to amaze me with his brilliant mind and kind heart. You have transformed my life more than you can imagine.

To **dad**. Thank you for using the little time we had to inject me with a life-long supply of love.

Table of Contents

Dedication	ii
Table of Contents	iii
List of Tables	ix
List of Figures	x
Abstract	xi
List of Abbreviations and Symbols Used	xii
Acknowledgements	xiii
Chapter 1 – Introduction	1
Chapter Overview	1
1.1. The blood-brain barrier	1
1.1.1. The neurovascular unit	1
1.1.2. Discovery	2
1.1.2.1. First observations of the separation between the blood and the brain	2
1.1.2.2. The role of cerebral endothelium	3
1.1.2.3. The role of astrocytes	3
1.1.2.4. The role of the basement membrane	4
1.1.2.5. The role of microglia	4
1.1.2.6. The role of neurons	4
1.1.2.7. The role of pericytes	5
1.1.3. Summary of BBB functions and barrier roles of the NVU	6
1.1.4. The selective nature of the BBB	8
1.1.4.1. Mechanisms of endothelial selectivity:	9
1.1.4.1.1. Paracellular selectivity	9
1.1.4.1.1.1. Tight junction proteins	9
1.1.4.1.2. Transcellular selectivity	9
1.1.4.1.2.1. Transcellular diffusion	11

1.1.4.1.2.2. Vesicular influx	11
1.1.4.1.2.3. Carrier-mediated transporters	12
1.1.4.1.3. Endothelial enzymes	13
1.1.4.1.4. Immuno-privilege	13
1.1.5. BBB dysfunction	14
1.1.5.1. Open questions in the field of BBB dysfunction	15
1.1.5.1.1. What is BBB dysfunction?	15
1.1.5.1.2. What causes BBB dysfunction?	15
1.1.5.1.3. How does BBB dysfunction mediate changes in brain function?	15
1.1.5.1.4. Is BBB dysfunction always bad, or should it be simply referred to as ‘altered BBB function’?	15
1.1.5.1.5. Can BBB dysfunction be diagnosed in living patients and what are the clinical features of BBB dysfunction?	15
1.1.5.1.6. Can BBB diagnosis be coupled with targeted treatment?	16
1.1.6. A focus on cross-BBB influx/leakage	16
1.2. Detecting BBB leakage in living patients and animals	18
1.2.1. Imaging the living BBB – a historical perspective	18
1.2.1.1. Intra-operative fluorescein microscopy	18
1.2.1.2. Single photon emission computed tomography (SPECT)	19
1.2.1.3. Computed tomography (CT)	19
1.2.1.4. Positron emission tomography (PET)	19
1.2.1.5. Magnetic resonance imaging (MRI)	19
1.2.2. Non-imaging markers as indicators of BBB leakage	20
1.3. Quantitative mapping of BBB permeability from DCE-MRI data	21
1.3.1. Pharmacokinetic models for estimating BBB leakage	22
1.3.2. Fast and slow BBB leakage	24
1.4. Chapter Summary	24
Chapter 2 – Methods	25
Chapter Overview	25
2.1. Studying mechanisms of BBB dysfunction	26

2.1.1. Studying mechanisms of BBB leakage in slice-cultures	27
2.1.2. Studying mechanisms of BBB leakage in vivo	30
2.2. Studying BBB leakage in humans	33
2.2.1. The MRI acquisition protocol	33
2.2.2. The developed BBB software	37
2.2.2.1. Data pre-processing	37
2.2.2.2. Calculating contrast concentration	40
2.2.2.3. Mapping leakage-rates	43
2.2.2.4. Giving leakage-rates diagnostic context	45
2.2.3. Studying clinical manifestations of BBB dysfunction	47
2.2.3.1. BBB leakage and psychiatric symptoms in patients with bipolar disorder	47
2.2.3.1.1. Participants	47
2.2.3.1.2. Psychiatric Assessment	48
2.2.3.2. BBB leakage and cognitive symptoms in patients with lupus Participants	48
2.2.3.2.1. Participants	48
2.2.3.2.2. Cognitive Assessment	48
2.2.3.3. Acquiring a reference for normal BBB function	49
2.2.3.4. Statistical analysis	50
Chapter 3 – Mechanisms of BBB dysfunction	52
Chapter Overview	52
Manuscript title: Seizure-induced microvascular injury is associated with impaired neurovascular coupling and blood–brain barrier dysfunction	53
Abstract	53
3.1. Introduction	55
3.2. Materials and methods	57
3.2.1. In vitro experiments	57
3.2.2. In vivo experiments	58
3.2.3. Statistical reporting	59
3.2.3.1. NVC evaluation	59
3.2.3.2. Cell damage, BBB permeability, oxygen measurements	59

3.2.3.3. Characterization of the vasodilatory response upon seizure activity	59
3.3. Results	61
3.3.1. Pericytes retain contractility in slice cultures	61
3.3.2. Seizures are associated with loss of NVC	65
3.3.3. Seizures do not induce disturbances in neurometabolic coupling	67
3.3.4. Seizures induce pericytic constriction and mitochondrial depolarization	67
3.3.5. Seizures induce changes in capillary permeability in vitro	68
3.3.6. Seizures induce NVC alterations in vivo	70
3.3.7. Seizure-induced cellular injury and microvascular permeability in vivo	71
3.3.8. Seizure-associated NVC impairment occurs under normoxic conditions in vivo	72
3.4. Discussion	74
Chapter 4 – BBB leakage and psychiatric symptoms in bipolar patients	77
<hr/>	
Chapter Overview	77
Manuscript title: BBB imaging as a potential biomarker for bipolar disorder progression	79
Abstract	79
4.1. Introduction	80
4.2. Methods	81
4.2.1. Participants	81
4.2.2. BBB Imaging	82
4.2.2.1. DCE-MRI acquisition and preprocessing	82
4.2.2.2. Image analysis	82
4.2.3. Statistical analysis	83
4.3. Results	84
4.3.1. Participants	84
4.3.2. A sub-group of bipolar patients have a significantly higher level of BBB dysfunction	84
4.3.3. Extensive BBB leakage in bipolar patients is associated with greater psychiatric morbidity	87

4.3.4. Extensive BBB leakage is associated with metabolic dysregulation, yet not with class of mood-stabilizing drugs	88
4.4. Discussion	89
Chapter 5 – BBB leakage and cognitive symptoms in lupus patients	91
<hr/>	
Chapter Overview	91
Manuscript title: BBB leakage in systemic lupus erythematosus is associated with gray matter loss and cognitive impairment	93
Abstract	93
5.1. Introduction	94
5.2. Patients and Methods	95
5.2.1. Patients	95
5.2.2. Cognitive function	95
5.2.3. Imaging	96
5.2.3.1 MRI acquisition	96
5.2.3.2. Volume analysis	96
5.2.3.3. BBB leakage analysis	97
5.2.4. Statistical analysis	97
5.3. Results	98
5.3.1. Demographic and clinical characteristics	98
5.3.2. A sub-group of SLE patients have extensive BBB leakage	98
5.3.3. Extensive BBB leakage in SLE patients is associated with smaller gray matter volume	100
5.3.4. Extensive BBB leakage in SLE patients is associated with cognitive impairment	101
5.4. Discussion	104
Chapter 6 – Discussion	108
<hr/>	
Chapter Overview	108
6.1. What is BBB leakage?	108
6.1.1. How does endothelial selectivity change?	108
6.1.2. What transformation takes place in non-endothelial neurovascular unit	110

elements?	
6.2. What causes BBB leakage?	110
6.2.1. How do seizures cause BBB leakage?	111
6.2.2. How does lupus cause BBB leakage?	111
6.2.3. How does insulin-resistant bipolar disorder cause BBB leakage?	112
6.3. How does BBB leakage mediate changes in brain function?	112
6.4. Is BBB leakage always bad?	114
6.5. Can BBB leakage be diagnosed in living patients and what are the clinical features of BBB leakage?	115
6.6. Future directions	119
6.6.1. Diagnosing BBB leakage in clinical settings	119
6.6.2. Understanding the neuro-functional correlates of BBB dysfunction	120
6.6.3. Understanding changes in BBB efflux	121
6.6.4. Coupling BBB diagnosis with targeted treatments	121
6.7. Chapter Summary	122
References	124
<hr/>	
References, Chapter 1	124
References, Chapter 2	132
References, Chapter 3	135
References, Chapter 4	139
References, Chapter 5	142
References, Chapter 6	146
Appendix I, Copyright Permissions	153

List of Tables

Table 1 – Main functions of the blood-brain barrier	7
Table 2 – The elements of the neurovascular unit	8
Table 3 – Demographic and clinical features of patients with Bipolar Disorder	85
Table 4 – Demographic and clinical features of SLE patients	99
Table 5 – Comparison between SLE patients with extensive versus normal BBB leakage	103

List of Figures

Figure 1 – The neurovascular unit	2
Figure 2 – BBB discovery milestones	6
Figure 3 – Endothelial Selectivity	Error! Bookmark not defined.
Figure 4 – Milestones in in-vivo BBB imaging	20
Figure 5 – Pharmacokinetic models of contrast leakage	23
Figure 6 – Results Chapters	25
Figure 7 – Slice culture methodology	29
Figure 8 – In vivo methodology	32
Figure 9 – Summary of MRI acquisition protocol	36
Figure 10 – BBB software, analysis pipeline	38
Figure 11 – Microvasculature and pericytes in slice culture	62
Figure 12 – Pericytes retain motility and respond to seizures in vitro	64
Figure 13 – Seizures impair neurovascular coupling in slice cultures	66
Figure 14 – Recurrent seizures induce pericyte constriction and BBB leakage	69
Figure 15 – Seizures impair neurovascular coupling in vivo	70
Figure 16 – Seizures induce cellular injury and vascular leakage in vivo	72
Figure 17 – A sub-group of bipolar patients have extensive BBB leakage	86
Figure 18 – Extensive BBB leakage is associated with a worse neuropsychiatric status	87
Figure 19 – Extensive BBB leakage is associated with metabolic dysregulation	88
Figure 20 – A sub-group of SLE patients have extensive BBB leakage	100
Figure 21 – Extensive BBB leakage in SLE patients is associated with smaller gray matter volume	101
Figure 22 – Extensive BBB leakage in SLE patients is associated with cognitive impairment	102
Figure 23 – Summary of proposed disease mechanisms	118

Abstract

The research presented in this thesis studied the role of the blood-brain barrier in the development and progression of neuropathology. The blood-brain barrier is the specialized lining of the brain's capillaries. The high selectivity of this lining is thought to have evolved to protect the brain by: a) barring the influx of neurotoxic molecules from the bloodstream to the brain; b) maintaining the precise ionic balance necessary for proper neuronal function; c) regulating the efflux of waste-products/pathogens from the brain; and d) allowing selective influx of nutrients/hormones/immune-factors into the brain. The barrier is formed by six primary elements, collectively referred to as the 'neurovascular unit': 1) specialized and highly selective endothelial cells, interconnected by dense/complex tight junctions; 2) a basement membrane enwrapping the endothelial layer; 3) pericytes, anchored in the basement membrane; 4) a layer of astrocytic end-feet; 5) neighboring microglial cells; and 6) neurons. These elements are key to proper development and maintenance of the specialized phenotype of cerebral capillaries, and can affect the selectivity of the endothelium by altering the expression/function of endothelial influx/efflux transporters, enzymes and/or tight-junctions.

Altered blood-brain barrier (BBB) selectivity has been linked to numerous brain disorders, including brain insults (e.g., ischemic/hemorrhagic stroke, traumatic brain injury and seizures) and neuro-inflammatory diseases (e.g., multiple sclerosis, dementia, amyotrophic lateral sclerosis, and Parkinson's disease). A consensus in the field of BBB research states that BBB dysfunction triggers neuro-inflammatory signaling ($TGF\beta$, IL6, $TNF\alpha$, $IL1\beta$) that can lead to reorganization/dysfunction of neuronal networks and mediate the development of neurological symptoms. However, many gaps remain in the current understanding of mechanisms that cause altered BBB selectivity, and the contribution of these selectivity changes to the development/progression of specific disorders.

This thesis studied one facet of altered BBB selectivity – increased blood-to-brain influx, termed BBB leakage for simplicity. The first part of this thesis consists of a study in experimental animals, in which we explored mechanisms resulting in BBB leakage and the pathogenic processes that mediate subsequent brain tissue damage. The second part of this thesis consists of two clinical studies, examining the relevance of BBB leakage to neuropsychiatric symptoms in patients with bipolar disorder and patients with lupus.

Our animal study demonstrated that pericytes are likely mediators of BBB leakage and loss of vascular responsiveness to neuronal energy demands (impaired neurovascular coupling). Our clinical studies revealed neuroimaging evidence of extensive BBB leakage in ~25% of patients in each cohort, and a link between extensive leakage and severity of neuropsychiatric symptoms. Moreover, our analysis suggests that the slow/subtle nature of the observed leakage represents an increase in trans-endothelial rather para-endothelial influx. We propose that the chronic systemic inflammation associated with both disorders is a likely cause of altered trans-endothelial leakage that may, in-turn, underlie neuro-functional changes that impact neuropsychiatric outcomes.

These insights lay the foundation for the development of novel biomarkers and therapeutics that target mechanisms of BBB pathology. Moreover, the diagnostic software I developed for MRI-based quantification of BBB leakage has high translatability potential, and may enable routine assessment of BBB leakage in clinical settings. The ability to reliably identify patients with BBB leakage may serve as a stepping-stone towards diagnosis-coupled treatment strategies.

List of Abbreviations and Symbols Used

2D two dimensional	IL-6 interleukin 6
3D three dimensional	LAT1 L-Type Amino Acid Transporter
3T three Tesla	LAVA Liver Acquisition with Volume Acquisition
4AP 4-aminopyridine	LDL low density lipoprotein
A β amyloid beta	LFP Local field potential
ABCs ATP-binding cassette.	MAD Median Absolute Deviation
ACR American College of Rheumatology	MADRS Montgomery-Åsberg Depression Rating Scale
aCSF artificial cerebrospinal fluid	MEG magnetoencephalography
ALS amyotrophic lateral sclerosis	MitoSox Mitochondrial Superoxide Indicator
AMI affective morbidity index	MMPs matrix metalloproteinases
ASL Arterial spin labeling	MNI Montreal Neurological Institute
BBB Blood-brain barrier	MRI Magnetic resonance imaging
BCRP breast cancer resistance protein	MS multiple sclerosis
BIOTIC Biomedical Translational Imaging Centre	NaFlu sodium-fluorescein
BP blood pressure	NG2 neuronal/glial antigen 2
BRAVO Brain Volume	NIFTI Neuroimaging Informatics Technology Initiative
CNS central nervous system	NMDA N-Methyl-D-aspartate
CSF cerebrospinal fluid	NP neuropsychiatric
CT Computed tomography	NPSLE neuropsychiatric Systemic Lupus Erythematosus
CVLT California Verbal Learning Test	NSHA Nova Scotia Health Authority
DAPI 4',6-diamidino-2-phenylindole	NVC neurovascular coupling
DCE dynamic contrast-enhanced	NVU neurovascular unit
DCE-MRI dynamic contrast-enhanced magnetic resonance imaging	PDGFR β platelet-derived growth factor receptor beta
DCF dichlorofluorescein	PECAM Platelet endothelial cell adhesion molecule
DIC differential interference contrast	PET Positron emission tomography
DICOM Digital Imaging and Communications in Medicine	PI propidium iodide
DWI Diffusion-weighted imaging	SADS-L Schedule for affective disorders and schizophrenia
ECoG electrocochleographic	SDMT Symbol Digit Modalities Test
eGFR estimated glomerular filtration rate,	SLE Systemic Lupus Erythematosus
EM electron microscopy	SLEDAI-2K Systemic Lupus Erythematosus Disease Activity Index-2000
FLAIR Fluid-attenuated inversion recovery	SLICC/ACR,
fMRI functional magnetic resonance imaging	SNAP S-nitroso-N-acetylpenicillamine
GAF global assessment of functioning scale	SPECT Single photon emission computed tomography
GFP green fluorescent protein	SPM Statistical Parametric Mapping
GLUT1 Glucose transporter 1	TBI Traumatic Brain Injury
H2DCF-DA 2',7'-dichlorohydrofluorescein diacetate	TEMPOL tetramethylpiperidine-N-oxyl
HAM-A The Hamilton Anxiety Rating scale	TGF- β transforming growth factor beta
HOMA-IR homeostatic model assessment of insulin resistance	TNF- α Tumor necrosis factor alpha
HRP horseradish peroxidase	VEGF vascular endothelial growth factor
IL-1 β interleukin 1 beta	QEII Queen Elizabeth II Health Sciences Centre

Acknowledgements

I feel extremely grateful for the mentorship and brilliance of **Dr. Alon Friedman**, **Dr. Steven Beyea** and **Dr. Chris Bowen**. Thank you for all you have taught and continue to teach me. An immense thank you to **Dr. Cynthia Calkin** and **Dr. John G Hanly** – the exceptional clinician-researchers we got to collaborate with and learn from.

Thank you to **Dr. Ronel Veksler**, the mind behind the Veksler approach for BBB assessment; to **Dr. Ofer Prager**, for always pushing the boundaries of what is possible in in-vivo imaging; and to **Dr. Richard Kovács**, for establishing a cutting-edge model of functional microvasculature in vitro. Your shoulders were the foundation of this work. Thank you. Big thanks to **Colyn Munn**, for being an awesome office-mate and helping enhance software features, and to **Kay Murphy** for being the backbone of our lab.

Thank you to my multi-talented and wonderfully sweet husband **Tristan Cleveland**, for illustrating my drawing of Figure 1, and for helping finalize the formatting of this document when my eyes became temporarily out of commission. I am beyond lucky to get to be your wife.

I would also like to express my enormous gratitude to **Dr. Bill Baldrige**, for his guidance, kindness, and endless patience; and to **Dr. Kazue Semba**, **Pauline Fraser**, and **Catherine Currell**, for all their assistance, support, and warmth.

Lastly, I would like to thank the individuals who volunteered to participate in our studies. Thank you for sacrificing your time for advancing brain research.

Chapter 1 – Introduction

Chapter Overview

The blood-brain barrier (BBB) is the specialized lining of the brain's blood vessels. A growing body of evidence suggests that altered influx/efflux across the BBB can impact neuronal activity. The goal of this thesis was to:

- I. Explore mechanisms that drive increased blood-to-brain influx/leakage.
- II. Examine whether subtle blood-to-brain leakage bears implications on mental health (e.g., depression and cognition).

In this chapter, I will review key discoveries in BBB research and milestones in diagnostic BBB imaging, while framing my own work in the context of the current knowns and unknowns in the field.

1.1. The blood-brain barrier

The delivery of oxygen and glucose to brain tissue occurs primarily at the brain's capillaries. The brain's dense capillary network ensures that neurons are always in close proximity to a capillary, as exemplified by a recent study determining that cortical neurons are on average 17.8 μm away from a feeding capillary.¹ To protect the brain from substances that can impair neuronal function, the brain's capillaries form a selective barrier between the blood and the brain – the blood-brain barrier (BBB).

1.1.1. The neurovascular unit

The BBB is comprised of six main elements (Figure 1) – collectively referred to as the 'neurovascular unit':²

1. A layer of endothelial cells that:
 - a. Are tightly-sealed by dense and continuous tight-junction proteins.
 - b. Have scarce domains for non-selective trans-endothelial transport.
2. A basement membrane surrounding the endothelial layer.
3. Pericytes that are anchored in the basement membrane, engulfing the endothelium.

4. An ensheathing layer of astrocytic end-feet.
5. Adjacent microglial cells.
6. Neighboring neurons.

These six elements represent a single building block of the BBB, with the term ‘neurovascular unit’ (NVU) emphasizing the intricate and complex relationship between neurons and their vasculature.² In the following section, I discuss the ‘barrier roles’ of these six elements in the order of their scientific discovery. The specific roles of each NVU element in the adult BBB are summarized in table 2.

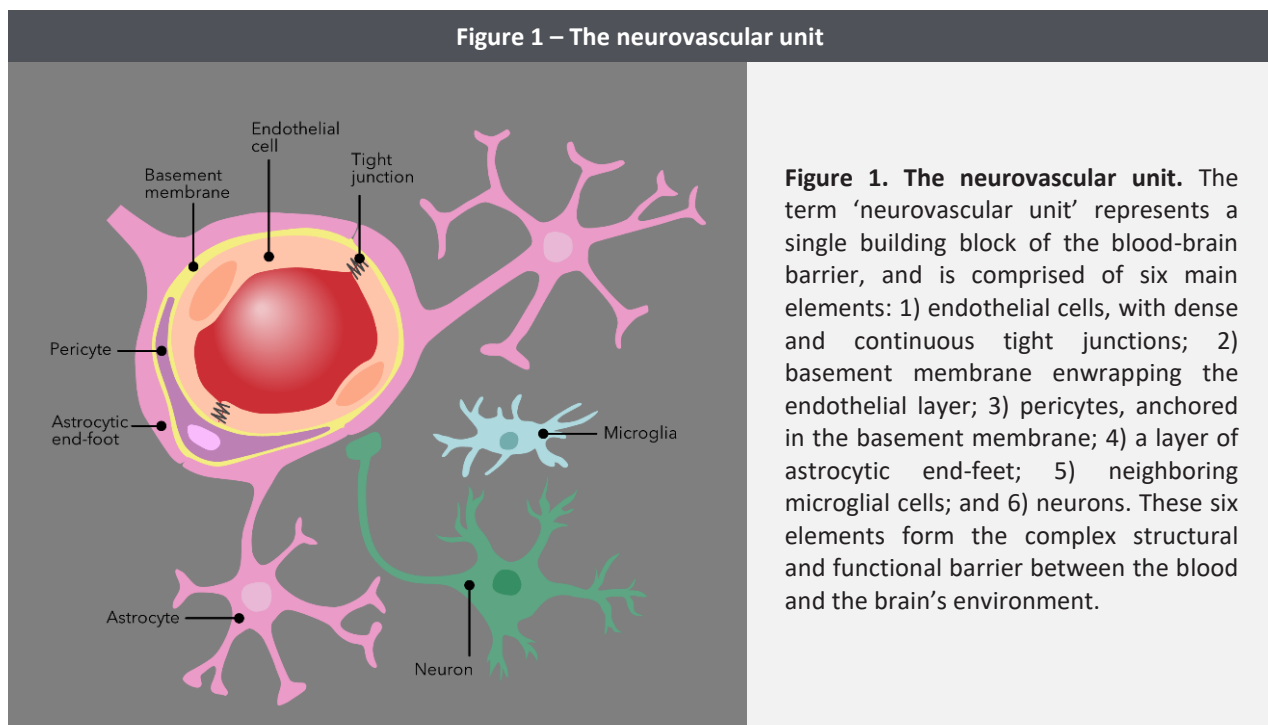


Figure 1. The neurovascular unit. The term ‘neurovascular unit’ represents a single building block of the blood-brain barrier, and is comprised of six main elements: 1) endothelial cells, with dense and continuous tight junctions; 2) basement membrane enwrapping the endothelial layer; 3) pericytes, anchored in the basement membrane; 4) a layer of astrocytic end-feet; 5) neighboring microglial cells; and 6) neurons. These six elements form the complex structural and functional barrier between the blood and the brain’s environment.

1.1.2. Discovery

Several scientific breakthroughs have contributed to our current understanding of the unique properties of the brain’s capillaries. Here I review key BBB discoveries from a historic perspective and a focus on the barrier roles of the six NVU elements.

1.1.2.1. First observations of the separation between the blood and the brain

The 1880s saw the emergence of tissue dyes that can stain living cells without killing them (i.e., vital stains). In 1885 the German scientist Paul Ehrlich was developing intravital dyes that change their color based on oxygen consumption. The dyes were injected into a living animal and were expected

to circulate throughout the body and stain all organs. To his surprise, cationic dyes (which bind serum albumin) stained all peripheral organs, but not brain tissue or the spinal cord. Ehrlich concluded that the brain has low affinity to the dye, and dismissed the idea that the brain's vasculature might selectively exclude it. Ehrlich went on to win a Nobel prize in 1908 for unrelated discoveries in the field of immunology.

Five years after Ehrlich's dye experiments, Max Lewandowsky observed that injection of neurotoxins into the dogs' ventricles produced seizures, while peripheral injections (even in larger doses) did not. Lewandowsky coined the term 'blood-brain barrier', and he is credited with being the first to hypothesize that it is the brain's capillaries that restrict certain substances from entering the brain.

In 1913, Ehrlich's student Edwin Goldman confirmed Lewandowsky's hypothesis and disproved Ehrlich's. Having injected the same dye directly into the cerebrospinal fluid (CSF) of rabbits and dogs, Goldman found that the same dyes do stain the brain and spinal cord but not peripheral organs – confirming a separation between peripheral circulation and the central nervous system (CNS).

1.1.2.2. The role of cerebral endothelium

The morphology of the BBB remained unknown until the advent of electron microscopy (EM). In 1966 Harvard's Morris J. Karnovsky introduced an improved technique for EM imaging with the horseradish peroxidase tracer (HRP, a small enzyme the reaction of which yields a specific color change).³ A year later Karnovsky joined forces with neurobiologist Tom Reese to use the new method for visualizing mouse neuroanatomy. HRP was injected intravenously, and the small tracer (40KDal) was expected to reach brain tissue. It did not. Upon further investigation, the duo realized the tracer reached the lumen of cerebral capillaries, but failed to cross cerebral endothelium.⁴ They also found dense tight junctions between adjacent endothelial cell, and relatively low pinocytotic activity (vesicles that transport non-specific substances across endothelial cells). They concluded that the tight junctions prevent para-cellular passage of HRP, while the scarce pinocytotic vesicles prevented trans-cellular HRP transport. The primary physical barrier between the blood and the brain was identified as the cerebral endothelium.

1.1.2.3. The role of astrocytes

The contribution of astrocytes (whose end-feet enwrap 97% of the endothelium)⁵ to the barrier properties of cerebral vasculature became apparent in 1987. The Raff lab demonstrated that isolated astrocytes transform non-CNS endothelium into non-leaky CNS-like vessels *in vivo*.⁶ In parallel *in vitro* experiments conducted by the Brightman group, endothelial cells cultured without astrocytes were shown to remain leaky, while those co-cultured with astrocyte developed sealing tight junctions.⁷ These findings also demonstrated the flexible phenotype of endothelial cells, and their ability to gain specialized morphology in cerebral vessels. Later studies also elucidated the role of astrocyte signaling in: (a) maintaining endothelial cells; (b) regulating the expression of selective endothelial transport proteins; and (c) facilitating the expansion/constriction of capillaries.^{8,9}

1.1.2.4. The role of the basement membrane

The 1990s saw a growth in the understanding of the basement membrane in the context of the BBB. The cerebral basement membrane was suggested to have several barrier roles: (a) serve as a filter for molecules based on charge and molecular size; (b) provide structural support and anchoring to endothelial cells, pericytes, and astrocytes; (c) mediate signaling between the anchored cells; (d) allow dynamic construction/degradation of connections to allow cell growth and migration.¹⁰ Interestingly, the proteins of the basement membrane were shown to be synthesized and deposited primarily by endothelial cells, pericytes and astrocytes.^{10,11}

1.1.2.5. The role of microglia

The early 2000s elucidated the role of microglia in regulating barrier leakiness – a role that manifests primarily in response to injury, infection, or systemic disease. Several animal studies showed that microglia (and astrocytes) secrete matrix metalloproteinases (MMPs)^{12,13} – enzymes that break-down tight junction proteins – presumably to allow mass migration of systemic immune cells (leukocytes) into the brain.¹⁴ In some cases, microglia may become phagocytic and engulf endothelial cells or other neurovascular components.^{14,15}

1.1.2.6. The role of neurons

In 2008, Liebner et al, demonstrated the role of neural tissue in BBB formation. The study identified a neuronal signaling pathway required for proper BBB development and function – the

Wnt axis.¹⁶ Neurons also have important roles in the mature BBB. The activity of neurons regulates the diameter of the capillary, in a process that matches blood-supply to energy-consumption. This process is termed ‘neurovascular coupling’, and was first observed in 1890 by Roy and Sherrington.¹⁷ Discoveries in the late 90s and early 2000s identified the signaling pathways involved in neuronal regulation of capillary diameter, and demonstrated the central role of pericytes in dilating/constricting the capillary.¹⁸ Changes in neuronal activity have been suggested to mediate circadian differences in the rate of brain-to-blood efflux;¹⁹ and glutamate – the main product of neuronal activation – has also been shown to increase cross-BBB influx.^{20–22} Together, the available evidence suggests that neuronal activity regulates both the diameter and the selectivity of neighbouring capillaries, however attempts to better understand this phenomenon are ongoing.

1.1.2.7. The role of pericytes

The role of pericytes in barrier integrity was discovered in 2010. Two separate studies by Armulik et al., and Daneman et al., used knock-out mice to show that the absence of pericytes affects the development of endothelial cells. Both studies demonstrated that pericyte-deficient mice develop cerebral endothelium with widespread transcellular transport domains and less coverage by astrocytic end-feet.^{23,24} While both studies also reported slight abnormalities in tight junction structure, the leakiness of the endothelium was attributed primarily to increased trans-cellular influx. Pericytes were concluded to play a critical role in inhibiting the expression of proteins mediating trans-endothelial transport.

Figure 2 – BBB discovery milestones

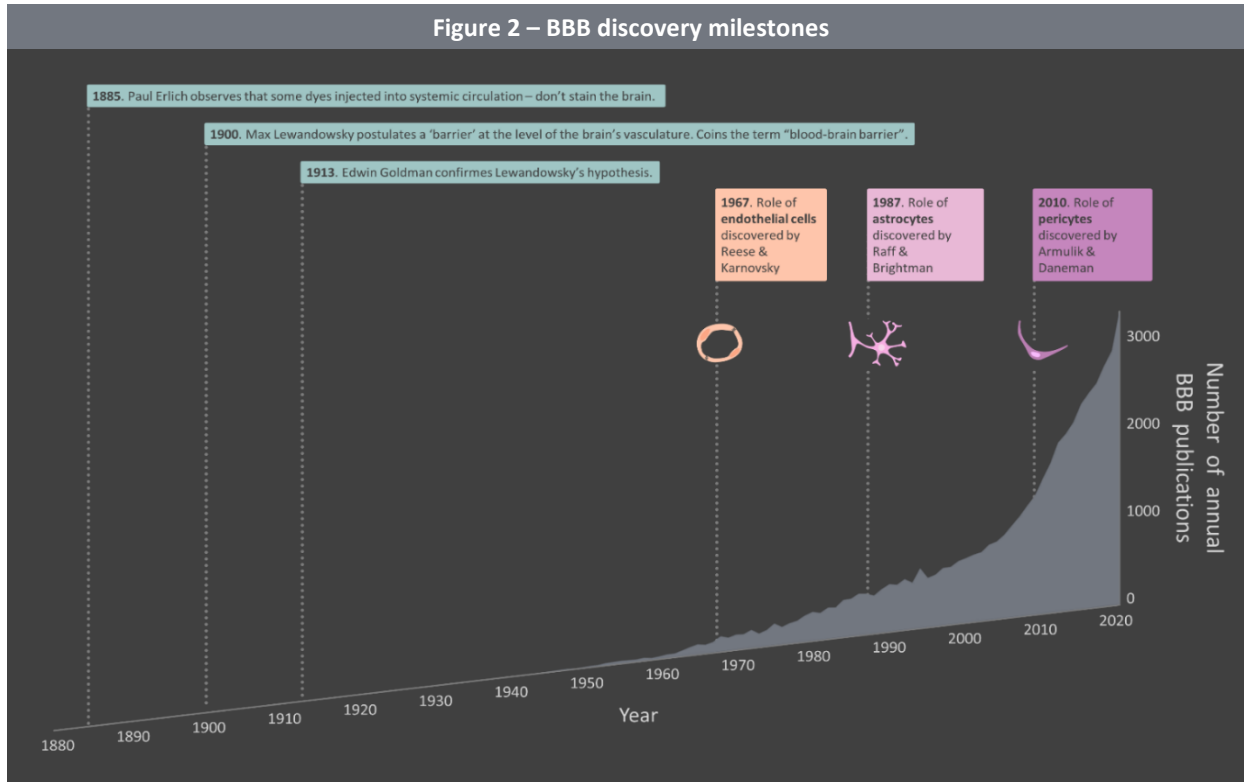


Figure 2. BBB discovery milestones. This figure presents key BBB discoveries, along with the number of annual BBB publications from 1880 to 2020 (based on a PubMed search with the terms “blood-brain barrier” or “blood brain barrier”). While **1885** is often regarded as the year the BBB was discovered, at the time the scientist conducting the experiment – Paul Ehrlich, did not interpret his observation in the context of a barrier. Ehrlich observed that some dyes injected into animal circulation stain peripheral organs, but not the brain or spinal-cord, and concluded that the brain simply does not ‘pick up’ certain dyes. In **1900**, Max Lewandowsky observed that some substances are toxic when injected into the brain’s ventricles, but not when injected into a vein. Lewandowsky suggested the existence of a barrier at the level of brain’s blood vessels and coined the term “blood-brain barrier.” In **1923**, Edwin Goldman observed that dye injection into the cerebrospinal fluid of dogs and rabbits stains the brain/spinal-cord, but not peripheral organs. Goldman disproved the theory that the brain ‘does not pick-up dye.’ The next definitive evidence for Lewandowsky’s hypothesis came with the advent of electron microscopy. In **1967**, Reese and Karnovsky identify the barrier properties of the cerebral endothelium, with its dense and continues tight junctions and scarce vesicular transport. In **1987**, two independent groups led by Raff and Brightman showed that endothelial cells grown without astrocytes form leaky vessels, while endothelial cells grown with astrocytes develop tight-junctions and a non-leaky phenotype. The studies concluded that astrocytes drive the specialization of the brain’s endothelium. In **2010**, two independent reports by Armulik and Daneman used pericyte-deficient mice to demonstrate that pericytes regulate expression levels of trans-endothelial transport and drive astrocytic end-feet to enwrap endothelial cells.

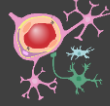





1.1.3. Summary of BBB functions and barrier roles of the NVU

Today, we have a clearer picture of the mysterious barrier Max Lewandowsky envisioned 120 years ago. Researchers have identified the selective nature of the BBB's endothelium – allowing the passage of some molecules, while barring others.^{25,26} These insights led to several conclusions regarding the main restrictive/regulatory/permissive functions of the BBB:

Bar	Regulate	Permit
<ul style="list-style-type: none">· Passage of molecules with neurotoxic potential	<ul style="list-style-type: none">· Passage of ions that can affect the precise ionic balance (homeostasis) necessary for proper neuronal function	<ul style="list-style-type: none">· Passage of nutrients, hormones, and growth factors essential for brain function· Clearance of neuronal waste products and expulsion of foreign agents· Communication with the systemic immune system

As reviewed in the previous section, researchers have also identified the elements comprising the building blocks of the BBB, and are beginning to understand the barrier roles of these elements. Astrocytes, pericytes, neuronal precursors, and the basement membrane – were all shown to be needed for proper embryonic development of the BBB's selective endothelium.^{7,10,16,23,24} However, proper development of a selective endothelium does not mean the job of the NVU elements is complete. In fact, it is just the beginning of a lifelong interplay of maintaining and modulating endothelial selectivity.^{9,27} The specific roles of the basement membrane, astrocytes, pericytes, neurons, and microglia in the adult BBB are summarized in table 2.

Table 2 – The elements of the neurovascular unit

Element:						
Features:	<p>Tightly inter-connected by tight junction proteins.²⁵</p> <p>Have scarce domains for non-specific transcellular transport.²⁵</p> <p>Have efflux pumps and enzymes that eject and break-down potentially neurotoxic substances, respectively.²⁵</p>	<p>A highly organized protein sheet, of 50-100 nm thickness.²⁸</p> <p>Consists of 4 main protein types, predominantly synthesized by the BBB's endothelial cells, pericytes and astrocytes.²⁸</p>	<p>Claw-shaped cells embedded in the basement membrane.²⁵</p> <p>Represent <2% of total brain cell population.²⁹</p> <p>Cover 30% of vessel circumference and 99% of vessels length.⁵</p> <p>Attach to endothelial cells via gap junctions and peg and socket junctions.³⁰</p>	<p>Star-shaped cells, whose end-feet enwrap 97% of the basement membrane.⁵</p> <p>Represent 20%-40% of total brain cell population.³¹</p>	<p>The immune with constantly moving branches.²⁵</p> <p>Represent ~12-16% of total brain cell population.³²</p>	<p>Represent ~15% of total brain cell population.³³</p>
Role in adult BBB:	<p>Produce the proteins that form tight junctions.²⁵</p> <p>Allow selective inward/outward transportation of nutrients and drugs.²⁵</p> <p>Regulate expression of channels for water and ion exchange on astrocytes.³⁴</p>	<p>Filters molecules based on size and charge.²⁸</p> <p>Provides anchoring for NVU cells.²⁸</p> <p>Facilitates signal transduction between NVU cells.²⁸</p> <p>Facilitate migration of systemic immune factors during CNS injury.²⁸</p>	<p>Provide structural support and stimulate expression of tight junctions.³³</p> <p>Provide contractility in response to neuronal activity (neurovascular coupling).³³</p> <p>Facilitate tight junction opening to systemic immune cells.³³</p>	<p>Modulate expression of endothelial carriers (glut1 and Pgp) and enzymes.³⁴</p> <p>Facilitate neurovascular coupling (via elongation/contraction of pericytes).³³</p> <p>Facilitate immune responses.³⁴</p> <p>Regulate neuronal environment and facilitate proper synaptic function.²⁵</p>	<p>Protect neurons and synapses.³²</p> <p>Surveil the tissue for signs of injury and trigger an inflammatory pathways in response to CNS injury.²⁵</p>	<p>Regulate neurovascular coupling (via direct signaling and recruitment of astrocytes) to elongate/constrict pericytes.³³</p> <p>Products of neuronal activation can increase BBB permeability.²⁰</p>

1.1.4. The selective nature of the BBB

In the previous section, I have reviewed the roles of the NVU elements in the development, regulation, and maintenance of the BBB and its specialized endothelium. Here, I provide a more detailed description of the specialized phenotype of the brain's endothelial cells, allowing the selective passage of nutrients, electrolytes, proteins, immune factors and potential neurotoxins between systemic circulation and brain tissue.^{25,26} The key features that underlie this selectivity, and distinguish the phenotype of the brain's endothelial cells from their peripheral counterparts, include:

- a) High expression of tight-junction proteins, that tightly seal the gaps between neighboring cells
- b) Low expression of vesicular trans-endothelial transport mechanisms
- c) Distinct expression of specific trans-endothelial transporters
- d) High expression of enzymes
- e) Thickness that is ~ 40% lower than of peripheral endothelium,³⁵ presumably to facilitate faster trans-endothelial transport

The expression of different transport mechanisms and enzymes at the brain's endothelium, hence, plays a critical role in the selectivity of the BBB, and its integrity as a physical, metabolic, electrical, and immunological interface. In this section, I provide an illustration (Figure 3) and a brief description and of the selectivity mechanisms of the brain's endothelium.

1.1.4.1. Mechanisms of endothelial selectivity:

1.1.4.1.1. Paracellular selectivity

Paracellular flux refers to passive diffusion of molecules across the gaps between endothelial cells of the BBB. The diffusion is driven by a concentration gradient, with molecules moving from high- to low- concentrations.

1.1.4.1.1.1. Tight junction proteins

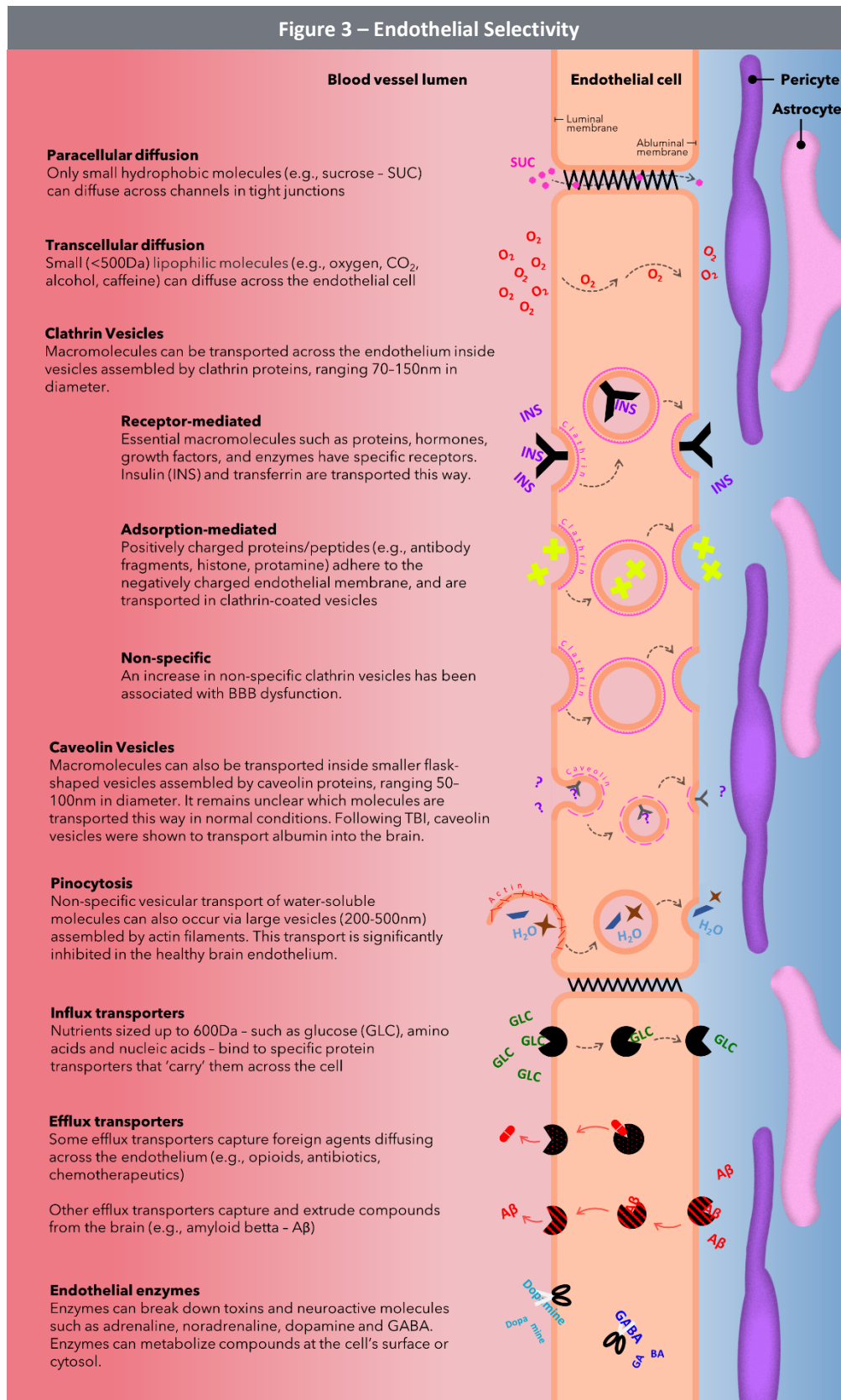
Under normal conditions, the gaps between adjacent endothelial cells at the BBB are sealed by tight junction proteins. The tight junctions of the BBB endothelium are far more dense, continuous, and complex than those in peripheral vasculature.^{36,37} The protein strands composing the BBB tight junctions include occludin, junctional adhesion molecules and members of the claudins family.³⁸

Tight junctions restrict paracellular diffusion of most molecules and microorganisms into the brain (including small ions, such as Na⁺ and Cl⁻), while allowing some flux of water, ions, and small (5–10nm in diameter) lipophilic molecules (e.g. sucrose) via size- and charge-selective pores formed by claudins.³⁹ This restricted movement results in significantly different electrical charges on each side of the endothelium (the luminal and abluminal walls), and an endothelial electrical resistance that is >1000 times higher than that in peripheral vasculature.⁹ Altered expression of tight junctions has been associated with genetic disorders and severe BBB injury following sepsis, stroke, intracranial hemorrhage, brain tumors, and cerebral edema.⁴⁰

1.1.4.1.2. Transcellular selectivity

In the present context, transcellular transport refers to the flux of substances through the brain's endothelial cells. The term *influx* is used to reflect blood-to-brain transport (from the luminal to abluminal side of the cell), and *efflux* reflects transport to the bloodstream. Several mechanisms of transcellular transport have been identified at the brain's endothelium:

Figure 3 – Endothelial Selectivity



Paracellular diffusion

Only small hydrophobic molecules (e.g., sucrose - SUC) can diffuse across channels in tight junctions

Transcellular diffusion

Small (<500Da) lipophilic molecules (e.g., oxygen, CO₂, alcohol, caffeine) can diffuse across the endothelial cell

Clathrin Vesicles

Macromolecules can be transported across the endothelium inside vesicles assembled by clathrin proteins, ranging 70-150nm in diameter.

Receptor-mediated

Essential macromolecules such as proteins, hormones, growth factors, and enzymes have specific receptors. Insulin (INS) and transferrin are transported this way.

Adsorption-mediated

Positively charged proteins/peptides (e.g., antibody fragments, histone, protamine) adhere to the negatively charged endothelial membrane, and are transported in clathrin-coated vesicles

Non-specific

An increase in non-specific clathrin vesicles has been associated with BBB dysfunction.

Caveolin Vesicles

Macromolecules can also be transported inside smaller flask-shaped vesicles assembled by caveolin proteins, ranging 50-100nm in diameter. It remains unclear which molecules are transported this way in normal conditions. Following TBI, caveolin vesicles were shown to transport albumin into the brain.

Pinocytosis

Non-specific vesicular transport of water-soluble molecules can also occur via large vesicles (200-500nm) assembled by actin filaments. This transport is significantly inhibited in the healthy brain endothelium.

Influx transporters

Nutrients sized up to 600Da - such as glucose (GLC), amino acids and nucleic acids - bind to specific protein transporters that 'carry' them across the cell

Efflux transporters

Some efflux transporters capture foreign agents diffusing across the endothelium (e.g., opioids, antibiotics, chemotherapeutics)

Other efflux transporters capture and extrude compounds from the brain (e.g., amyloid beta - Aβ)

Endothelial enzymes

Enzymes can break down toxins and neuroactive molecules such as adrenaline, noradrenaline, dopamine and GABA. Enzymes can metabolize compounds at the cell's surface or cytosol.

1.1.4.1.2.1. Transcellular diffusion

The brain endothelial cells allow limited passive diffusion across their membranes. Molecules that can diffuse freely include lipid-soluble gases (e.g., O₂ and CO₂), low molecular-weight alcohols (<500 Da, e.g., ethanol, butanol),⁴¹ and other psychoactive compounds such as caffeine, nicotine, cocaine, and heroin.⁴² This transport is driven by a concentration gradient and can be bi-directional.

1.1.4.1.2.2. Vesicular influx

A key feature distinguishing the brain's endothelium from peripheral capillaries is its low expression of sites for vesicular transport.⁴³ Termed *transcytosis* – vesicular transport allows the uptake and trafficking of large molecules from the bloodstream to the brain. Transcytosis involves *endocytosis* – the assembly of vesicles and encapsulation of cargo on the luminal side of the cell, and *exocytosis* – the release of encapsulated cargo at the abluminal side.⁴² While the rate of transcytosis in the brain's endothelium is considered low,⁴³ the mechanisms of vesicle assembly resemble those of peripheral capillaries and include: vesicles assembled by clathrin proteins, caveolin proteins and pinocytotic actin filaments.

Clathrin

Clathrin vesicles range between 70–150nm in diameter and are formed by the complexes of the clathrin protein.⁴² The clathrin proteins create an inward fold at the luminal cellular membrane that captures cargo and forms a clathrin-coated sac that can be trafficked through the cell's cytoplasm. Clathrin transport can be:

- **Ligand-specific** – large ligands such as proteins, hormones, growth factors, and enzymes can bind to specific membrane receptors that trigger ligand encapsulation in a clathrin coated sac.⁹ Ligands that can undergo *receptor-mediated* clathrin encapsulation include insulin, transferrin, low density lipoprotein (LDL) and amyloid beta (A β).⁴⁴
- **Charge-specific** – positively charged molecules can trigger clathrin-mediated encapsulation by adhering to the negatively charged membrane of the cell. This transport is termed *adsorptive transcytosis*, and is driven by the electrostatic interactions at the cellular membrane.⁴⁴ Molecules that penetrate the brain via this route include positively charged proteins/peptide such as cationized albumin, antibody fragments and histones.⁴⁴

- **Non-specific** – some water-soluble molecules may also undergo uptake in clathrin vesicle, yet the extent and the content of non-specific clathrin transport in the healthy BBB remains unknown.⁴²

Caveolin

Caveolin vesicles range between 50–100nm in diameter and are assembled by caveolin proteins, that create and coat flask-shaped cargo-containing capsules.⁴² While receptor-mediated caveolin transport was shown to traffic albumin in peripheral endothelium, this receptor was found to be absent from the brain's endothelial cells.⁴⁴ Notably, a shift from ligand-specific clathrin transport to non-specific caveolin transport has been suggested to contribute to increased cross-BBB leakage in aging,⁴⁵ and to play a role in post TBI (traumatic brain injury) transcytosis of albumin.⁴⁶ The exact cargo and expression of caveolar transcytosis in the healthy and diseased brain require further investigation.

Pinocytosis

Pinocytosis vesicles can range between 200-500nm in diameter and are formed by actin filaments that can engulf large amounts of extracellular fluid and water-soluble molecules.⁴² This is a highly-nonspecific form of transcytosis, and is often referred to as '*cell drinking*' or '*fluid-phase*' transcytosis.⁴² In the healthy brain, the expression of this transcytosis mechanisms at the brain's endothelium is considered to be highly inhibited, however pathological changes in inhibition have been suggested to contribute to non-specific influx of macromolecules (including albumin) into the brain.^{42,46}

1.1.4.1.2.3. Carrier-mediated transporters

While trans-endothelial transport of macromolecules requires vesicles, certain smaller molecules (<600 Da) can be trafficked by carrier proteins.²⁵ Some carriers act as blood-to-brain influx transporters, while others expel molecules in brain-to-blood efflux.⁴⁷

Influx transporters

The luminal side of the brain's endothelial cells has several transporters that can bind small nutrients circulating the bloodstream and deliver them to the brain. These include the specific transporter for glucose (GLUT1), transporters for amino acids (LAT1), and transporters for nucleic acids.^{9,47}

Efflux transporters

Efflux transporters eject compounds into the bloodstream at the luminal side of the endothelial cells. Some carry their cargo from the brain (e.g., neuronal waste products captured on the abluminal endothelial membrane), while others capture cargo inside the cell's cytosol (e.g., potentially neurotoxic compounds that diffused into the endothelial cell).⁴⁷ These transporters require energy in the form of ATP, and are termed ATP-binding cassettes (ABCs).⁴⁸

One of the most expressed efflux transporters at the BBB is the P-Glycoprotein.⁴⁸ P-Glycoprotein plays a key role in the clearance of A β peptides from the brain, and restricts a large range of compounds (including anticancer drugs, antibiotics and opioids) from entering the brain.⁴⁹ The expression of P-Glycoprotein transporters has been shown to increase in diseases such as ALS⁵⁰ and epilepsy,⁵¹ and is hypothesized to underlie drug-resistance in affected patients.^{50,51} Conversely, reduced P-Glycoprotein expression/function has been linked to ageing,⁵² and was suggested to play a role in failed clearance of A β peptides in Alzheimer's disease.^{49,53}

1.1.4.1.3. Endothelial enzymes

The brain's endothelium also has a unique expression profile of enzymes, acting as an additional defense system that degrades potential neurotoxins before they can enter the brain.⁴⁸ Some enzymes metabolize neurotransmitters circulating in the bloodstream (e.g., adrenaline, noradrenaline, dopamine, and GABA) to prevent them from affecting brain function; others metabolize drugs and toxins. Endothelial enzymes are suggested to contribute to the inability of various therapeutics to reach the brain.⁵⁴

1.1.4.1.4. Immuno-privilege

While the brain is largely considered to be separated from the systemic immune system, emerging data suggests that peripheral immune cells – specifically lymphocytes T and B – routinely enter the brain to provide additional surveillance for pathogens and repair of injured tissue.^{55–57} Lymphocyte are suggested to have both para-cellular and trans-cellular routes of crossing the endothelium. Para-cellular passage is thought to involve tight-junction remodeling, while trans-cellular passage is believed to be mediated by interaction between PECAM proteins (Platelet endothelial cell adhesion molecule) present on the surfaces of both lymphocyte- and endothelial- cells.^{55,58} To help quell infection upon pathogen-detection lymphocytes trigger: a) endothelial signaling encouraging further

lymphocyte migration towards the BBB, and b) increase in the expression of endothelial proteins for trans-endothelial lymphocyte trafficking.^{55,57} Importantly, overstimulation of this response has been shown to underlie severe neuro-inflammation, edema and tissue damage.^{55,57}

1.1.5. BBB dysfunction

In the previous section I have reviewed the mechanisms underlying the para-cellular and trans-cellular selectivity of the BBB's endothelium. Notably, both para-cellular and trans-cellular pathways have been implicated in BBB dysfunction. These findings challenge the classic interpretation of BBB dysfunction, that was often referred to as 'BBB-breakdown' and assumed to involve free para-cellular diffusion across broken-down tight-junctions.⁵⁹⁻⁶¹ In a 2013 collaboration with Dr. Jens Dreier, our lab has shown that increased influx across the dysfunctional BBB can take place despite fully intact tight junctions.⁶² Numerous studies have since demonstrated that the expression of transcellular influx and efflux mechanisms is indeed not static, and can be altered in Alzheimer's disease,^{49,53} epilepsy,⁵¹ traumatic brain injury,^{41,46} ageing,^{45,52} and even between night and day.^{19,63} Together, these findings suggest that acquired 'breakdown' of para-cellular selectivity may represent severe BBB pathology in the core and/or surrounding-tissue of lesions such as tumors and stroke,^{41,59-61} while maladaptive modulation of trans-cellular influx/efflux may play a role in earlier/milder disease stages. However, this hypothesis requires further investigation, as the characteristics and temporal features of altered trans- and para-cellular selectivity remain far from clear, along with their exact contribution to BBB-mediated pathogenesis.

There is little doubt in the literature that BBB dysfunction contributes to the development and progression of neuropathologies,⁶⁴ yet many gaps in our understanding of BBB dysfunction persist. To position my work in a broader context, in the next section I lay out my perspective on the main open questions in the field. The specific questions that were the focus of this thesis are delineated in section 1.1.6.

1.1.5.1. Open questions in the field of BBB dysfunction

1.1.5.1.1. What is BBB dysfunction?

- a) How does endothelial selectivity (Figure 3) change?
 - Which para-cellular/trans-cellular mechanisms are involved and when?

- Are there different phases of altered selectivity and what drives their progression?
 - Which substances leak and which fail to be cleared/metabolized?
 - Can endothelial selectivity be therapeutically restored?
- b) What transformations take place in non-endothelial NVU elements?
- Which NVU elements undergo transformation, and in what order?
 - What mechanisms drive NVU transformation?
 - How does NVU transformation alters endothelial selectivity?
 - Can NVU transformations be blocked?

1.1.5.1.2. What causes BBB dysfunction?

- a) What brain insults/pathologies result in BBB dysfunction, and how?
- b) What systemic diseases result in BBB dysfunction, and how?
- c) Can mechanisms resulting in BBB dysfunction be blocked?

1.1.5.1.3. How does BBB dysfunction mediate changes in brain function?

- a) What mechanisms underlie changes in function/structure of neuronal networks? In what order/time-frame?
- b) Do specific mechanisms underlie specific change patterns in network function/structure?
- c) Can changes in network function/structure be prevented?

1.1.5.1.4. Is BBB dysfunction always bad, or should it be simply referred to as 'altered BBB function'?

- a) Does altered BBB selectivity have protective/beneficial effects?
- b) What are the benefits and drawbacks of reversing altered BBB selectivity?

1.1.5.1.5. Can BBB dysfunction be diagnosed in living patients and what are the clinical features of BBB dysfunction?

- a) What methods can reliably diagnose BBB dysfunction in living patients, and what type of dysfunction do they reveal?
- b) What fluctuations in influx/efflux correspond to normal vs pathological BBB phenotype in different brain regions/networks/hemispheres?
- c) What kind of clinical symptoms are associated with BBB dysfunction?

- d) Does the presence of BBB dysfunction exacerbate existing clinical symptoms?
- e) Do specific symptoms (or their severity) correspond to differences in affected endothelial selectivity mechanism, the involved NVU elements, the duration and extent of BBB dysfunction, the affected brain regions/networks?

1.1.5.1.6. Can BBB diagnosis be coupled with targeted treatment?

- a) Can mechanisms associated with BBB dysfunction be targeted for the management or prevention of neuropathologies?

1.1.6. A focus on cross-BBB influx/leakage

My thesis focused on studying altered influx from the bloodstream to the brain, termed 'BBB leakage' for simplicity. Specifically, I examined:

- I. Mechanisms that cause BBB leakage (question 1.1.5.1.2) and pathological processes triggered by BBB leakage (question 1.1.5.1.3).

In an animal study published in 2019 (chapter 3), I examined the role of pericytes and neurons in BBB leakage, and the potential role of impaired coupling between them in BBB-mediated tissue damage.⁶⁵

Rationale: Pericytes and neurons have been shown to play important roles in BBB development, maintenance, and regulation; however, their role in mediating BBB leakage remains poorly understood. Moreover, pericytes regulate the supply of blood flow to neighboring neurons to meet neuronal energy demands (neurovascular coupling). Hence, impairment in pericyte-neuron coupling may potentially result in hypoxic conditions in surrounding tissue.

- II. The ability to diagnose BBB leakage in living patients and to understand its clinical correlates (question 1.1.5.1.5).

In two clinical studies published in 2019 and 2020 (chapters 4 & 5), I tested whether neuroimaging evidence of slow trans-cellular BBB leakage can be found in patients without

gross brain abnormalities (such as tumors or stroke lesions); and whether such leakage is associated with neuropsychiatric manifestations.^{66,67}

Rationale: The prevalent methods for diagnosing BBB leakage in living patients focus on robust and fast para-cellular leakage.⁶⁸⁻⁷⁰ Animal studies suggest that BBB dysfunction is also likely to involve increased trans-cellular leakage,^{41,46,62} however clinical evidence of this phenomenon remains scarce, nor is it clear whether such leakage is associated with neuropsychiatric morbidity. In a recent study of individuals with traumatic brain injury, we have shown the feasibility of diagnosing trans-cellular BBB leakage.⁷¹ Here, I provide the first exploration of the clinical relevance of such leakage, and its association with the severity of mood symptoms in patients with bipolar disorder and cognitive symptoms in patients with lupus.

The rationale behind these research goals is discussed in further detail in the introduction of each results chapter. The next two sections of the present chapter provide a short historical overview of existing technologies for diagnosing BBB dysfunction, followed by a review of current analysis approaches for MRI-based BBB assessment.

1.2. Detecting BBB leakage in living patients and animals

1.2.1. Imaging the living BBB – a historical perspective

As detailed above, the BBB discoveries between 1885 and 1960s originated from animal experiments with vital (i.e., non-fatal) dyes.⁴ In this approach, a dye is injected intravenously and is allowed to circulate the blood stream of the living animal for several minutes. However, detection of the dye in brain tissue requires the sacrifice of the animal, extraction of its brain and ex-vivo imaging. Hence, the study of the living BBB necessitated the development of alternative imaging approaches. In this section (and its accompanying figure 4), I provide a brief summary of such imaging modalities.

1.2.1.1. Intra-operative fluorescein microscopy

An early imaging breakthrough that allowed BBB visualization in living patients came from surgeries for brain tumor resection. As the surgery required a partial removal of the skull and exposure of the brain, in 1948 George Moore was able to image the surface of the brain using a fluorescent microscope.^{72,73} Moore coupled the procedure with an intravenous injection of a fluorescent dye that does not normally cross the BBB (the dye binds to proteins in the blood – primarily the BBB-impermeable albumin). He observed that the dye delineates tumors, and later studies confirmed that tumors are indeed surrounded by abnormal vascularization, and leakage of the capillary wall.^{74,75} In 1970 this method was also used to study tumor tissue after its resection. The tumor was extracted 30 to 60 minutes post dye injection, and the presence of the fluorescent dye was studied ex-vivo.⁷⁶

The first analogous study I was able to identify in animals was published in 1984 using cats,⁷⁷ and was termed intravital fluorescein microscopy. In 2010 our lab has established a method for intravital fluorescein microscopy in rats, allowing detailed and quantitative assessment of BBB permeability.⁷⁸ The approach was developed by Dr. Ofer Prager, who later enhanced it to allow simultaneous assessment of cortical blood-flow and diameter of cortical blood-vessels.⁷⁹ The first part of my PhD research utilized this approach to study mechanisms associated with BBB leakage, in collaboration with Dr. Prager and Dr. Richard Kovács.⁶⁵ The methodology of the approach is discussed in greater detail in the next chapter of this thesis (Methods, Section 1.2. Studying mechanisms of BBB leakage in-vivo). Notably, intra-operative fluorescein microscopy is still used today in specific clinical

settings (brain surgeries that require detailed mapping of blood-flow and permeability),⁸¹ and in animal studies of BBB leakage.^{82,83}

1.2.1.2. Single photon emission computed tomography (SPECT)

Today the popularity of single photon emission computed tomography (SPECT) remains limited, mainly due to its ionizing radiation (gamma rays), and relatively low resolution. However, in 1969 SPECT provided early validation of BBB differences between healthy and pathological tissue in living humans.⁸⁴ Later studies confirmed the phenomenon with more advanced tracers and rotating gamma-scanners,^{59,85} and replicated the findings in animals.⁸⁶

1.2.1.3. Computed tomography (CT)

Computed tomography (CT) was first used for BBB imaging in living rabbits in 1970.⁸⁷ In 1975 CT was used for imaging the BBB of living patients.^{88,89} Due to its limited resolution, CT is particularly useful for detecting hemorrhages and large BBB lesions. This application of CT is common clinical practice, and CT is regularly used for imaging patients with brain insults/tumors. This method has the advantage of widespread availability in clinical settings, but is disadvantaged by its X-ray radiation and limited sensitivity to non-robust BBB leakage.

1.2.1.4. Positron emission tomography (PET)

1980 marked the year of the first human BBB study using positron emission tomography (PET).⁹⁰ Advances in the technology enabled imaging the activity of specific BBB transporters in animals⁹¹ and in humans.^{51,92} Notably, PET allows the study of both trans-endothelial influx and efflux. Similar to SPECT and CT, PET imaging requires exposure of patients to ionizing radiation and is limited in resolution.

1.2.1.5. Magnetic resonance imaging (MRI)

The first magnetic resonance imaging (MRI) of a live human was performed in 1977.⁹² The emergence of magnetic tracers compatible with MRI in the early 1980s,⁹³ offered the first paradigm for non-invasive and non-ionizing BBB imaging. The first human studies focused on patients with brain tumors, providing evidence of tracer accumulation in and around tumor tissue due to BBB leakage.^{94,95} The 1990s saw a growth in BBB studies using MRI both in humans^{96,97} and animals.⁹⁷ Researchers realized that the accuracy of MRI-based BBB assessment benefits from continuous MRI acquisition post-injection,⁹⁸⁻¹⁰⁰ and the procedure became known as ‘dynamic contrast-enhanced MRI’ or DCE-MRI, for short. However, to date there is no consensus regarding the DCE-MRI duration necessary for accurate BBB assessment, or the optimal mathematical approach for deriving

physiologically-relevant information from the data.^{101,102,103,104} More on that in section 3 of this chapter.

Excitingly, contrast-free MRI approaches for BBB imaging (using arterial spin labeling)¹¹⁹ are currently under development, and may prove especially useful for BBB assessment in patients with renal pathology (in whom gadolinium-based contrast may exacerbate kidney damage).¹²⁰

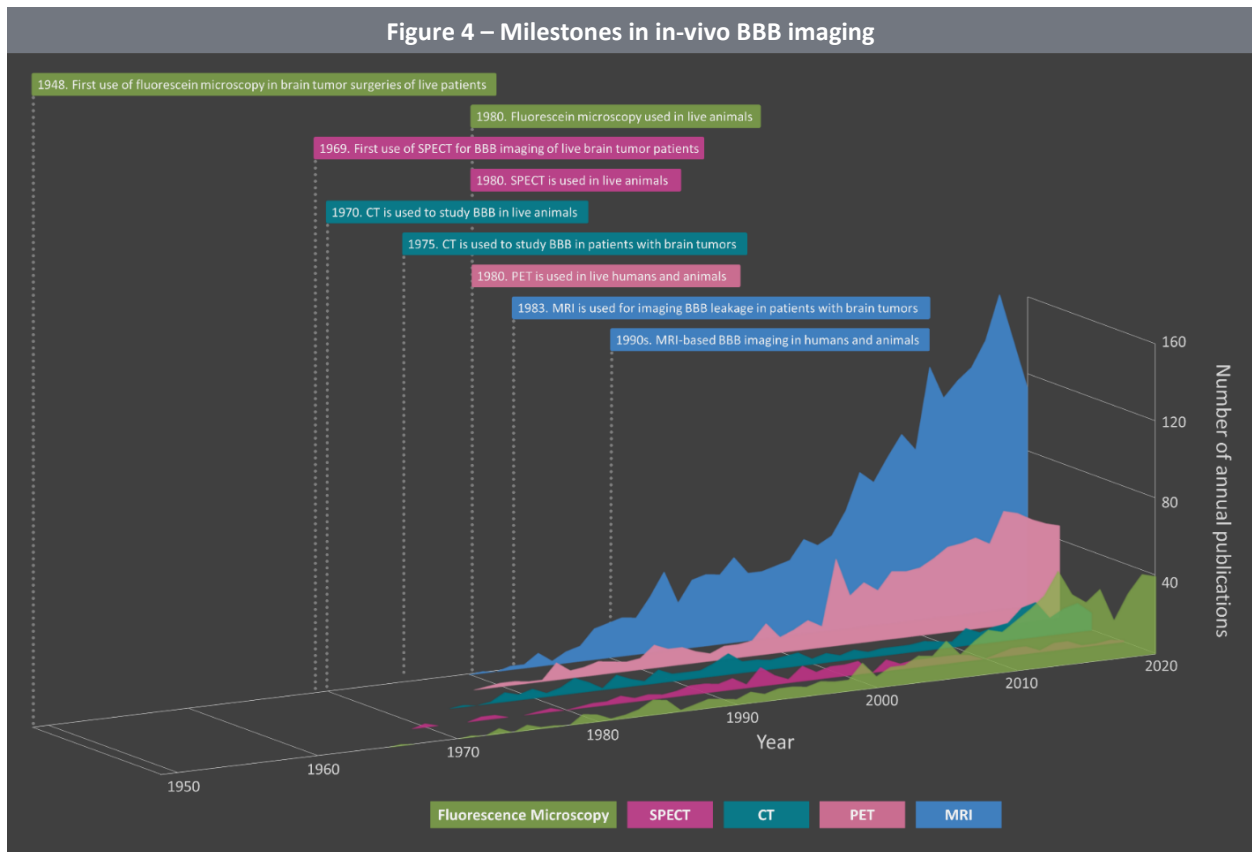


Figure 4. Milestones in in-vivo BBB imaging. Today, the main technologies that allow BBB imaging of living animals/humans are intraoperative fluorescent microscopy (green); single positron emission computed tomography (SPECT, burgundy); computed tomography (CT, teal); single positron emission tomography (PET, pink); and magnetic resonance imaging (MRI, blue). For each technology, the figure presents key breakthroughs in in-vivo BBB imaging, along with the annual number of relevant publications (in-vivo BBB imaging in animals or humans). The number of publications was determined using PubMed: for each technology, the search was conducted with three elements: (1) [“blood-brain barrier” or “blood brain barrier”] + (2) [optional terms describing the technology] + (3) [optional terms relevant to in-vivo imaging in animals and/or humans].

1.2.2. Non-imaging markers as indicators of BBB leakage

The advances in neuro-imaging techniques offer exciting opportunities for characterizing the living BBB. However, while these techniques provide detailed BBB mapping, the procedures tend to be

costly and not easily accessible. These limitations have led several groups to investigate the potential of non-imaging indicators of BBB leakage. Unlike the neuro-imaging techniques, these approaches do not rely on injected tracers. Instead, they either : a) test for the presence of brain-borne proteins (such as s100b or GFAP) in a subject's blood sample;^{105,106} or b) test for the presence of blood-borne albumin or immunoglobulins in a subject's cerebrospinal-fluid (CSF).^{107,108} However, recent findings raise growing concerns regarding the validity of these markers, as their serum/CSF concentrations can also be affected by BBB-unrelated factors.^{109,110} For instance, the s100b marker was discovered to also have non-neuronal origins (secreted to the circulation by adipose tissue),¹⁰⁹ and CSF levels of albumin/immunoglobulins were shown to depend on the rate of CSF production and rate of venous washout.¹¹⁰ Hence, while blood-markers may provide valuable information regarding the presence/absence of BBB leakage when neuro-imaging techniques are inaccessible, the search for reliable such markers is ongoing.

1.3. Quantitative mapping of BBB permeability from DCE-MRI data

MRI-based BBB assessment has seen a significant growth in popularity, thanks to its non-ionizing radiation, minimal invasiveness, and relatively high resolution. However, extracting diagnostically relevant information from raw MRI data is no trivial task. Numerous processing steps are required to access the first critical part of this puzzle – how much contrast is present in every voxel of the brain (voxel is the 3D equivalent of a pixel) at each time point the brain was imaged. These processing steps are detailed in the next chapter of this thesis (Methods, Section 2. Studying BBB leakage in humans). Once this puzzle piece is at hand, the next major challenge is to understand whether contrast leaks from capillary to non-capillary tissue. The crux of this challenge lies in the fact that capillaries are too small to be visible in MRI (millimeter-scale resolution), and each voxel contains both capillary and non-capillary tissue (cells and the space between cells). To overcome this limitation scientists have turned to mathematical models, that make assumptions regarding the tissues in each voxel and the passage routs between them. These mathematical models are also known as pharmacokinetic models, as they aim to characterize the kinetics of a drug in the brain, with the drug in this case being the MRI contrast agent.

1.3.1. Pharmacokinetic models for estimating BBB leakage

The goal of pharmacokinetic models is to estimate the rate of contrast leakage within each voxel (from the capillary within the voxel to the voxel's non-capillary tissue). In figure 5 below, I illustrate the main characteristics and assumptions of the four most recognized pharmacokinetic models:

1.3.1.1. The Tofts Model

The most widely used model was proposed in 1991 by Paul Tofts.¹⁰⁴ This model assumes that under pathological conditions the injected contrast agent can diffuse freely from the capillary, in a potentially bi-directional process driven by a concentration gradient and reflective of para-cellular flux between endothelial cells (presumably due to disruption of tight junctions). Tofts further assumed that contrast that left the capillary cannot enter cells and is restricted to the space between them (referred to as the 'extra-vascular, extra-cellular space' or 'interstitial space' – marked in gray in Figure 5 below). For simplicity, an additional assumption stated that the capillary occupies a negligible portion of the voxel, and that contrast presence within the capillary lumen can be ignored. To quantify the rate of the assumed diffusion, the model analyzes contrast dynamics during the first ~3 minutes post contrast injection.

1.3.1.2. The Modified Tofts Model

In 1999, Tofts updated his model to no longer dismiss the fact that some of the voxel's contrast can be within the capillary lumen.¹⁰³

1.3.1.3. The Patlak Model

Another widely used model was developed by Clifford Patlak in 1983.¹¹¹ Patlak's model assumed that contrast diffusion back into the capillary is unlikely, based on two sub-assumptions: a) contrast can be absorbed irreversibly, e.g., by tissue cells; and b) contrast concentration within the capillary is much greater than outside the capillary. Notably, while both the Tofts and Patlak models were classically used for characterizing the bolus phase of contrast circulation in the brain (the first 3 or 5 minutes post-injection), the accuracy of the Patlak model was shown to benefit from longer DCE acquisition.¹¹² The Patlak model was further confirmed to be fit for characterizing both fast and slow BBB leakage (lasting beyond the phase of initial contrast wash-in).¹¹²⁻¹¹⁴

1.3.1.4. The Veksler Model

In 2010, our lab started developing a model that is fit for characterizing the slow and subtle BBB leakage we observed in in-vivo animal studies.^{78,115} This approach was later adapted to DCE-MRI by Dr. Ronel Veksler and Dr. Yoash Chassidim, and has become known as the Veksler model.^{116,117} Unlike methods that focus on the initial bolus of the contrast, the Veksler approach focuses on the period of contrast-washout from blood vessels (6-20 minutes post contrast injection). The approach first identifies voxels that consist solely of vascular tissue (the superior sagittal sinus) and estimates the washout-rate of the vasculature. For the rest of the brain's voxels – that contain capillaries, cells, and interstitial space – the model estimates whether: a) contrast accumulates in the voxel due to trans-endothelial leakage, or b) contrast does not accumulate due to properly functioning endothelial cells.

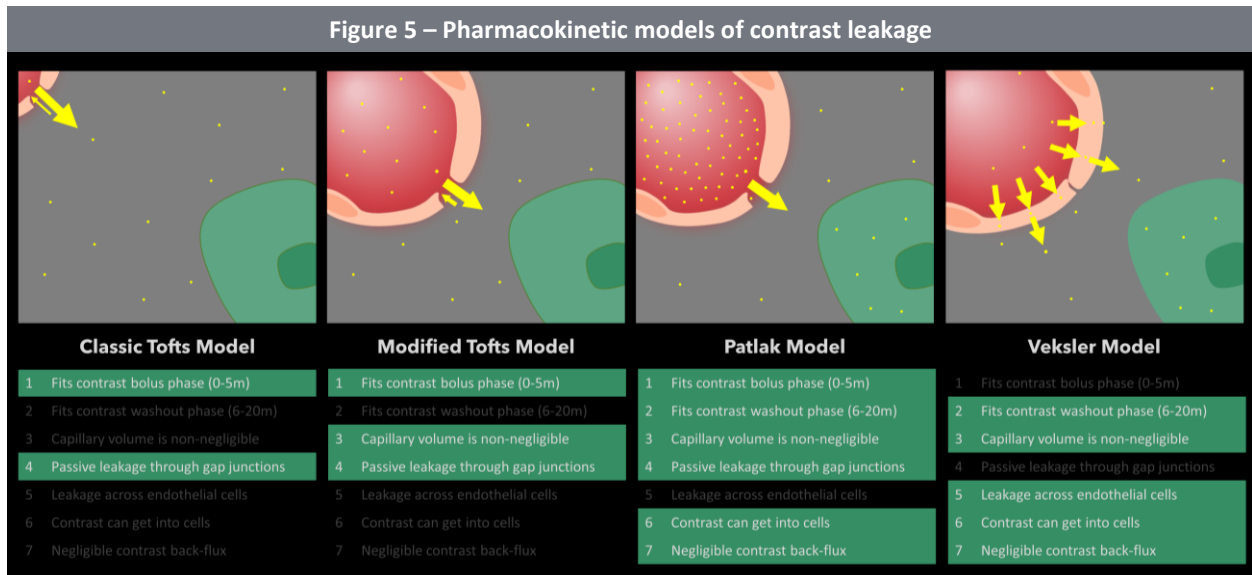


Figure 5. Pharmacokinetic models of contrast leakage. Each square represents a voxel, partially occupied by a capillary cross-section (delineated by two adjacent endothelial cells in light salmon), a neighboring cell (green), and the space outside the capillary and between cells (i.e., ‘extra-vascular, extra-cellular space’, depicted in gray). Yellow circles represent contrast-agent molecules and yellow arrows represent the assumed directionality of contrast diffusion. The classic Tofts model characterizes contrast leakage in the first minutes post injection, and assumes that: a) the capillary volume is negligible, and contrast within it does not contribute to the overall contrast concentration of the voxel; b) contrast can diffuse freely according to the concentration gradient, presumably through open gap junctions; c) contrast can only diffuse into the space between cells (gray), without entering cells (green); and d) contrast can flow back into the capillary. The modified Tofts model eliminates the first assumption, taking into account the contrast present within the capillary. The Patlak model eliminates the assumption of back-flow into the capillary, by assuming that: a) contrast can enter cells and accumulate within them irreversibly; and b) the capillary has a much greater concentration of contrast compared to its surroundings, making freely diffused back-flux unlikely. The Patlak model was also shown to be appropriate for fitting contrast dynamics that take place on a slower time scale. The Veksler model focuses on slow leakage and adds the assumption that it can be a product of trans-endothelial transport.

1.3.2. Fast and slow BBB leakage

For my BBB research I created a software that implements two of these pharmacokinetic models: modified Tofts and Veksler. The MRI acquisition protocol was also designed accordingly, capturing both the bolus phase of contrast circulation (0-3minutes post injection) and the washout phase of the contrast (6-20minutes post injection). The aim of this acquisition was to allow future comparison between the two types of leakage captured by these models:

- Fast BBB leakage (Tofts model) – likely to correspond to severe BBB leakage, due to para-cellular influx between gap-junctions. Such leakage is the hallmark feature of brain lesions caused by tumors, stroke, or multiple sclerosis (MS).^{68–70}
- Slow BBB leakage (Veksler model) – likely to represent more subtle BBB leakage, due to changes in trans-cellular endothelial transport.⁷¹ Such leakage can also be found in patients with tumors, stroke, or MS, however, it is more likely to be found in the gray matter surrounding the lesions.^{71,117,118}

While the developed software does allow the calculation of both types of leakage, the clinical studies of this thesis focused on the analysis of slow/trans-cellular BBB leakage and its neuropsychiatric correlates. A detailed analysis of fast/para-cellular leakage in the studied patient-cohorts, and the interplay between the two leakage types will be the focus of future research.

1.4. Chapter Summary

Despite the many discovered aspects of BBB structure and function – the current understanding of the BBB in health and disease remains incomplete. The knowledge gaps that were studied in this thesis include: i) mechanisms that cause BBB leakage; ii) pathological processes triggered by BBB leakage; iii) clinical diagnosis of trans-cellular BBB leakage; and iv) clinical correlates of trans-cellular BBB leakage. As will be further elaborated in the discussion chapter, the findings of this thesis also provide indirect insights into some of the other open questions in the field.

Chapter 2 – Methods

Chapter Overview

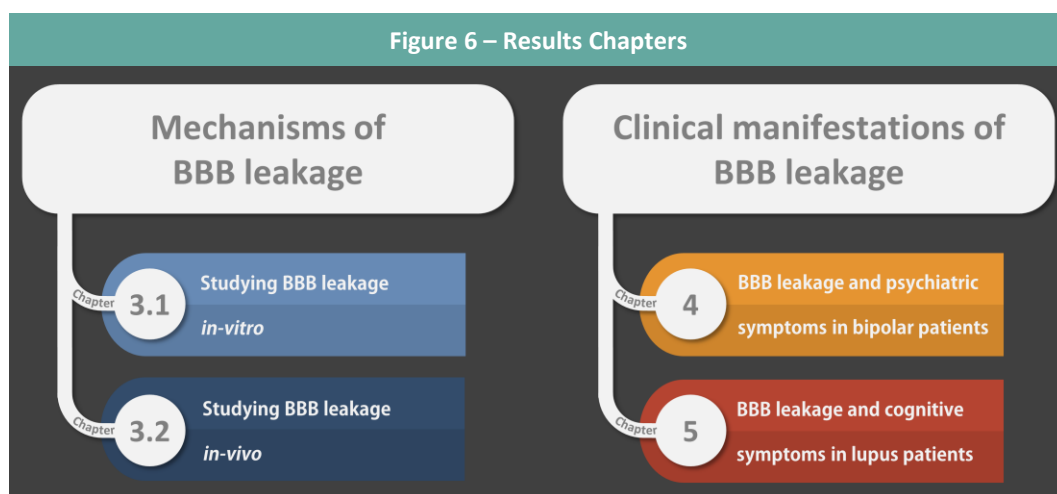
My PhD research had two primary focuses:

- I. Mechanisms that trigger cross-BBB influx/leakage and mediate subsequent neuronal dysfunction.
- II. Clinical diagnosis of BBB leakage and examination of associated symptoms.

Hence, the methodology of this thesis includes:

- I. Animal research, allowing the study of cellular mechanisms using in-vitro and in-vivo models of BBB injury.
- II. Clinical research, allowing the characterization of BBB leakage in living patients and the study of BBB-associated clinical manifestations.

The structure of the results chapters can be summarized in the following manner:



In the current chapter I will present the methodologies that allowed us to study the BBB in slice cultures, live rats, and finally – human subjects.

2.1. Studying mechanisms of BBB dysfunction

Many important insights into the function and dysfunction of the BBB have originated from studies in rodents. The brain microvasculature of rodents is similar to that of humans, and consists of the same elements of the neurovascular unit (NVU) reviewed in the introduction chapter and its first figure: endothelial cells (adjoined by tight junction proteins), basement membrane enwrapping the endothelial layer, pericytes anchored in the basement membrane, astrocytic end-feet (covering ~97% of the vascular surface area),¹ and nearby microglial cells and neurons.² This similarity has led to the development of several rodent models of BBB dysfunction, in which altered BBB selectivity can be induced either mechanically (e.g. weight drop,³ stroke induction),⁴ chemically (e.g., exposure of the vasculature to bile salts or serum albumin),⁵ genetically (by knocking-out or knocking-in genes that alter BBB development/function),^{6,7} or via kindling (e.g., induction of status epilepticus using kainic-acid⁸ or pilocarpine).⁹ Here, we sought out to establish a novel model of BBB dysfunction, that mimics the subtle and confined BBB leakage following focal transient seizures. Focal transient seizures were induced via focal application of 4AP (4-aminopyridine, an inhibitor of voltage-gated potassium channels)¹⁰ on the exposed cortex of living rats.

To allow the study of the effects of transient seizures at the cellular level, we had to overcome a major challenge in BBB research: the lack of in-vitro models of BBB dysfunction. To overcome this obstacle, we established a collaboration with Dr. Richard Kovács at the Neurophysiology Institute of the Charité Medical University in Berlin. Dr. Kovács has previously developed a slice culture model of the vasculature that maintains the complex architecture and dynamics of the BBB (organotypic vasculature), despite the absence of blood flow.¹¹ In this collaboration, we induced transient seizures in the Kovács slice culture model. This paradigm allowed us to study the effects of neural seizure activity on the neurovascular unit at the capillary level, and the mechanisms underlying seizure-induced BBB leakage. Specifically, we tested the hypothesis that pericyte dysfunction plays a role in mediating BBB leakage and loss of neurovascular coupling, that may in-turn lead to ischemic neuronal injury.

In the next section, I will present a description of the experimental settings of the models we established for transient seizures in-vitro and in-vivo. The section will put an emphasis on the

imaging methodologies used for the quantification of BBB leakage in both models. Other aspects of the methodology will appear in greater detail in the paper presented in Chapter 3 – “Seizure-induced microvascular injury is associated with impaired neurovascular coupling and blood–brain barrier dysfunction.”

2.1.1. Studying mechanisms of BBB leakage in slice-cultures

Slice preparation:

The slice cultures were prepared as previously described by Kovács et al.¹¹ In brief, the brains of 6-8 day-old Wistar rats were removed (Figure 7A,B), and submerged in carbogen-containing medium. The brains were sliced using a microtome, to obtain 400µm-wide hippocampal slices (Figure 7C). Medium-submerged slices were maintained in an incubator, with a humidified atmosphere containing 5% CO₂. The vascular tone of the cultured capillaries was maintained using the thromboxane analogue U46619 – an agent causing vascular constriction that compensates for the absence of blood flow and adrenergic input.¹¹

Seizure-induction and electrophysiological recordings:

Seizure activity was induced in CSF-submerged slices using two different methods: (1) adding 4-aminopyridine (100 µM) to the CSF, or (2) lowering the CSF-concentration of magnesium and elevating the CSF-concentration of potassium. Both methods induce stereotypic seizure-like discharges.^{11,12} Electrophysiological recordings were performed in area CA3 of the slice cultures (Figure 7C).

Fluorescent labeling of the vascular lumen, pericytes and astrocytes:

To confirm the organotypic architecture of the vasculature, the slices were incubated with antibodies for laminin – a major constituent of the vascular basement membrane (Figure 7E). Pericytes were labeled with either: neuronal/glial antigen 2 proteoglycane (NG2), or mitochondrially-targeted fluorescent ethidium derivative (MitoSoxTM) – which accumulates within the mitochondria-rich pericytes. Pericytes were also confirmed based on their morphology (appearing as a “bump on a log” structure enwrapping a capillary, Figure 7F). Astrocytic end-feet were labeled using calcein-AM (Figure 7F).

Monitoring pericytic injury:

To examine whether seizures lead to pericyte injury, we monitored the integrity of pericytic mitochondria. Since MitoSox™ accumulates predominantly within pericytic mitochondria, leakage of MitoSox from the mitochondria into the pericytic cytosol was used as an indicator of mitochondrial breakdown.¹³

Studying neurovascular coupling:

Neurovascular coupling was assessed by examining the ability of capillaries to appropriately dilate in response to seizures. The diameter of capillaries was measured as the distance between the astrocytic end-feet enwrapping the capillary cross-section (Figure 7F). To test whether deficiencies in neurovascular coupling are associated with reduced oxygen supply to the tissue, the level of tissue-oxygenation was also continuously monitored and recorded (using Clark-style oxygen microelectrodes, Unisense, Denmark).

Assessment of cross-BBB influx/leakage:

To study seizure-induced changes in capillary leakage, slice cultures were incubated with 2',7'-dichloro-2,7-difluoro-4,6-diacetamido-3,6-dimethyl-5-carboxyfluorescein diacetate (H2DCF-DA, 20 μ M, 30 min). H2DCF-DA leads to accumulation of its oxidation end-product – DCF, within the vascular lumen (Figure 7G). DCF flux from the capillary lumen to the peri-vascular space was used as an indicator of BBB leakage (Figure 7H).

Figure 7 – Slice culture methodology

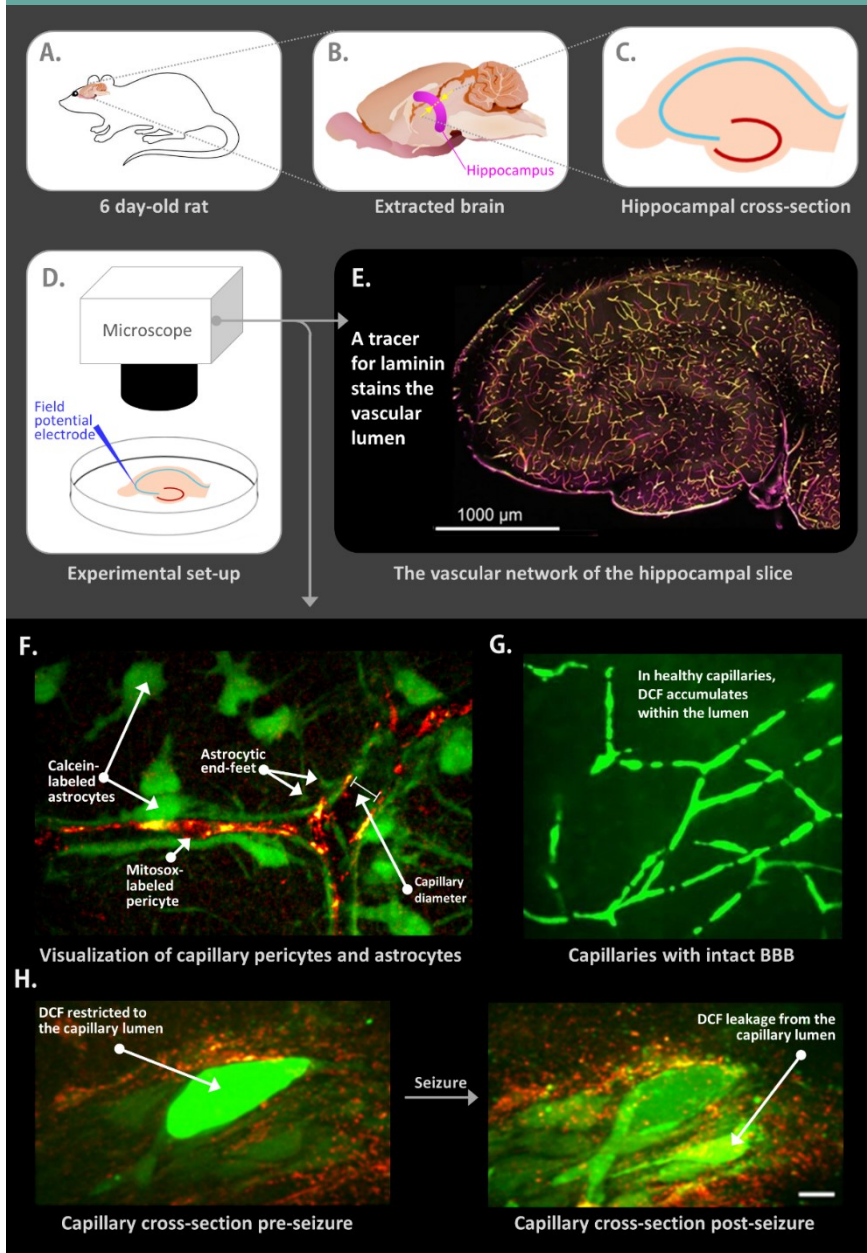


Figure 7. Slice culture methodology **A.** Experiments were conducted in sacrificed 6 day-old rats. **B.** The rat brain was extracted, and a 400uM cross-sectional slice of the hippocampus was cut (**C.**) The slice was maintained in conditions mimicking the brain’s microenvironment. **D.** Fluorescent microscopy was used continuously during the experiments, along with electrophysiological recordings from area CA3 of the hippocampus. **E.** A tracer for laminin was used for labeling the vasculature of the slice. **F.** CalceinAM and MitosoxTM were used for labeling astrocytes and pericytes, respectively. The labeling revealed astrocytic end-feet enwrapping the capillaries, and allowed the continuous monitoring of capillary diameter in response to seizures. Mitosox accumulated in the mitochondria of pericytes, revealing the classic “bump on a log” structure of pericytes. **G.** The tracer DCF normally accumulates within blood vessels and remains inside the vascular lumen. **H.** The cross-section of a capillary before and after a seizure, demonstrates that seizures induce leakage of DCF from the capillary lumen. Such leakage is indicative of BBB dysfunction.

2.1.2. Studying mechanisms of BBB leakage in vivo

Animal preparation:

Male rats were anesthetized (with ketamine (100 mg/ml, 0.08 ml/100g) and xylazine (20 mg/ml, 0.06 ml/100 g), and placed in a stereotactic frame. A craniotomy was performed, removing the part of the skull above the motor-sensory cortex of the right hemisphere. The dura was also removed, exposing the cortical tissue. A ring of bone-cement was anchored around the exposed cortex, creating a small ‘reservoir’ for continuously-perfused artificial CSF (aCSF). The aCSF was supplied using a peristaltic pump (Peri-Star, WPI).

Seizure-induction and electrophysiological recording:

Transient, focal seizures were induced by changing the solution supplied to the fluid-reservoir above the exposed tissue (Figure 8A). The pump continuously perfusing the reservoir was switched from supplying aCSF to delivering aCSF containing the convulsive agent 4AP (500mM). Electrophysiological activity was recorded using epidural (electrocochleographic; ECoG) electrodes (DSI, St Paul, MN).

Studying neurovascular coupling:

Similar to the slice culture experiments, the in vivo experimental set-up was also designed to allow the study of neurovascular coupling (i.e., the responsiveness of the vascular diameters to seizures). The diameter of arterioles was monitored continuously, and quantified as the cross-section of the vessel. To test whether reduced neurovascular coupling was accompanied by deficits in oxygenation, the oxygen level of the tissue was also continuously recorded (using Clark-style oxygen microelectrodes, Unisense, Denmark).

Assessment of cellular injury:

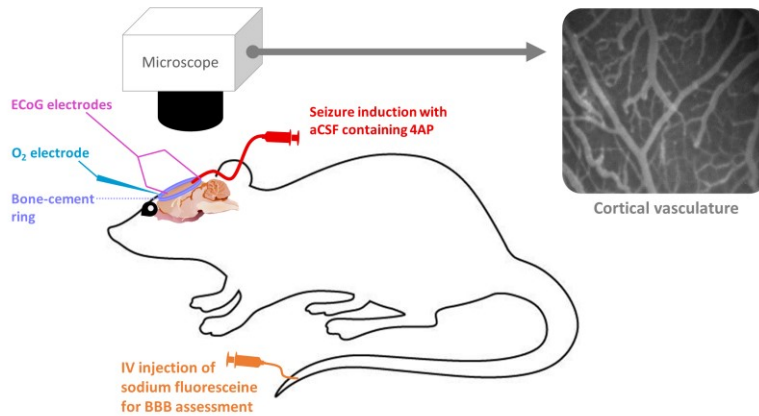
To examine whether seizures induce cellular damage that could underlie BBB injury, we used the fluorescent dye propidium iodide – a marker of cell-membrane injury that binds to exposed cellular DNA/RNA. The dye was intravenously injected into the rat’s tail (0.5 mg/kg body weight, 0.5 mg/ml in saline), and its fluorescence in the exposed cortex was monitored using fluorescent microscopy.

Assessment of BBB permeability:

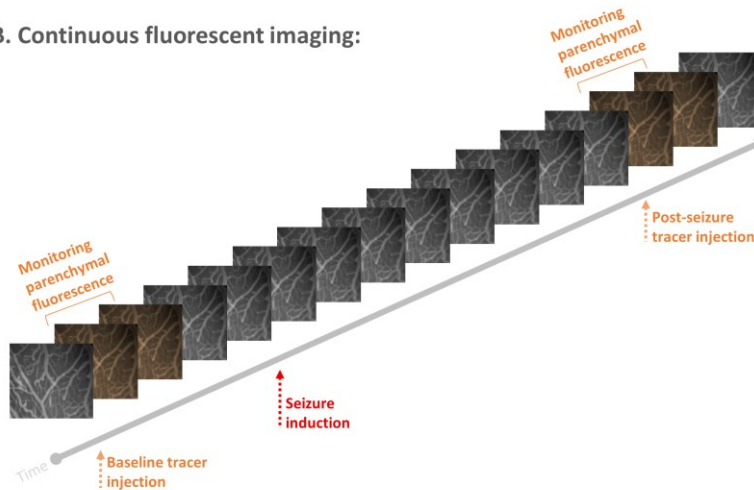
Seizure-induced BBB permeability was assessed using the fluorescent dye sodium-fluorescein (NaFlu, Novartis). Normally this dye does not cross the BBB, due to its large molecular weight (376 Da). The dye was injected intravenously into the rat's tail (1 mg/ml in saline), and the exposed cortex was monitored using fluorescent microscopy for 3 minutes post injection (Figure 8B). Images were taken with a frequency of 5Hz. The images captured whether dye fluorescence remained within arterioles or leaked into non-vascular tissue due to BBB dysfunction (Figure 8C). Dye accumulation in non-vascular tissue was later quantified using image processing algorithms. Images were first registered to correct for movements during the 3min image acquisition. Next, pixels representing vascular and non-vascular tissue were identified, and a curve of the 3min fluorescence was constructed for every pixel. These curves were used to determine whether fluorescence has accumulated in the pixel. For each pixel, fluorescence accumulation was quantified as the area under the fluorescence time-curve, and was used as a measure of BBB permeability.

Figure 8 – In vivo methodology

A. Experimental set-up:



B. Continuous fluorescent imaging:



C. Quantification of tracer leakage:



Figure 8. In vivo methodology.

A. A craniotomy was performed on anesthetized rats, exposing the tissue of the right motor-somatosensory cortex. A ring of bone-cement was anchored above the exposed cortical tissue to serve as a reservoir for continuously perfused artificial cerebrospinal fluid (aCSF). Transient, focal seizures were induced by switching from cortical perfusion with aCSF to perfusion with aCSF containing the convulsive agent 4-aminopyridine (4AP). Electrocorticographic electrodes were used for recording electrophysiological activity; and O₂ electrodes were used for recording tissue oxygenation. Sodium fluoresceine was injected intravenously for assessing BBB permeability, and the cortical tissue was continuously imaged using fluorescent microscopy (**B**). BBB permeability was quantified based on the dynamics of the injected tracer in non-vascular tissue. Prior to seizures, injected tracer remained within the blood vessels. A single transient seizure was sufficient to cause tracer accumulation in non-vascular tissue – a phenomenon indicative of BBB leakage.

2.2. Studying BBB leakage in humans

In the in-vitro and in-vivo experiments, the cross-BBB leakage was assessed using dyes that normally do not cross the BBB. A similar paradigm is used for assessing the BBB of living human patients. However, instead of using fluorescent dyes and fluorescent microscopy (allowing direct imaging of exposed brain tissue), we used a magnetic dye and magnetic resonance imaging (MRI). MRI has several advantages over direct imaging, with the primary benefit of eliminating the need to expose the subject's brain with a craniotomy. MRI also allows 3D whole-brain mapping of BBB permeability, as opposed to the above-described 2D methods of imaging the surface of the cortex, or of the extracted hippocampus.

To map BBB leakage using MRI, the magnetic dye is injected intravenously into the subject's arm, and the brain is scanned repeatedly over a period of ~20 minutes -- to determine whether the dye leaks into brain tissue. The details of the acquisition protocol are presented in the next section, and its accompanying figure 9. The drawbacks of this approach include the relatively long acquisition time (subjects must try to remain motion-less for 20 minutes), and the inability to examine patients with impaired renal function (the magnetic dye can further damage their kidneys). MRI-based BBB assessment is also challenging in terms of data analysis. The recorded MR signals do not directly reflect dye concentration in the tissue, and several computational steps are required to convert the images to data of physiological relevance. The software developed during my PhD integrates all these computational steps into a single automatic and stream-lined process, and calculates the rate of BBB leakage in every voxel of the brain (a voxel is the 3D equivalent of the 2D pixel). The steps of the developed software are detailed later in this chapter and summarized in figure 10.

2.2.1. The MRI acquisition protocol

BBB assessment requires a specialized protocol of MRI acquisition. Here, I describe the acquisition protocol used in the clinical studies presented in chapters 4 and 5. All study participants underwent MR scanning at the Biomedical Translational Imaging Centre (BIOTIC, QEII Hospital, Halifax, NS, Canada), on a 3T MRI scanner (Discovery MR750, GE Healthcare, Waukesha, WI, US), with a 32-

channel MR Instruments head coil. The acquisition protocol consists of four sequences of T1-weighted imaging:

- A) The first sequence acquires a high-resolution T1-weighted scan (Figure 9A). What sets this sequence apart is its relatively small voxel size (1x1x1mm), allowing a detailed view of brain-anatomy and differentiation between small brain structures. This sequence aids the mapping of each participant's brain onto the standardized brain template developed by the Montreal Neurological Institute (MNI), in a process termed spatial normalization (see next section – ‘analysis pipeline’). The high-resolution anatomical sequence is also useful for measuring the volumes of different brain structures, using the [VolBrain](#) freeware.¹⁴

*Acquisition parameters of the
T1-Weighted Sagittal
anatomical Scan*

TE/TR: 2/6ms
FOV: 224mm
Acquisition matrix: 224x224x168
Voxel size: 1x1x1mm
Flip angle: 9°

- B) The second sequence consists of three scans of the brain, each acquired with a different flip angle (Figure 9B). This step is critical for later transforming the images from values of MR-intensity to values of T1-relaxation times. More on that in the next section – ‘analysis pipeline’.

*Acquisition parameters of the
T1-Weighted Axial Scan*

TE/TR: 2/10ms
FOV: 240mm
Acquisition matrix: 192x192x34
Voxel size: 1.25x1.25x6mm
Variable flip angle: 5°/10°/30°

- C) Next, the magnetic contrast agent is intravenously injected into the participant's arm (Gadobenate Dimeglumine, MultiHance, Bracco Imaging, Montreal, QC, Canada, Injection dose: 0.1mmol/kg), and the brain is scanned continuously to capture the dynamics of the contrast in brain-tissue (Figure 9C). This sequence is, therefore, called dynamic contrast-enhanced MRI (DCE-MRI), and in our protocol it consists of two parts:

Part I — the brain is scanned every 4 seconds between 0- and 3-minutes post injection (54 brain scans).

Part II — the brain is scanned every 20 seconds between minutes 6 and 20 post injection (additional 46 brain scans).

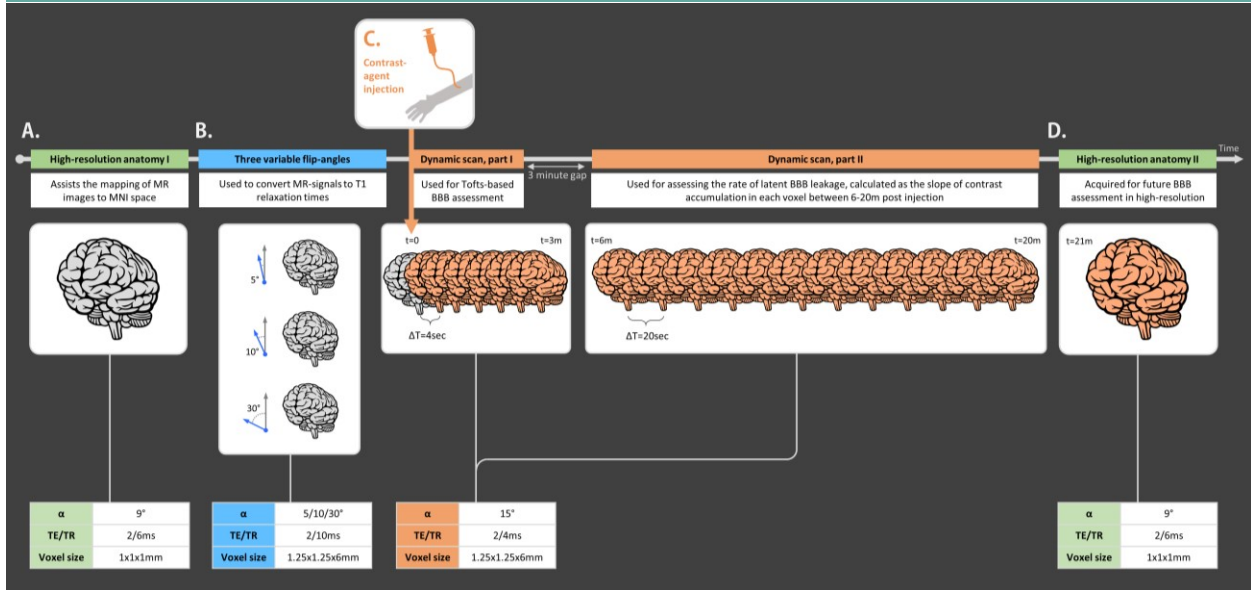
The 0-3-minute acquisition captures robust/fast contrast kinetics, allowing the calculation of BBB permeability using the Tofts model.¹⁵ The 6-20-minute acquisition captures the subtle/slower accumulation of contrast in the tissue, quantified using the Veksler model of BBB leakage.^{16,17}

*Acquisition parameters of the
T1-Weighted Axial Dynamic
Scan*

TE/TR: 2/4ms
FOV: 240mm
Acquisition matrix: 192x192x34
Voxel size: 1.25x1.25x6mm
Flip angle: 15°
 $\Delta t=4\text{sec}$, 0-3min post-injection.
 $\Delta t=20\text{sec}$, 6-20min post-injection

D) The last sequence acquires another high-resolution T1-weighted scan (Figure 9D), with identical acquisition parameters to sequence A. This scan is acquired for future analysis, meant to test the potential of a simplified acquisition protocol. Future work will test whether comparing a single T1 image acquired before contrast injection (sequence A) to a single scan acquired 20 minutes after injection (sequence D), could allow reliable screening for BBB leakage without the need for dynamic scanning (sequence C). If this hypothesis is correct, the 20 minutes interval post-injection can be dedicated to acquiring other types of sequences commonly requested by physicians (e.g., T2-weighted imaging, fluid-attenuated inversion recovery [FLAIR], diffusion weighted imaging [DWI], or functional MRI [fMRI]). This would simplify the integration of BBB imaging into standard clinical practice, as the overall duration of the MR protocol would not need to be substantially lengthened.

Figure 9 – Summary of MRI acquisition protocol



2.2.2. The developed BBB software

Once the MR sequences are acquired, they are analyzed using a custom pipeline written in MATLAB. For simplicity I shall refer to the pipeline and its graphical user interface as the *BBB software*. The BBB software requires a single input from the user: selection of the directory containing the MR data. Once the software knows where the data is stored, the user simply presses the button ‘run analysis’ for automatic execution of all computational steps required for quantifying BBB leakage in every voxel of the brain. The analysis consists of:

2.2.2.1. Three steps of data pre-processing (Figure 10 A-C)

2.2.2.2. Two steps calculating contrast concentration (Figure 10 D,E)

2.2.2.3. Two steps mapping contrast leakage-rates (Figure 10 F,G)

2.2.2.4. Two ‘post-processing’ steps, giving leakage-rates diagnostic relevance (Figure 10 H,I).

2.2.2.1. Data pre-processing

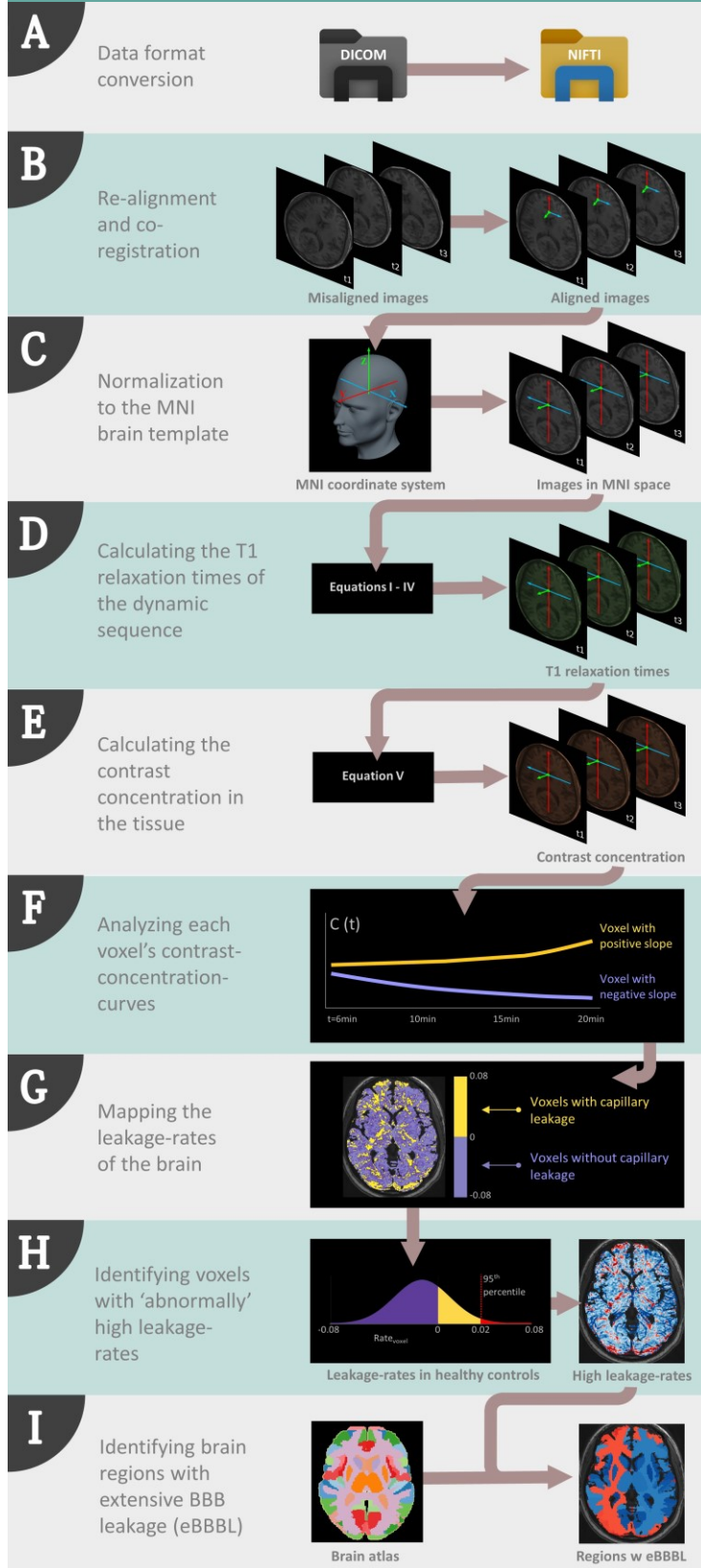
Data pre-processing involves steps that are performed on all sequences of the acquisition protocol to prepare the data for voxel-based analysis of contrast dynamics. The three pre-processing steps run by the BBB software are:

A) Data format conversion

The MRI machine exports images as 2-dimensional slices) in a format called DICOM (Digital Imaging and Communications in Medicine). This format is a standard method for transmitting medical images and their associated information (acquisition parameters, patient demographics, etc.). While specialized applications allow the viewing of data in DICOM format, customized image-analysis necessitates the separation of images from the additional information encoded in the DICOM format. The BBB software performs this separation using the third-party application [mcVerter.exe](#) that:

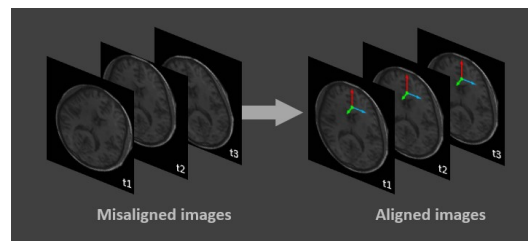
- Extracts the 2D slice-image from each DICOM (slice= 256x256 voxels)
- Arranges the slices of a given scan into a 3D brain-representation (brain=256x256 voxels x 26 slices)
- Saves the 3D data in a format called NIFTI (Neuroimaging Informatics Technology Initiative, Figure 10A). The DCE sequence is saved with an added fourth dimension representing time.

Figure 10 – BBB software, analysis pipeline



B) Re-alignment and co-registration.

The DCE acquisition consists of two sequences: 54 scans between 0-3 minutes and 46 scans between 6-20 minutes. The two sequences allow us to study the changes in contrast over time, in every voxel of the brain. This approach is known as ‘voxel-based analysis’. Successful voxel-based analysis requires all scans of a sequence to be accurately aligned, with every given voxel representing the exact same part of the brain across all scans. To overcome potential misalignment of voxels due to patient movement between scans, the BBB software uses the robust re-alignment algorithm developed by the Statistical Parametric Mapping initiative (SPM).¹⁸ More specifically, the software executes the [SPM12](#) algorithm to: a) create a reference scan (as the average of the 46 scans between 6-20 minutes); and b) re-align all scans of the dynamic sequence to the reference (Figure 10B). This re-alignment procedure relies predominantly on geometric transformations of rotation and translation.



Relevant excerpt from Figure 10

Once all scans within the dynamic sequence are properly aligned, another SPM12 re-alignment procedure is initiated to align the rest of the T1-weighted sequences (sequences A, B and D in figure 9) to the same reference. While the alignment of scans within the same sequence is termed ‘re-alignment’, the process of aligning different sequences is often referred to as ‘co-registration’. Post re-alignment and co-registration, all voxels of the acquired sequences match in size and orientation, representing the same part of the brain across all sequence scans.

Due to the critical importance of proper voxel alignment for voxel-based DCE analysis, the BBB software tests the quality of the re-alignment results by calculating the mean-square-error between every two consecutive scans in the DCE sequence. Scans that remain misaligned (as reflected by a large mean-square-error) are automatically omitted from the sequence. Sequences with >1 scan that

fails re-alignment are extremely rare (most-commonly old datasets from one specific imaging center).

C) Normalizing all scans to the MNI brain template.

This step can be thought of as another co-registration process, only this time all scans are mapped to a standardized brain template. The BBB software maps all scans to the MNI brain template (Figure 10C), developed based on the scans of >300 healthy brains.¹⁹ This mapping is termed ‘normalization’, as it is designed to compensate for the variability in brain shapes across humans. While all humans are likely to have similar gross anatomy, common variations include the morphology of gyri, sulci, corpus callosum, as well as minor differences in overall brain volume.²⁰ This part of the pipeline also uses an SPM12 algorithm. The algorithm first focuses on the anatomical sequence, mapping its superficial brain structures to the MNI template using affine geometric transformations that include translation, rotation, scaling, shear, and nonlinear warping. The ‘mapping instructions’ are saved in 12 transformation parameters, that are then used to transform the rest of the sequences (since all sequences were co-registered in the previous step). After normalization, all sequences represent the brain as 27 slices of 157x189 voxels that are aligned with the MNI template.

2.2.2.2. Calculating contrast concentration

Once all voxels of all scans are aligned, the software can focus on the information stored within them. The brightness of each voxel reflects the signal recorded by the MR scanner. The brighter the voxel, the more contrast it contains. However, the relationship between voxel brightness and actual contrast concentration is not linear, and depends both on tissue characteristics and acquisition parameters.²¹ Consequently, additional steps (Figure 10 D,E) and mathematical operations are required in order to convert voxel-based brightness-information to voxel-based levels of contrast:

D) Calculating the T1 relaxation times of the dynamic sequence.

The basis of contrast-enhanced MRI lies in the fact that the contrast agent shortens the longitudinal relaxation time (T1) of the tissue it reaches. This is the reason why the DCE sequence is T1-weighted, which means that the acquisition parameters (such as echo time, repetition time, flip angle, etc.) are optimized towards capturing the longitudinal relaxation-time of protons in the tissue.

However, while this acquisition is more sensitive to T1 relaxation, components of T2 relaxation and proton density are also present in the recorded signal.²² The signal may also be affected by the specifics of the MRI machinery, such as receiver coil geometry/sensitivity and amplifier gains.²² Raw T1-weighted images can be useful for qualitative inspection (e.g., in hospital settings). However, quantitative analysis over several time-points requires the conversion of T1-weighted values to definitive T1 relaxation times. The separation of the T1 component from the DCE sequence is possible through the acquisition of an additional, specialized MR sequence prior to contrast injection. The earliest strategies date back to the 1970s and rely on lengthy sequences that produce curves of ‘true’ T1 relaxation.²³ Here we implemented a faster method,²² acquiring a series of 3 rapid scans – each with a different flip-angle ($\alpha = 5^\circ, 10^\circ$ and 30° ; figure 9B). The BBB software uses these three scans to estimate the pre-contrast T1 relaxation times, based on the equation optimized by Deoni et al:^{24,25}

Equation I:

$$\frac{S(\alpha)}{\sin(\alpha)} = \frac{S(\alpha)}{\tan(\alpha)} \cdot E_1 + M_0(1-E_1) \quad ; \quad E_1 = e^{-TR/T1}$$

This equation formulates a relationship between:

- The flip angle of each scan – α
- The raw T1-weighted signal corresponding to each α – $S(\alpha)$
- The repetition time of the three scans – TR
- The actual longitudinal relaxation time — T1
- The longitudinal magnetization at equilibrium – M_0

T1 and M_0 are the unknowns of the equation. The equation can be solved in its linear form:

Equation II:

$$y = E_1 \cdot x + f(E_1) \quad ; \quad y = \frac{S(\alpha)}{\sin(\alpha)} \quad ; \quad x = \frac{S(\alpha)}{\tan(\alpha)}$$

Once the 3 sets of α and $s(\alpha)$ are fed to equation II, its slope (E_1) can be estimated using linear regression. T1 is then easily derived from:

Equation III:

$$T1 = \frac{-TR}{\ln(E_1)}$$

Using the series of 3 scans, equations I, II & III are solved for every voxel of the brain – resulting in voxel-specific T1 values. These T1 values are called the ‘T1 map’, and serve as the cypher for computing the actual T1 values of the DCE sequence. The set of variables required for the calculation of T1 at a particular time-point – T1(t) – can be summarized with the following representation:

Equation IV:

$$T1(t) = f(T1_{map}, TR_{DCE}, \alpha_{DCE}, S(t), S_{t=0})$$

Hence, for every voxel, T1(t) is a function of:

- The voxel’s T1 map value – T1_{map}
- The repetition time of the DCE sequence – TR_{DCE}
- The flip angle of the DCE sequence – α_{DCE}
- The voxel’s raw T1-weighted signal at time t – S(t)
- The voxel’s raw T1-weighted signal at baseline (prior to contrast injection) – S_{t=0}

The calculations summarized in equation IV were covered in detail by Jackson et al.²⁶

E) Calculating the contrast concentration in the tissue.

Once the DCE data represents true T1 relaxation times, the contribution of the contrast-agent to each voxel’s T1 can be computed. This is achieved using the Solomon-Bloembergen equation,²⁷ allowing the calculation of contrast concentration at each time point – C(t):

Equation V:

$$C(t) = \frac{1/T1(t) - 1/T1_{map}}{\text{Contrast Relaxivity}}$$

For every voxel, equation V formulates the relationship between:

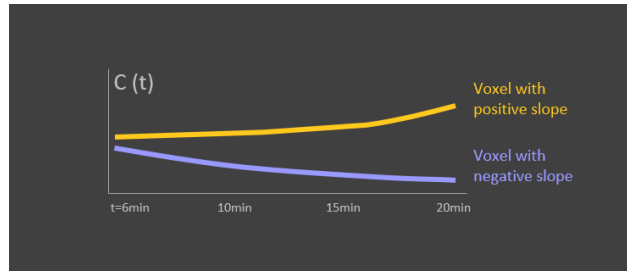
- The voxel's actual longitudinal relaxation time calculated in the previous step — $T1(t)$
- The voxel's pre-contrast T1 value — $T1_{map}$
- The relaxivity of the contrast-agent (a characteristic of the contrast-agent that is listed on its label) — Contrast Relaxivity

2.2.2.3. Mapping leakage-rates

Knowing the levels of contrast concentration in each voxel over time sets the stage for tackling the chief objective of the analysis. The software is now ready to estimate how leaky are the capillaries within each voxel. In the introduction chapter, I discussed the main challenge of this stage. The limited resolution of MRI results in voxels that contain both capillary and non-capillary tissue. Hence, to estimate how contrast leaks between the types of tissue inside each voxel, we enlist the help of more math. Mathematical models allow the calculation of leakage-rates between the tissue types within a voxel, by making certain assumptions regarding contrast kinetics. As reviewed in the introduction chapter, there are four widely used pharmacokinetic models that differ in assumptions and time interval of interest (Figure 5). I designed the BBB software to calculate BBB leakage based on two of these pharmacokinetic models: the modified Tofts model, allowing the characterization of fast, para-cellular leakage (0-3minutes post injection),²⁸ and the Veksler model, characterizing slow, trans-cellular leakage (6-20minutes post injection).²⁹ Since my PhD targeted understanding the role of slow/subtle BBB leakage in neuropsychiatric symptoms, my analysis focused on the Veksler approach. The approach identifies voxels that accumulate contrast during the time period when contrast is being washed out of the brain – i.e., the washout phase. The implementation of the approach consists of the following steps:

F) Analyzing each voxel's contrast-concentration-curves.

- Constructing a contrast-concentration-curve for every voxel. At this stage of the analysis, the data is re-arranged. Each voxel is treated as a separate entity, and a curve representing its concentration over time is constructed:



Relevant excerpt from Figure 10

- Calculating the slope of the contrast-concentration-curves for every voxel. The Veksler approach characterizes each curve using linear regression, under the assumption that the changes in contrast 6-20 minutes post injection are slow enough to satisfy the linear equation:

Equation VI:

$$C(t) = A \cdot t + B$$

Equation VI can be easily solved for every time-curve using linear regression, producing the value of the curve's slope A (Figure 10F). The calculated slope represents the rate of contrast change in each voxel.

- Identifying voxels containing only vascular tissue and calculating their average slope. This step relies on the identification of a major drainage vessel in the brain – the superior sagittal sinus. The ~20 voxels comprising the cross-section area of the superior sagittal sinus are identified automatically using a sophisticated, in-house-developed algorithm of iterative morphological operations. The slopes of the identified voxels are averaged, to produce a single value representing the rate of contrast washout from the brain's vasculature – $\text{Rate}_{\text{washout}}$.
- Comparing each voxel's rate of contrast change to the rate of vascular contrast washout. Each voxel's rate of contrast change is normalized to the vascular washout rate, resulting in a unitless value $\text{Rate}_{\text{leakage}}$:

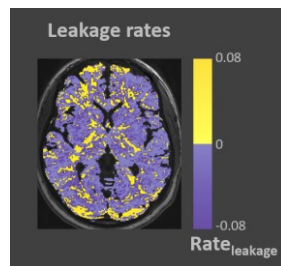
Equation VII:

$$\text{Rate}_{\text{leakage}} = \frac{\text{Rate}_{\text{change}}}{\text{Rate}_{\text{washout}}}$$

$\text{Rate}_{\text{leakage}}$ represents the rate of leakage from each voxel's capillary to its non-capillary tissue.

G) Mapping the leakage rates of the brain.

Once all voxel-specific leakage-rates have been calculated, they can be mapped back to a 3D representation of the brain (a matrix of 189x156x27 voxels). The slices of the 3D leakage-rate map can be viewed, as in the following example of a patient with lupus:

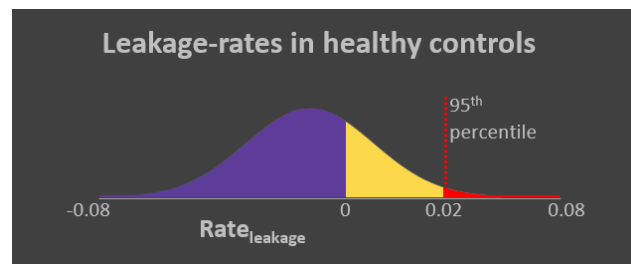


Relevant excerpt from Figure 10

2.2.2.4. Giving leakage-rates diagnostic context

H) Identifying voxels with leakage-rates reflecting BBB dysfunction.

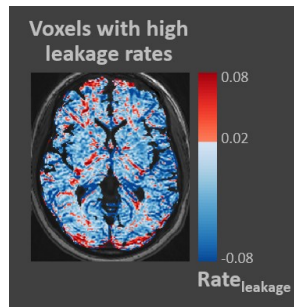
The leakage-rates in a given subject span between -0.08 and 0.08. To understand which values reflect 'abnormal' leakage, we studied the distribution of values in a population of 50 healthy controls.³⁰ The 95th percentile of the distribution was identified as $\text{Rate}_{\text{leakage}}=0.02$, and defined as the threshold separating 'normal' and 'abnormal' leakage-rates:



Relevant excerpt from Figure 10

Application of this threshold to patient data results in leakage maps in which shades of red denote suprathreshold voxels ($\text{Rate}_{\text{leakage}} \geq 0.02$) and shades of blue represent subthreshold voxels (Figure

10H). The extent of overall BBB pathology in a patient can then be represented as the percent of ‘red’ voxels.



Relevant excerpt from Figure 10

I. Identifying brain regions with high percentage of abnormal BBB leakage.

The 3-dimensional map identifying voxels with ‘abnormally’ high BBB leakage rates (Figure 10H) is next segmented into 126 regions of anatomical/functional significance using the [MNI brain atlas](#) (Figure 10I). The BBB software categorizes all ~800,000 voxels of a patient’s brain into 126 regions, and tallies the voxels with abnormal BBB leakage in each region. The total of such voxels in a region is divided by the region’s size (number of all voxels comprising the region). This calculation characterizes each region with a single value – percent of region with abnormal BBB leakage. Next, the software compares the patient’s region-specific values to those of controls. Regions with values two standard deviation higher than the control group are considered to have extensive BBB leakage (Figure 10I):



Relevant excerpt from Figure 10

2.2.3. Studying clinical manifestations of BBB dysfunction

The developed BBB software provides a novel way of looking inside the brain and understanding brain pathology. It exposes subtle BBB leakage in otherwise healthy-looking brains, lacking any apparent lesions or structural abnormalities. This software allowed us to be the first to explore the link between subtle BBB leakage and neuropsychiatric symptomatology.

To begin to understand the answer to this question, we studied two disorders – each characterized by the fact that some patients develop far worse neurological outcomes than others. We, therefore, sought to understand whether BBB pathology could help explain the difference in symptom severity among patients with similar diagnoses. Specifically, we studied:

- patients with bipolar disorder – a condition with high prevalence of treatment-resistance³¹ (morbidity that does not respond to mood-stabilizing medication).
- patients with lupus – a disease in which ~40% of patients experience cognitive impairment throughout their illness.³²

Both patient groups were scanned with the described MR protocol at the Biomedical Translational Imaging Centre (BIOTIC, QEII Hospital, Halifax, Nova Scotia) in a collaboration with Dr. Chris Bowen and Dr. Steven Beyea.

2.2.3.1. BBB leakage and psychiatric symptoms in patients with bipolar disorder

2.2.3.1.1. Participants

A total of 36 patients with bipolar disorder types I or II were consecutively recruited in collaboration with Dr. Cynthia Calkin, the head of the Mood and Metabolism Program at the Queen Elizabeth II Health Sciences Center, Halifax, Nova Scotia (Bipolar Registry and TRIO-BD study). Diagnoses were based on the DSM-5 criteria and required a consensus of at least 3 psychiatrists.³³

Exclusion criteria included:

- 1) Diabetes

- 2) Pregnancy
- 3) Age under 18 years old
- 4) Contra-indication to MRI or gadolinium (e.g., estimated glomerular filtration rate [eGFR] < 60)
- 5) Lack of full capacity to consent.

The study was approved by the Nova Scotia Health Authority (NSHA) Research Ethics Board, and participants provided written informed consent.

2.2.3.1.2. Psychiatric Assessment

Mood symptom and progression of bipolar illness were assessed using:

- 1) The Montgomery-Åsberg Depression Rating Scale (MADRS).³⁴
- 2) The Hamilton Anxiety (HAM-A) scale.³⁵
- 3) The global assessment of functioning scale (GAF), reflecting illness effects on social, occupational, and psychological functioning).³⁶
- 4) The affective morbidity index (AMI), reflecting severity and length of manic/depressive episodes.³⁷

2.2.3.2. BBB leakage and cognitive symptoms in patients with lupus Participants

2.2.3.2.1. Participants

A total of 65 patients with Systemic Lupus Erythematosus (SLE) were recruited in collaboration with Dr. John G. Hanly, Division of Rheumatology, Queen Elizabeth II Health Sciences Center, Halifax, Nova Scotia. SLE was diagnosed using the revised American College of Rheumatology criteria.³⁸ Patients were recruited consecutively, without pre-screening for cognitive impairment.

Exclusion criteria included:

- 1) Contra-indication to MRI or gadolinium (e.g., estimated glomerular filtration rate [eGFR]<60).
- 2) Lack of full capacity to consent

The study was approved by the Nova Scotia Health Authority (NSHA) Research Ethics Board, and participants provided written informed consent.

2.2.3.2.2. Cognitive Assessment

Cognitive performance was assessed in five cognitive domains:

- 1) Information processing speed was tested using the Symbol Digit Modalities Test (SDMT), measuring an individual's ability to pair numbers with geometric figures – based on a given example.³⁹
- 2) Executive abilities were examined using the Fixed Design Fluency test, assessing an individual's ability to generate different designs/drawings, based on specific instructions/guidelines (e.g. draw maximal number of unique designs using only 4 straight lines).⁴⁰
- 3) Attention span was assessed using a paradigm of the California Verbal Learning Test (CVLT-II), counting the number of words recalled correctly after a single presentation of a word-list (trial 1).⁴¹
- 4) New learning was assessed using a paradigm of the CVLT-II, counting the total of words recalled over five presentations of the same word-list (trials 1-5).⁴¹
- 5) Delayed spontaneous recall was assessed a paradigm of the CVLT-II, counting the number of words recalled spontaneously after a 20-minute delay.⁴¹

2.2.3.3. Acquiring a reference for normal BBB function

The two groups of patients allowed us to examine the link between BBB pathology and symptom severity. The accumulation-rates of the two groups were analyzed in the context of the 50 healthy controls scanned in Israel,³⁰ as detailed in the pipe-line section above (and Figure 10H). To provide an additional reference for normal BBB function, we recruited a group of subjects without neuropsychiatric symptoms from Nova Scotia (also through the Queen Elizabeth II Health Sciences Center). Control volunteers were recruited consecutively, and underwent MR imaging and BBB assessment. A group of 14 control subjects was recruited as part of the bipolar study, and was matched for sex, age, and metabolic status to the bipolar cohort. Nine subjects from this group also fulfilled the criteria to serve as controls for the SLE study (and were matched in sex and age to the SLE cohort).

Controls – exclusion criteria for the bipolar study:

- 1) Neuropsychiatric history (mood or cognitive symptoms)
- 2) Diabetes
- 3) Pregnancy
- 4) Contra-indication to MRI or gadolinium (e.g., estimated glomerular filtration rate [eGFR] < 60)

5) Lack of full capacity to consent

Controls – additional exclusion criteria for the SLE study:

6) SLE

7) Insulin resistance

3) Age under 35 or over 70 years old

2.2.3.4. Statistical analysis

To investigate the link between BBB leakage and patient symptomatology, we employed a data-driven approach. The BBB of each participant was mapped, and the extent of BBB pathology was calculated as the percent of brain voxels with BBB leakage (percent of red voxels in figure 10H). Hence, the brain of each participant was represented by a single parameter of BBB leakage. The difference in this parameter between patients and controls was assessed using the Wilcoxon rank sum test. Next, I performed an outlier analysis to identify patients with unusually high parameter values (i.e., percent of brain volume with BBB leakage). The outlier analysis was performed using the Median Absolute Deviation (MAD) approach, as it is considered more robust than traditional thresholding using standard deviations around the mean.⁴² The MAD threshold was calculated as:

Equation VIII:

$$\text{Threshold} = \text{Median}(X) + 2 \cdot \text{Median}(|X - \text{Median}(X)|)$$

Based on:

- The vector representing parameter values of all subjects — X
- The median of all subjects — $\text{Median}(X)$
- The vector representing the absolute difference between each subject and the group median — $(|X - \text{Median}(X)|)$

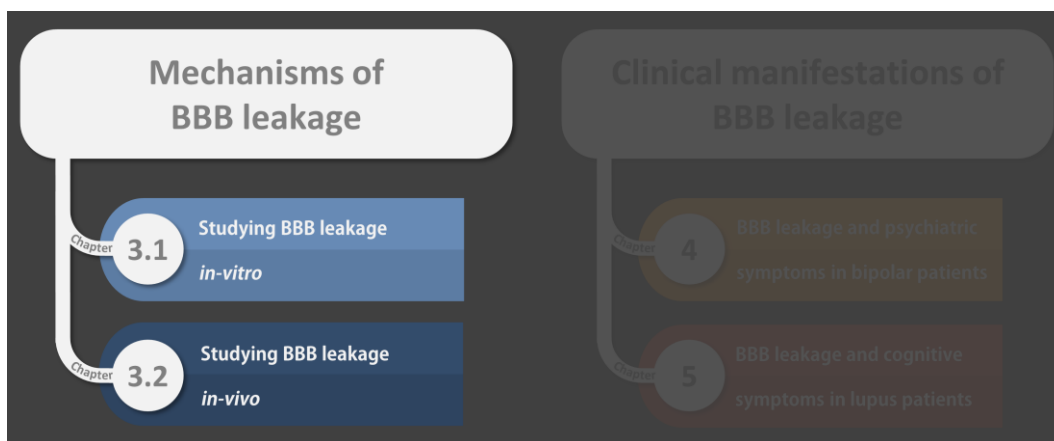
The outlier analysis divided the patients of each study into two groups: patients with ‘normal BBB leakage’ and patients with ‘extensive BBB leakage’. This data-driven division allowed us to explore group differences in symptoms. Symptoms that were represented by continuous scores/values were

compared using the Wilcoxon rank sum test, and symptoms of categorical nature were compared using the Chi-square test. The false discovery rate method was used to correct for multiple comparisons, and 0.05 was set as the level of significance. Multivariate analysis was used for the identification of potential confounds. All statistical analyses were performed in MATLAB_2018a.

Chapter 3 – Mechanisms of BBB dysfunction

Chapter Overview

This is the first of the three results chapters of this thesis, corresponding to the three manuscripts published during my PhD. The current chapter addresses the first goal of my research: understanding mechanisms that enhance BBB leakage and the processes that mediate subsequent neuronal dysfunction.



This research focused on examining the effects of neuronal activity during seizures on pericytes and their ability to regulate neuronal oxygen supply (neurovascular coupling). In this study I collaborated with Dr. Ofer Prager – an expert in cortical imaging of live animals, and Dr. Richard Kovács – who specializes in slice culture models of microvasculature. Together we established novel models of transient seizures in-vivo and in-vitro, allowing us to explore both arteriolar and capillary changes in BBB integrity and neurovascular coupling.

The experiments conducted in this study tested the following hypotheses:

- I. Neuronal activity during seizures results in impaired neurovascular coupling.
- II. Impaired neurovascular coupling results in hypoxia and ischemic tissue damage.
- III. Neuronal activity during seizures results in pericyte injury.
- IV. Pericyte injury mediates BBB leakage.

V. Pericyte injury mediates impaired neurovascular coupling.

Hypotheses I and II were tested both *in vitro* and *in vivo*, providing a characterization of neurovascular coupling and tissue oxygenation in organotypic capillaries and in cortical arterioles supplied by cerebral circulation, respectively. Hypotheses III-V were tested *in-vitro*, by characterizing cellular alterations at the capillary level.

Our findings confirmed the validity of the first hypothesis, showing that neuronal activity during seizures, indeed, leads to reduced vascular responsiveness to neuronal activity. However, our results did not show that this impairment in neurovascular coupling is associated with tissue hypoxia, as oxygen levels in the tissue remained well above hypoxic levels throughout both *in-vitro* and *in-vivo* experiments (potentially due to innate oversupply of oxygen to neuronal tissue known as the ‘oxygen paradox of neurovascular coupling’, as will be further discussed in the discussion chapter).

Remarkably, our findings did support hypotheses III-V, as neuronal seizure-activity was found to induce pericyte injury (via breakdown of pericytic mitochondria) and rigor, followed by impaired neurovascular coupling and BBB leakage. We, hence, argue that pericytes are likely mediators of neurovascular un-coupling and BBB leakage. While neurovascular un-coupling did not induce hypoxia in acute settings, the potential role of long-lasting coupling-impairment in dysfunction/damage of neuronal networks warrants further examination.

Manuscript title:

Seizure-induced microvascular injury is associated with impaired neurovascular coupling and blood–brain barrier dysfunction

Epilepsia, 2019

Authors:

Prager O*, [Kamintsky L](#)* (*equal first co-authorship), Hasam-Henderson LA, Schoknecht K, Wuntke V, Papageorgiou I, Swolinsky J, Muoio V, Bar-Klein G, Vazana U, Heinemann U, Friedman A, Kovács R.

Abstract

Objective: Blood–brain barrier (BBB) impairment, redistribution of pericytes, and disturbances in cerebral blood flow may contribute to the increased seizure propensity and neurological comorbidities associated with epilepsy. However, despite the growing evidence of postictal disturbances in microcirculation, it is not known how recurrent seizures influence pericytic membrane currents and subsequent vasodilation.

Methods: Here, we investigated successive changes in capillary neurovascular coupling and BBB integrity during recurrent seizures induced by 4-aminopyridine or low-Mg²⁺ conditions. To avoid the influence of arteriolar dilation and cerebral blood flow changes on the capillary response, we measured seizure-associated pericytic membrane currents, capillary motility, and permeability changes in a brain slice preparation. Arteriolar responses to 4-aminopyridine–induced seizures were further studied in anesthetized Sprague Dawley rats by using electrocorticography and tissue oxygen recordings simultaneously with intravital imaging of arteriolar diameter, BBB permeability, and cellular damage.

Results: Within the preserved vascular network in hippocampal slice cultures, pericytes regulated capillary diameter in response to vasoactive agents and neuronal activity. Seizures induced distinct patterns of membrane currents that contributed to the regulation of pericytic length. During the course of recurrent seizures, individual vasodilation responses eroded, and BBB permeability increased, despite unaltered neurometabolic coupling. Reduced vascular responsiveness was associated with mitochondrial depolarization in pericytes. Subsequent capillary constriction preceded BBB opening, suggesting that pericyte injury mediates the breach in capillary integrity. In vivo findings were consistent with slice experiments, showing seizure-related neurovascular

decoupling and BBB dysfunction in small cortical arterioles, accompanied by perivascular cellular injury despite normoxic conditions.

Significance: Our study presents a direct observation of gradually developing neurovascular decoupling during recurrent seizures and suggests pericytic injury as an inducer of vascular dysfunction in epilepsy.

3.1. Introduction

Brain disorders such as depression, anxiety, and dementia are eight times more common in epilepsy patients than in the general population.¹ With growing evidence of microvascular dysfunction in epileptic tissue, the role of blood–brain barrier (BBB) injury in seizure disorders is gaining particular interest.^{2–4} BBB dysfunction and subsequent infiltration of serum albumin into the brain were shown to initiate epileptogenic alterations such as astrocytic transformation, neuroinflammation, excitatory synaptogenesis, and pathological plasticity.^{5,6} As prolonged BBB opening is associated with delayed structural and functional disturbances of neuronal networks,⁷ it is tempting to speculate that BBB injury in the epileptic brain contributes to epilepsy comorbidities. However, the mechanisms underlying seizure-related BBB dysfunction remain poorly understood. Among the components of the BBB neurovascular unit, pericytes may be of particular relevance, as they play a crucial role in BBB integrity⁸ and contribute to microcirculatory dysfunction.^{9–11} Moreover, pericytes were shown to redistribute following kainic acid–induced status epilepticus as well as in chronic epileptic tissue.^{12–14}

Despite some debate regarding the exact nomenclature of contractile cells along the microvascular axis,^{15–17} morphologically defined pericytes (spindle-shaped cells engulfing microvessels measuring 4–10 μm in diameter) were shown to regulate local blood supply in response to neuronal metabolic demands, a phenomenon termed neurovascular coupling (NVC).

Deficiencies in NVC were previously reported in neurological disorders associated with BBB injury, including Alzheimer's disease,¹⁸ stroke,⁹ and subarachnoid hemorrhage.¹⁹ Seizures were reported to compromise stimulus-induced vascular reactivity,^{20,21} and tissue oxygenation around the epileptic focus²² and in deep cortical layers.²³ Moreover, several studies implicate post-seizure hypoxia and vasoconstriction in seizure-related memory and behavioral deficits^{24,25} and point to pericyte-like mural cells as the mediators of capillary constriction.²⁶ This is in line with a recent study showing a correlation between mural cell remodeling, vascular pathology, and seizure severity by monitoring pericytic coverage in vivo over the course of several days after status epilepticus.²⁷ Together, these studies highlight the importance of an in-depth understanding of the development of metabolic and NVC abnormalities associated with recurrent seizures.

To allow a detailed investigation of capillary responses and BBB function in a controlled microenvironment, we established a slice culture model of organotypic microvasculature that allows the recording of seizure-associated membrane currents in pericytes along with the measurement of vasomotility, BBB permeability, and mitochondrial respiration.²⁸ We present the first characterization of distinct pericytic current patterns associated with seizure-induced vasomotility and demonstrate successively developing dysfunction of pericytes. We further show in vitro at the capillary level and in vivo at the arteriolar level that recurrent seizures trigger enhanced microvascular permeability and a gradual loss of NVC.

3.2. Materials and methods

All experimental procedures were approved by the animal ethics committee of the respective universities, and the experiments were performed in adherence to the Care and Use of Mammals in Neuroscience and Behavioral Research (National Research Council, 2010) and the ARRIVE guidelines.

3.2.1. In vitro experiments

Slice cultures were prepared and maintained as described earlier.²⁸ Wistar rats and heterozygous transgenic mice expressing green fluorescent protein (GFP) at the platelet-derived growth factor receptor β (PDGFR β) promoter²⁹ were sacrificed at postnatal day 6-8 or 2-3, respectively. Entorhinal cortex-hippocampus slices (400 μ m) were maintained under interface conditions (medium containing 50% minimal essential medium, 25% Hank balanced salt solution, 25% horse serum, pH 7.4; all from Gibco).

Immunofluorescent reconstruction of the vascular unit was obtained with a Nikon (Tokyo, Japan) A1r multiphoton microscope (AMBIO Imaging Core Facility, Charité– Medical University Berlin) by using antibodies for laminin (Thermo Scientific), neuronal/glial antigen 2 proteoglycan (NG2), or PDGFR β (Santa Cruz Biotechnology).

Electrophysiological recordings were performed in area CA3 of the slice cultures in artificial cerebrospinal fluid (aCSF) containing (in mmol/L) 129 NaCl, 26 NaHCO₃, 10 glucose, 3 KCl, 1.25 NaH₂PO₄, 1.6 CaCl₂, and 1.8 MgCl₂ (perfusion = 5 mL/min, 32°C, pH = 7.4). Epileptiform activity was induced via perfusion with a zero magnesium (Mg²⁺)-containing aCSF or by the voltage-gated potassium channel inhibitor 4-aminopyridine (4AP; 100 μ mol/L). Both methods induce stereotypic ictal discharges resembling seizure activity.^{30,31} Local field potential (LFP) recordings of seizure-like events are referred to as “seizures” throughout the text. LFP and whole cell patch clamp recordings on visually identified pericytes were obtained by using a MultiClamp 700B amplifier and pClamp10 software (Axon CNS; Molecular Devices). Recording electrodes were filled with aCSF (for LFP) or with a solution containing (in mmol/L) KCH₃SO₄ 130, KCl 20, HEPES 10, MgCl₂ 2, EGTA 0.2, Na₂ATP 2, Na₂GTP 0.5, Na₂Phosphocreatine 5, and in some cases Alexa Fluor 488 0.1. Changes in

tissue partial oxygen pressure (pO_2) were recorded by using Clark-style oxygen microelectrodes (Unisense) polarized and calibrated as described previously.³²

Fluorescent monitoring of vascular responsiveness was performed in slice cultures stained with the mitochondrially targeted ethidium derivative MitoSox and calcein-AM (5 and 4 $\mu\text{mol/L}$, respectively).²⁸ Labeling of astrocytic endfeet by calcein-AM allowed for reconstruction of the vessels, whereas pericytes were visualized by the accumulation of MitoSox or by GFP fluorescence in slice cultures obtained from PDGFR β -bac-GFP mice (Figures 11DE and 12BD). Changes in the permeability of the BBB were measured in slice cultures preincubated with 2',7'-dichlorohydrofluorescein diacetate (20 $\mu\text{mol/L}$, 30 minutes), resulting in accumulation of the oxidation end-product dichlorofluorescein (DCF) in the vascular lumen.

A spinning-disk confocal microscope system (Andor iXon EM+, Andor Revolution; Acal BFi) was used for imaging in parallel with the LFP recordings. Z scans containing the entire vessel were obtained at each time point, and changes in MitoSox/DCF fluorescence, pericyte length, and capillary diameter were evaluated offline and presented here as percentage of pre-treatment values in response to sequential seizures.

3.2.2. In vivo experiments

Animal preparations were performed as previously described.^{33,34} A craniotomy window was drilled over the motor-somatosensory cortex of deeply anesthetized (ketamine/xylazine) male rats, and the dura was carefully removed. The exposed cortex was continuously perfused with aCSF containing (in mmol/L) 129 NaCl, 21 NaHCO₃, 1.25 NaH₂PO₄, 1.8 MgSO₄, 1.6 CaCl₂, 3 KCl, and 10 glucose, with or without 4AP (500 $\mu\text{mol/L}$).

To study NVC, we applied simultaneous recording of electrocorticographic (ECoG) activity and imaging of anatomically defined arterioles and venules (DL-658 M-TIL; Andor Technology).^{33,34} A subdural ECoG electrode was located within the imaging area next to the selected arteriole, and a reference epidural electrode was placed posterior to the window. ECoG signals were recorded at 200 Hz (DSI) and band-pass filtered at 1-45 Hz.³⁵ Changes in arteriolar diameter relative to pre-4AP values were measured as previously described.³⁶ To assess the neuronal activity, we calculated the normalized power of the ECoG signal for each seizure. Arteriolar responses were calculated as the

averaged diameter during each seizure, divided by the average pre-seizure diameter. For continuous monitoring of pO₂, a miniaturized Clark-type electrode was positioned near an arteriole of interest, and the duration and magnitude of the seizure-associated initial dip, the peak magnitude, and the duration of dip-to-peak recovery were quantified.

Fluorescent imaging of BBB permeability was obtained by using the BBB-impermeable dye sodium fluorescein (NaFlu molecular weight = 376 Da, 1 mg/mL in saline; Novartis). To further confirm changes in BBB permeability, in a subset of experiments the fluorescent dye Evans blue albumin complex (molecular weight = 66 kDa) was injected intravenously. Assessment of cellular damage was performed through intravenous injection of propidium iodide (0.5 mg/kg body weight, 0.5 mg/mL in saline³³).

3.2.3. Statistical reporting

All results are presented as mean \pm SEM. Statistics were performed using the SPSS 24 software packet (IBM). $P < 0.05$ was considered significant.

3.2.3.1. NVC evaluation

Paired Wilcoxon analysis was used to compare parameters (vasodilation, seizure power, seizure duration, vasodilation/ power, $n = 9$, $P = 0.05, 0.02, 0.11, 0.04$, respectively) of early versus late seizures.

3.2.3.2. Cell damage, BBB permeability, oxygen measurements

Paired Wilcoxon analysis was used to compare perivascular cell damage, microvascular permeability, and pO₂ before and following seizures ($n = 7, 10, 4$, $P = 0.043, 0.0049, 0.273$, respectively).

3.2.3.3. Characterization of the vasodilatory response upon seizure activity

Correlation between pericytic length and vascular diameter was described by Pearson coefficient ($n = 20$, 0.711 , $P = 0.005$). Mann-Whitney test was used to compare the first seizure-induced changes in pericytic length/vascular diameter between low-Mg²⁺ and 4AP ($n = 20$ vs 10 , $P = 0.042, 0.055$, for length and diameter, respectively). Paired Wilcoxon analysis was used to compare vasodilation or the pO₂ changes associated with first versus fourth seizure ($n = 9$ and 10 cultures presenting with at least four seizures, $P = 0.028, 0.05$ for low-Mg²⁺ and 4AP, respectively and $n = 6$ $P = 0.833$ for pO₂ changes under low-Mg²⁺ conditions).

3.3. Results

3.3.1. Pericytes retain contractility in slice cultures

Immunofluorescent laminin labeling revealed an extensive network of vessels and organotypic arborization throughout the slices, with the exception of an atypical dense meshwork of vessels at the bottom of the culture (Figure 11A). Notably, whereas the slicing procedure did result in the collapse of large arterioles and venules (diameters $> 20 \mu\text{m}$), microvessels (4-10 μm in diameter, from here on referred to as “capillaries”) retained their lumen and became sealed at the cut surface.

Putative pericapillary pericytes in slice cultures were visualized using NG2 or PDGFR β labeling, and were found at the abluminal side of the vascular wall, surrounded by small pockets of laminin (Figure 11B). However, NG2 labeling was also observed in the parenchyma, likely representing oligodendrocyte precursor cells. To achieve long-term visualization of capillaries and pericytes in the living slice culture, we used a combination of calcein-AM and the mitochondrial superoxide indicator MitoSox.²⁸ In addition to parenchymal/neuronal staining, bulk application of MitoSox also penetrated capillaries and underwent oxidation in the mitochondria of pericytes but not in endothelial cells. The accumulation of the oxidized dye within mitochondria (and to a lesser extent in the nucleus) revealed the typical “bump on a log” structure of pericytes, with lengthy arms extending to a distance of up to $\sim 50 \mu\text{m}$, often embracing a blood vessel (Figures 11C and 12A). Upon release of oxidized mitochondrial MitoSox into the cytosol (see below), the entire structure of individual pericytes became visible (Figure 11DE), allowing reconstruction of the morphology and clear distinction of these cells from endothelial cells or perivascular glia. Simultaneous calcein-AM application labeled glial cells without crossing vascular walls, indicating the presence of a diffusion barrier.²⁸ The outer vascular diameter was delineated as the distance between astrocytic endfeet (Figures 11C and 12A).

The observed accumulation of MitoSox in pericytes (yet not endothelial cells) was confirmed in a transgenic mouse expressing GFP on the PDGFR β promoter that allows pericytic visualization.²⁹ Although the size of the pericytes was slightly smaller compared to slice cultures from rats, MitoSox labeling in the transgenic model was colocalized with GFP in cells of the typical “bump on a log” morphology (Figure 11F and 11G). While some GFP fluorescence was also observed in non-mural

cells throughout the parenchyma, both MitoSox accumulation and GFP expression were significantly lower in such cells compared to pericytes (normalized MitoSox 3.9 ± 0.3 vs 2.0 ± 0.2 and GFP fluorescence 16.7 ± 1.4 vs 8.9 ± 0.8 in pericytes and non-mural cells, respectively; $n = 26$). We thus conclude that pericytic accumulation of oxidized MitoSox is not exclusive to rats, and may be a general property of pericytes across different species.

Figure 11 – Microvasculature and pericytes in slice culture

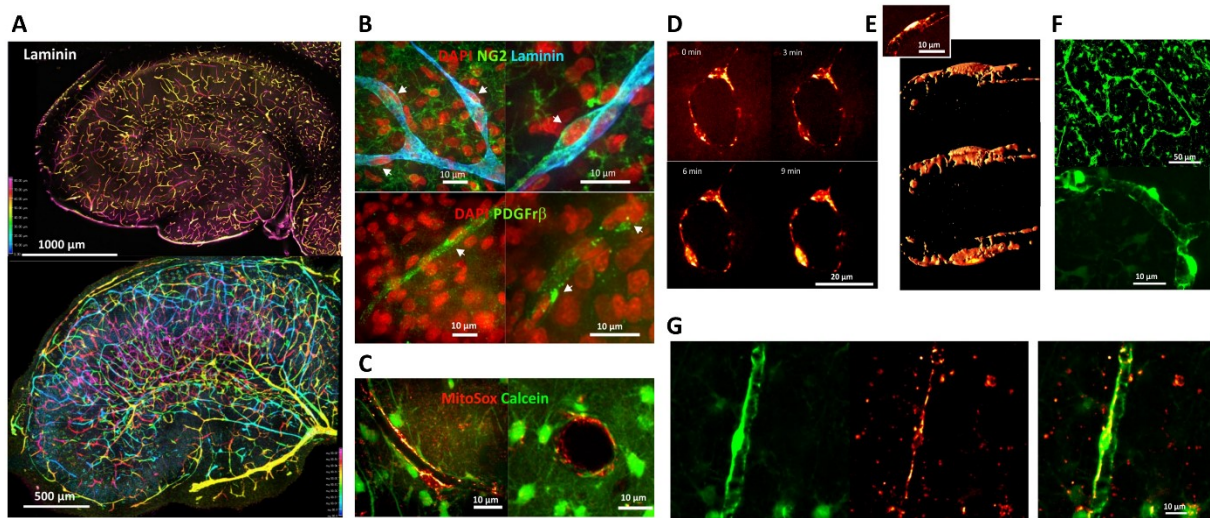


Figure 11 – Microvasculature and pericytes in slice culture. A, Immunofluorescent laminin labeling revealed the organotypic arborization of the vascular network of the hippocampal slice (depth-coded colors) as compared to the arborization pattern of an acute slice of the same thickness. B, Top: Neuronal/glial antigen 2 proteoglycan (NG2)-positive pericytes (marked with arrowheads) were evident within laminin pockets, and were frequently located at the branching points of capillaries (false colors; blue = laminin, green = NG2, red = 4,6-diamidino-2-phenylindole [DAPI]). Bottom: Immunofluorescent platelet-derived growth factor receptor β (PDGFR β) labeling marked pericytes as areas of dense dye concentration along the wall of vessels (arrowheads; green = PDGFR β , red = DAPI). C, Calcein-MitoSox co-labeling in situ resulted in the delineation of capillaries by both calcein-filled astrocytic endfeet and MitoSox-positive spindle-shaped pericytes, as seen in both longitudinal (left) and cross-sectional (right) images of vessels. D, Pericytic morphology was confirmed at the end of experiments, using laser-induced (100% intensity continuous illumination) release of MitoSox from the mitochondria into the cytosol. E, Volume rendering of individual pericytes following cytosolic MitoSox accumulation, as depicted from three different angles (the insert shows the maximum intensity projection of the raw confocal images). Note the typical “bump on a log” appearance and the one arm enwrapping the whole vessel. In contrast to endothelial cells, pericytes never covered the entire surface of a vessel. F, Slice cultures from PDGFR β -green fluorescent protein (GFP) transgenic mice showcase capillary networks (top) delineated by spindle-shaped and helical mural cells enwrapping the capillary wall (bottom). G, Colocalization of MitoSox labeling and GFP fluorescence in PDGFR β -positive mural cells. Maximum intensity projection of a capillary segment presents (from the left) GFP, MitoSox fluorescence, and their overlap. Although MitoSox is present throughout the parenchyma, it reaches far greater intensity inside pericytes.

The contractility of pericytes in slice cultures was previously demonstrated in response to direct mechanical stimulation or increasing intraluminal pressure.²⁸ Here we investigated pericytic motility in response to vasoactive substances and seizures (Figure 12A-D). Bath application of the thromboxane analogue U46619 induced dose-dependent pericytic shortening, which was reversible upon washout or by application of the nitrogen monoxide donor S-nitroso- N-acetylpenicillamine (200 $\mu\text{mol/L}$; Figure 12C).

To examine whether vasoconstriction and dilation are associated with specific pericytic membrane currents, we employed whole cell patch clamp recordings in visually identified pericytes ($n = 23$; Figure 12Da and 2Db). In a subset of recordings, Alexa Fluor 488 was included in the pipette solution and the dye-filled cells were transferred to the confocal microscope for subsequent morphological analysis. Patch clamped cells showed the typical “bump on a log” structure, with arms embracing the vessel, resembling the morphology of the PDGFR β -GFP-positive cells. Pericytes had a resting membrane potential of -77.8 ± 1.4 mV (-85.8 ± 1.4 mV following correction for the junction potential), and either high (87.7 ± 12.1 M Ω , $n = 7$) or low (37.8 ± 2.9 M Ω , $n = 16$) input resistance, likely corresponding to individual or GAP junction coupled cells, respectively.³⁷ Interestingly, whereas mechanical stimulation occurring during seal-formation constricted pericytes and capillaries, clamping the cells to a membrane potential with zero net-current reversed this vasoconstriction. U46619 (100 nmol/L) induced a tonic low-amplitude inward current across the pericytic membrane (79 ± 11.8 pA), superimposed with spontaneous epochs of inward currents (81.6 ± 27 pA, lasting a few hundred milliseconds) in nine of 15 pericytes (Figure 12Dc). Whereas the application of the voltage-dependent potassium channel blocker 4AP had no overt effect on membrane currents in cells clamped to -80 mV, subsequent induction of seizures triggered high-amplitude phasic inward currents (up to 1 nA). The amplitude of these phasic inward currents decreased toward the end of seizures, occasionally turning into an outward current that reaches or exceeds the baseline recorded prior to U46619 application (Figure 12Dd). Together, these findings support the notion that the MitoSox-labeled spindle-shaped cells are pericytes that not only retain their motility in culture but also exhibit specific membrane currents in response to neuronal activity.

Figure 12 – Pericytes retain motility and respond to seizures in vitro

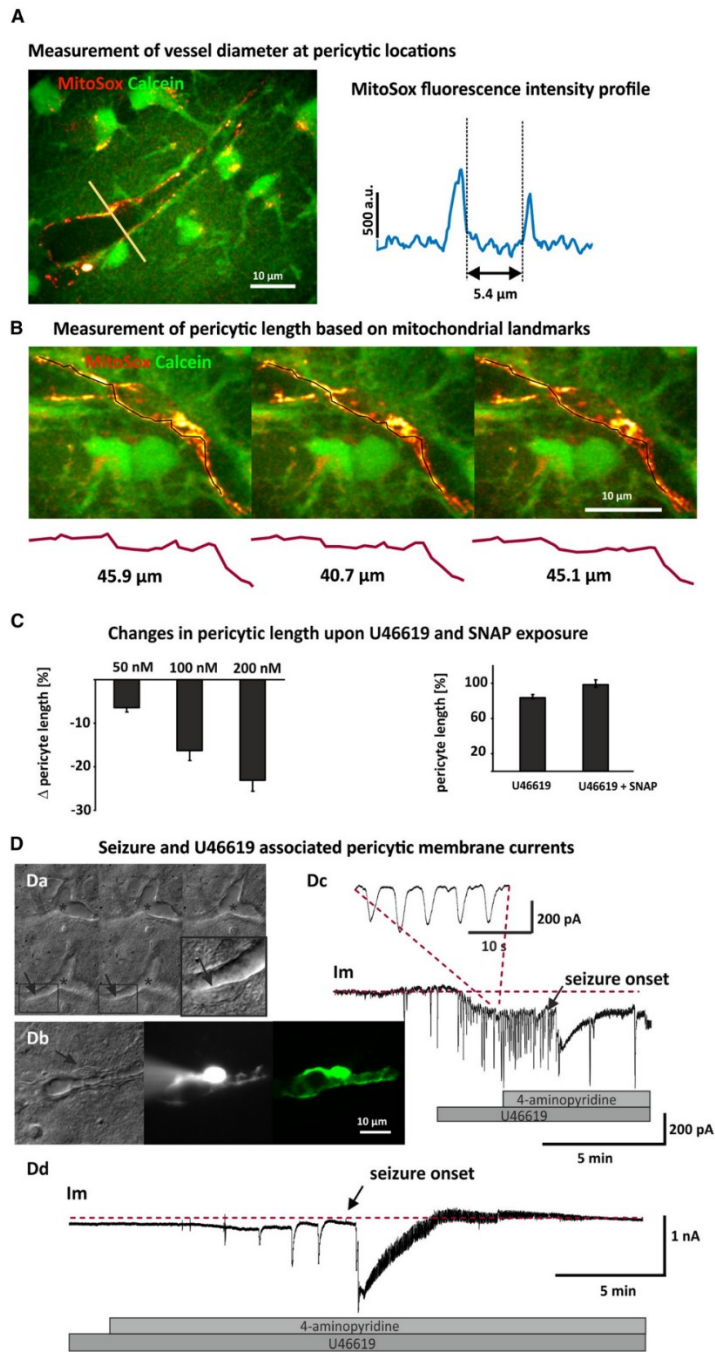


Figure 12 – Pericytes retain motility and respond to seizures in vitro.

Pericytes retain motility and respond to seizures in vitro. A, Co-labeling of the slices with calcein-AM and MitoSox allowed for measurement of vascular diameter. The diameter of the capillary was calculated by positioning a line that crosses both the pericytic body and its processes at the maximal intensity projection of the Z planes containing the vessel. The inflection points in the MitoSox intensity profile along that line correspond to the diameter of the vessel (neglecting the thickness of the endothelial layer). B, Representative image sequence showing pericyte shortening upon treatment with the vasoconstricting U46619 and elongation in response to seizure activity. Pericytic length was measured using distinguishable MitoSox-labeled mitochondria at distal locations (see also Video S2). The mitochondrial landmarks were connected with a freehand-line (at a maximum intensity projection containing the entire pericyte), and the length at maximal constriction/elongation was divided by the initial length of the pericyte to represent percent change. C, Shortening of the pericytes in response to U46619 was found to be dose dependent (right panel) and reversible upon application of the nitric oxide donor S-nitroso-N-acetylpenicillamine (SNAP; left panel, at 100 nmol/L U46619). D, Whole cell patch clamp recordings on visually identified pericytes. Da, Sequence of differential interference contrast (DIC) images focusing through a vessel. Asterisks mark the vessel lumen. A spindle-shaped pericyte (arrows) was adjacent to the bifurcation of the vessel. The black frames mark the position of the pericyte, which is shown magnified in the last frame. Db, Image sequence from a pericyte filled with Alexa Fluor 488 via the patch pipette. From the left: DIC image, epifluorescent image during the whole cell recording, and maximum intensity projection of a Z stack obtained in the confocal microscope. Dc, Application of the vasoconstricting U46619 induces tonic and

phasic inward currents across the pericytic membrane (traces on the right and excerpt show the phasic inward currents on [excerpt with a shorter time scale]). In contrast, the onset of 4-aminopyridine-induced seizures was accompanied by large inward currents (arrow). Dd, The large inward current persisted throughout seizure duration, occasionally reversing polarity and turning into an outward current prior to seizure cessation (lower trace; red dotted line represents the zero current level before application of U46619). Im, membrane current.

3.3.2. Seizures are associated with loss of NVC

To investigate whether seizure-associated pericytic membrane currents result in an adequate vascular response, we next measured changes in pericytic length and capillary diameter in response to seizures as induced by two different proconvulsive treatments: 4AP and low-Mg²⁺. The vascular tone of the cultured capillaries was maintained by U46619 to compensate for the absence of blood flow and adrenergic input.²⁹ The first low-Mg²⁺-induced seizure was characterized by pericytic relaxation ($7.2 \pm 1.1\%$ elongation compared to the length before seizure onset, $n = 20$) and capillary vasodilation ($12.5 \pm 2.1\%$, reaching maximal values at seizure cessation, $n = 20$), followed by constriction to pre-seizure values (Figure 13A). The changes in pericytic length correlated with the changes in capillary diameter (Pearson coefficient = 0.711, $P < 0.005$), highlighting the vasoregulatory role of pericytes in vitro. Importantly, the vasodilatory responses decreased significantly with subsequent seizures (dilating $9.6 \pm 2.2\%$ in response to the first seizures vs $0.4 \pm 2.6\%$ in response to the fourth, $P = 0.028$; Figure 13A). Upon the fourth seizure, changes in diameter were not different from zero ($P = 0.889$, $n = 9$). Notably, despite the reversible nature of U46619-induced vasoconstriction (see above), recurrent seizures resulted in constriction that could not be reversed even upon U46619 washout (capillary diameter decreased to $85 \pm 3.2\%$ of the initial diameter following U46619 application and to $77 \pm 4\%$ after recurrent seizures, $n = 9$). Such irreversible vasoconstriction was previously termed “terminal rigor.”¹¹ Following exposure to 4AP, the first seizure was also associated with pericytic relaxation ($13.3 \pm 2.8\%$) and capillary dilation ($22.7 \pm 7.4\%$), values slightly greater than those measured for the first seizure in the low-Mg²⁺ model ($P = 0.042$ and 0.055 for pericyte length and capillary diameter, respectively; $n = 10$). Similar to the low-Mg²⁺ findings, we observed a decrease in vasodilatory responses (with a $22.7 \pm 7.5\%$ vs $6.4 \pm 7\%$ increase in diameter, associated with the first and the fourth seizure, respectively, $P = 0.05$) and occasionally complete vascular unresponsiveness after ≥ 5 4AP- induced seizures. These results show that neuronal activity in organotypic slice cultures induces capillary dilation, and that these responses diminish over the course of recurrent seizures, irrespective of the type of proconvulsive treatment.

Figure 13 – Seizures impair neurovascular coupling in slice cultures

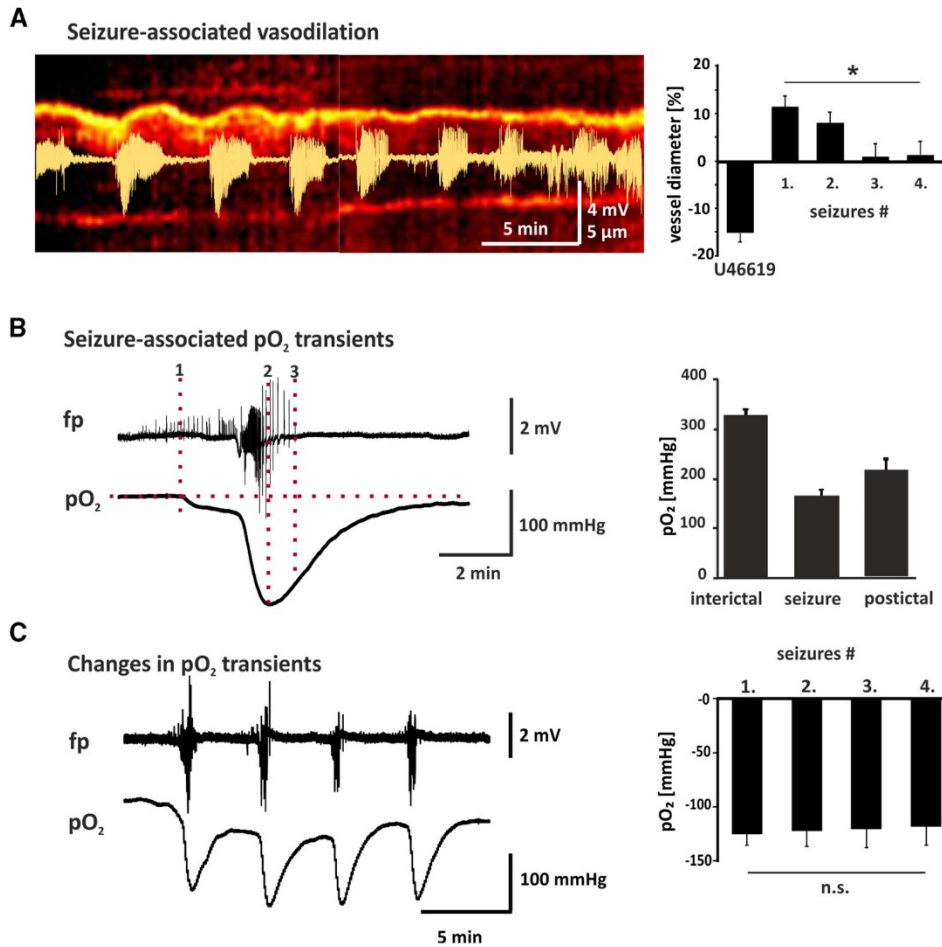


Figure 13 – Seizures impair neurovascular coupling in slice cultures. A, Pericytic processes at both sides of a capillary are represented by the red lines on the kymograph (x-t series), demonstrating the diameter changes associated with the seizures (field potential traces are superimposed on the lumen). Changes in vascular diameter in response to U46619 and the first four seizures are presented as percentage of initial diameter. Whereas early seizures were accompanied by adequate vascular responses, later seizures failed to induce vasodilatation ($9.6 \pm 2.2\%$ in response to the first seizure vs $0.4 \pm 2.6\%$ to the fourth, $*P = 0.028$, Wilcoxon test, $n = 9$ capillaries, right panel). B, Seizures were accompanied by a decrease in tissue pO₂, reaching complete recovery several minutes post-seizure. Notably, seizure-related pO₂ decreases never reached hypoxic levels (188 ± 17 mm Hg, $n = 66$ seizures) starting from a baseline pO₂ of ~ 313 mm Hg. C, Early vs late pO₂ responses to seizures remained unaltered ($P = 0.953$, Wilcoxon test, $n = 6$), pointing to stable oxygen consumption and unaltered neurometabolic coupling. fp, field potential; n.s., not significant.

3.3.3. Seizures do not induce disturbances in neurometabolic coupling

We next set out to explore whether the observed loss of vascular responsiveness could be attributed to a gradually developing disturbance in neurometabolic coupling and consequent failure of energy metabolism, as described for low-Mg²⁺ conditions.³⁰ As slice preparations are continuously perfused with oxygen, decreases in pO₂ represent increased mitochondrial respiration and allow the monitoring of neurometabolic coupling.³² In the submerged slice (at a depth of 80-120 μm from slice surface, 95% O₂, perfusion > 6 mL/min), baseline pO₂ levels were measured at 313.3 ± 13 mm Hg (Figure 13B). Seizures were accompanied by a characteristic pO₂ response, with the initial tonic phase resulting in a decrease of 124 ± 9 mm Hg (reaching minimal values 58 ± 2 seconds after seizure onset, n = 66 seizures in 17 slice cultures). pO₂ levels remained lower throughout the duration of the seizures (188 ± 17 mm Hg), yet completely recovered to baseline values within ~5 minutes of seizure cessation (232.4 ± 10 seconds). Remarkably, even during pO₂ minima, the tissue remained hyperoxic in all cultures. No significant differences in pO₂ responses were found between the first and fourth seizure in a sequence (*P* = 0.833; Figure 13C), pointing to stable oxygen consumption and intact neurometabolic coupling. Together, these findings suggest that neither hypoxia nor disturbances of neuronal energy metabolism are responsible for neurovascular decoupling.

3.3.4. Seizures induce pericytic constriction and mitochondrial depolarization

As seizures are known to enhance oxidative metabolism and superoxide formation,³¹ which may in turn lead to MitoSox oxidation, we next examined whether seizures enhance MitoSox fluorescence in pericytes. These experiments were carried out without pre-constriction of the capillaries, because U46619-induced changes in pericyte length alter mitochondrial distribution and fluorescence intensity irrespective of MitoSox oxidation (with a ~10% increase in fluorescence upon constriction and a ~-5% decrease upon relaxation). In the absence of the vasoconstricting U46619, individual seizures no longer induced vasodilatation or the corresponding length-dependent changes in MitoSox fluorescence, indicating the complete absence of vasotonus in culture. However, periods of >40 minutes of recurrent seizures were associated with a gradual decrease in capillary diameter (-8.1 ± 2.1%) and pericytic length (-8.9 ± 1.7%, n = 22), despite the absence of U46619 (Figure 14B). This constriction was irreversible and persisted even when seizures terminated following

perfusion with normal aCSF. Irreversible constriction was preceded by a slow and cumulative enhancement in fluorescence outside the mitochondria, all throughout the pericytic cytosol ($29.3 \pm 9.0\%$, $n = 22$; Figure 14BC). As mitochondrial retention of MitoSox depends on the presence of a negative mitochondrial membrane potential,³⁸ this cytosolic enhancement is likely to reflect dye leakage from depolarized mitochondria. To examine the potential contribution of superoxide-dependent oxidation of MitoSox to the observed enhancement in cytosolic fluorescence, slices were treated with the free radical scavenger tetramethylpiperidine-N-oxyl (TEMPO; $500 \mu\text{mol/L}$, coapplied with 4AP). Interestingly, despite the general suppression of MitoSox fluorescence, TEMPO did not prevent the translocation of MitoSox into the cytosol ($47.15 \pm 10.7\%$ increase in the cytosol at the end of the recording, compared to the fluorescence following U46619 application, $n = 9$). Together, these results associate vasoconstriction and pericytic rigor with depolarization of pericytic mitochondria, independent of free radical formation.

3.3.5. Seizures induce changes in capillary permeability in vitro

Although slice preparations are generally devoid of a BBB, in slice cultures we observed clear evidence of a diffusion barrier, with calcein failing to penetrate the capillary lumen nor entering pericytes or endothelial cells. Having also found that DCF (a substrate of the multidrug resistance-associated protein 2) does accumulate in the lumen, we were granted a unique opportunity to explore seizure-induced changes in BBB permeability in vitro (Figure 14D). In normal aCSF, DCF fluorescence increased continuously within the lumen, reaching $203 \pm 43.5\%$ of the initial value during the first 10-minute recording period and a further $139 \pm 30.7\%$ between 10 and 20 minutes ($n = 11$ slice cultures). While the largest increase in fluorescence ($9.91 \pm 1.01\%$) was observed between the first and second scans and likely reflects laser-induced auto-oxidation of the reduced dye (H2DCF) in the lumen, the gradual and continuous increase throughout the rest of the recording (by about 4%) most likely represents ongoing DCF uptake. Upon seizure induction, DCF fluorescence within individual microvessels underwent a biphasic change; the continuous slow increase was followed by a rapid fluorescence decrease within the lumen in six of 14 cultures (Figure 14E and 14F). Remarkably, this rapid decrease coincided with terminal constriction and continuous fluorescence enhancement in the surrounding neuropil, indicating cross-BBB leakage and not photobleaching. Occasionally, dye extravasation appeared as small protrusions at capillary borders, further indicative of increased permeability (Figure 14F, arrowhead).

Figure 14 – Recurrent seizures induce pericyte constriction, mitochondrial depolarization, and BBB leakage

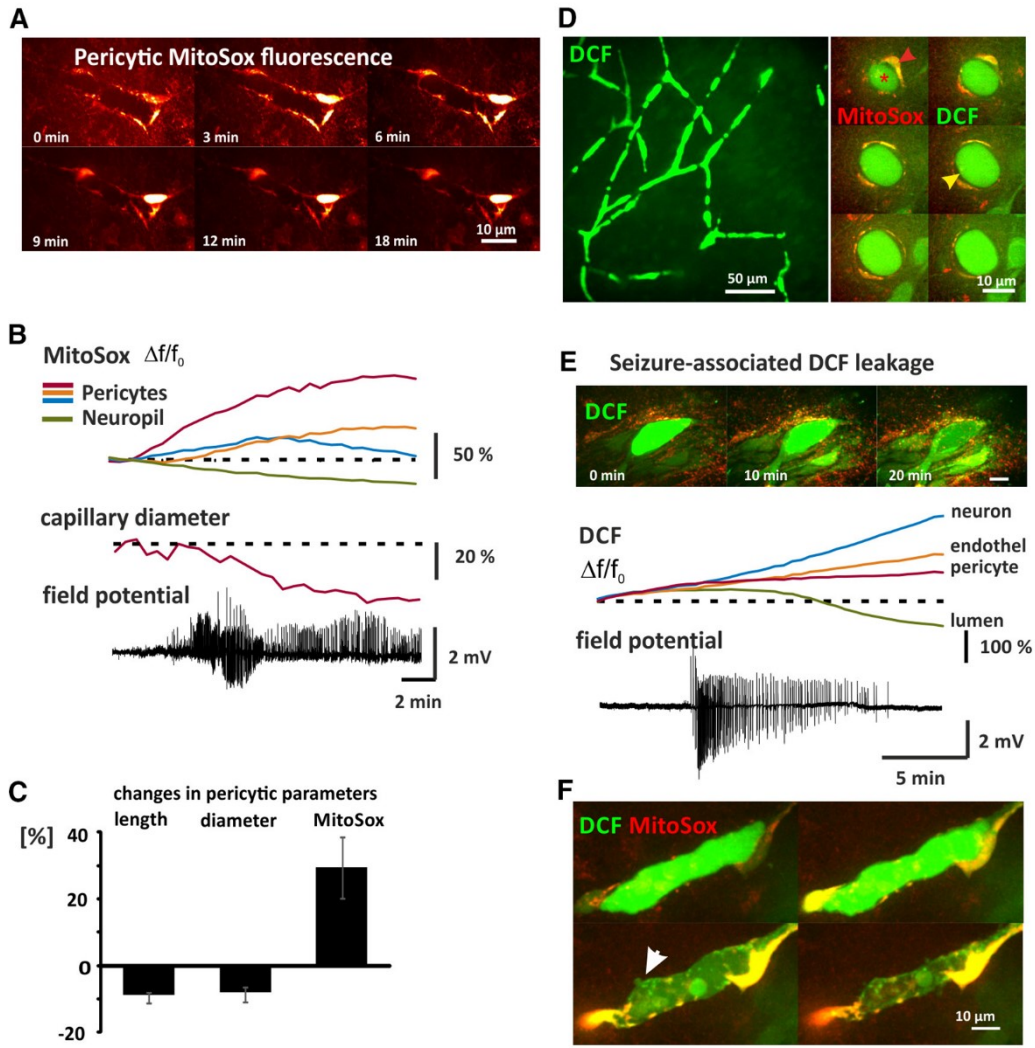


Figure 14. Recurrent seizures induce pericyte constriction, mitochondrial depolarization, and blood–brain barrier leakage. A, Prolonged seizure activity led to increased cytosolic MitoSox fluorescence in the pericytes ($29.3 \pm 9\%$, $n = 22$), indicative of mitochondrial leakage of MitoSox. B, These changes were concomitant with pericytic shortening ($-8.9 \pm 1.7\%$, $n = 22$) and a decrease in capillary diameter ($-8.1 \pm 2.1\%$, $n = 22$), as summarized in C. D, Superficial capillaries in the area CA3 (left) visualized by the dichlorofluorescein (DCF) accumulation in the capillary lumen. Double labeling with DCF and MitoSox clearly shows pericytes engulfing the capillary (capillary cross sections at different Z planes, right). The narrow dark gaps between the lumen and the pericytes represents the unlabeled endothelial cells. E, Neurovascular decoupling and terminal vasoconstriction were accompanied by a sudden release of DCF from the lumen, indicative of increased permeability of the BBB (upper panel). Maximum intensity projection of a DCF-filled vessel (lower panels) shows pericytic, endothelial (endothel), and neuronal DCF fluorescence increase (as expected for ongoing H2DCF oxidation), yet decreasing intraluminal fluorescence following the seizure (scale bar = 10 μm). F, Representative DCF leakage from a vessel during 20 minutes of recurrent seizure activity. Arrowhead marks an individual site of DCF release.

3.3.6. Seizures induce NVC alterations in vivo

The resolution of the slice culture model allowed us to characterize the functionality of microcirculation and individual pericytes; we next sought to validate the presence of a neurovascular decoupling of larger vessels in vivo. Using intravital microscopy and the open-window technique, we imaged pial arterioles (defined here as vessels measuring 30-60 μm in diameter) while monitoring ECoG activity during 4AP- induced seizures ($n = 9$; Figure 15). Local perfusion of the exposed neocortex with 4AP induced recurrent seizures with an onset latency of 24.43 ± 5.14 minutes.

Figure 15 – Seizures impair neurovascular coupling in vivo

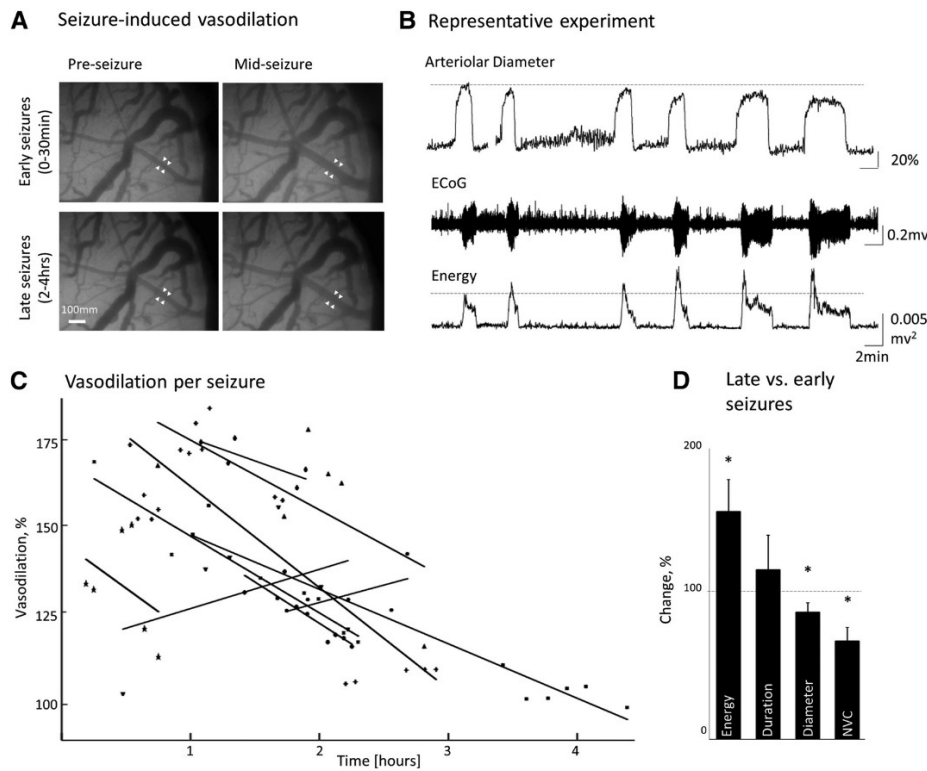


Figure 15. Seizures impair neurovascular coupling in vivo. A, Direct cortical imaging enabled continuous measurement of vascular diameter, as demonstrated for a representative experiment in B. Whereas early seizures (0-30 minutes) elicited a $59.33 \pm 8.46\%$ increase in arteriolar diameter, late seizures (2-4 hours) were accompanied by diameter increases of only $35.11 \pm 4.55\%$. C, The gradual decrease in vascular responses to seizures was evident in seven of nine animals ($P = 0.028$, Wilcoxon test, $n = 9$ animals). D, Comparison of early (0-30 minutes) versus late (2-4 hours) seizures confirmed a significant reduction in diameter responses ($P = 0.05$, Wilcoxon test, $n = 9$ animals), despite an overall increase in seizure power ($P = 0.02$) and a lack of change in seizure duration. Hence, with a decrease in dilatations and an increase in power, the dilatation to seizure power ratio (denoted as NVC [neurovascular coupling]) was also significantly smaller in response to late seizures ($P = 0.02$). ECoG, electrocorticogram; *, $P < 0.05$.

Individual seizures lasted 3.09 ± 0.47 minutes, with 4.77 ± 1.15 -minute inter-seizure intervals (18.22 ± 2 seizures per animal, $n = 9$ rats), and were accompanied by reversible vasodilation (of up to 60%). Importantly, seizure-associated changes in arteriole diameter gradually decreased in 7 of 9 animals (Figure 15C). Specifically, whereas early seizures (0-30 minutes of 4AP) induced vasodilation of $59.33 \pm 8.46\%$ ($n = 9$), late seizures (2-4 hours of 4AP) were associated with dilations of only $35.11 \pm 4.55\%$ ($n = 9$, $P = 0.05$; Figure 15B). The reduction in vascular responses could not be attributed to a decline in seizure severity, as seizure power invariably increased over time ($P = 0.02$, early vs late seizures; Figure 15D) with no changes in seizure duration ($P = 0.11$; Figure 15D). Consequently, the ratio between the vasodilatory response and the power of late versus early seizures was found to be significantly smaller ($P = 0.04$; Figure 15D), further confirming arteriolar neurovascular decoupling. As pericytes and capillaries are not visible in this preparation, the finding of neurovascular decoupling at the arteriolar level suggests that smooth muscle cells are also prone to loss of responsiveness.

3.3.7. Seizure-induced cellular injury and microvascular permeability in vivo

Having found pericytic injury and neurovascular decoupling, we proceeded to test whether these were accompanied by cellular damage in vivo. Visualization of cellular injury (using the intravenously injected membrane integrity marker propidium iodide)³³ pointed to cumulative perivascular enhancement after 2-4 hours of ongoing recurrent seizures (Figure 16B), reflective of cellular injury ($P = 0.06$, $n = 7$ animals, compared to pre-seizure values; Figure 16).

Our finding of pericytic injury and increased microvascular permeability in slice cultures prompted us to examine BBB permeability changes during recurrent seizures in vivo. In line with the literature^{3,39} and our in vitro findings, we observed seizure-related vascular leakage, with increased fluorescence of the intravenously injected BBB-impermeable dye (NaFlu) around and along arterioles and venules (Figure 16B). Quantitative assessment of parenchymal tracer accumulation confirmed a significant increase in endothelial permeability (compared to pre-seizure conditions, $n = 10$, $P = 0.0049$; Figure 16B). Notably, parenchymal increase in NaFlu fluorescence is likely to involve dye release from capillary BBB, as it appeared throughout the tissue and not only in the proximity of penetrating arteries and arterioles. Moreover, the leakage was not restricted to the pial

surface but was present in deeper cortical layers, as evidenced by the presence of the albumin-binding dye Evans blue in the parenchyma (Figure 16A, yellow arrows).

Figure 16 – Seizures induce cellular injury and vascular leakage in vivo.

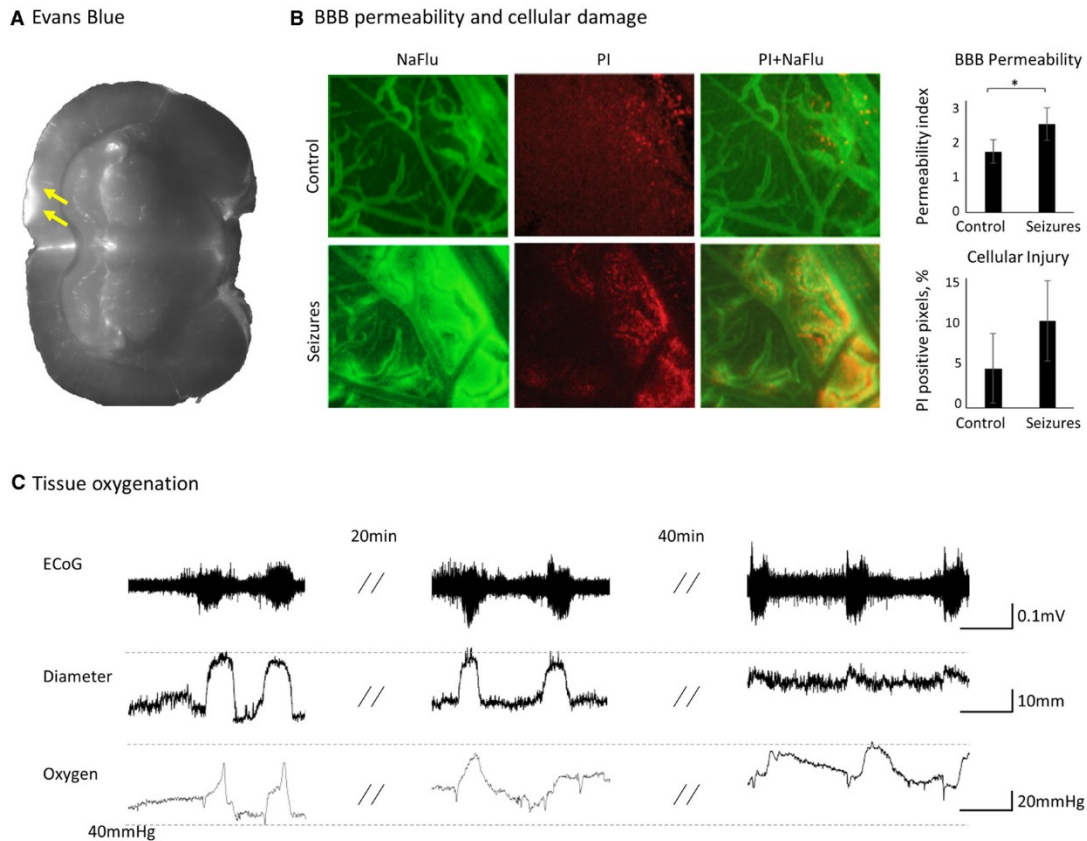


Figure 16. Seizures induce cellular injury and vascular leakage in vivo. A, Fluorescent imaging of Evans blue (intravenously injected premortem) demonstrates the extravasation of the dye in surface and deep cortical layers surrounding the window of 4-aminopyridine administration. B, In vivo imaging has revealed overlapping seizure-related increases in sodium fluorescein (NaFlu) and propidium iodide (PI) fluorescence in perivascular (arteriolar and venular) regions, reflective of blood–brain barrier (BBB) dysfunction (* $P = 0.0049$, Wilcoxon test, $n = 10$ animals) and cellular injury, respectively. C, Despite the impaired vascular responses to latent seizures, we never observed pO₂ values reaching the hypoxic threshold of 10 mm Hg with the Clark-style electrode ($P = 0.273$, Wilcoxon test, $n = 4$ animals). ECoG, electrocorticogram; *, $P < 0.05$.

3.3.8. Seizure-associated NVC impairment occurs under normoxic conditions in vivo

The balance between metabolic demands and perfusion during seizures remains a matter of debate, with some studies showing that blood supply meets metabolic demands,^{40,41} whereas others

suggesting the contrary.⁴² More recently, postictal hypoperfusion was highlighted as the potential link between seizures and neurological comorbidities in epilepsy.^{24,25} We thus examined the potential effects of neurovascular decoupling on tissue oxygenation, using Clark-style pO₂ microelectrodes⁴³ located adjacent to the responding arterioles (Figure 16C, n = 4). Consistent with previous reports,⁴⁴ individual seizures induced a characteristic biphasic pO₂ response: a rapid decrease at seizure onset (the “initial dip”) followed by a gradual increase that far exceeded the pre-seizure pO₂ levels (the “overshoot”). The rapid dips upon seizure onset (from a baseline of 39.86 ± 12.84 mm Hg to 26.46 ± 4.39 mm Hg) lasted 23.25 ± 11.65 seconds, whereas the recovery phase lasted 113.5 ± 30.2 seconds ($t_{\text{recovery}} = t_{\text{peak}} - t_{\text{dip}}$), reaching overshoot values of 79.87 ± 20.15 mm Hg. Importantly, despite neurovascular decoupling, the pO₂ overshoots of late seizures did not decrease compared to early events ($P = 0.273$), ruling out aggravated hypoxia as the mediator of enhanced cellular injury and BBB dysfunction.

3.4. Discussion

We report that recurrent seizures induce pericytic injury *in vitro* and are associated with neurovascular decoupling and BBB dysfunction at arteriolar and capillary levels. Seizure-induced capillary constriction was accompanied by loss of mitochondrial integrity in pericytes, highlighting the role of energy metabolism in microvascular injury. Our findings may help understand the mechanisms behind the postictal microcirculatory hypoperfusion underlying behavioral and cognitive symptoms associated with seizure disorders.²⁵

The viability of endothelial cells and pericytes, and the resealing of small vessels in the slice culture preparation,^{28,45,46} granted us the opportunity to study capillary neurovascular responses, without potential contribution of precapillary dilation and changes in blood flow. In light of the controversy surrounding the nomenclature of mural cells along the vascular axis,¹⁷ for simplicity we relied on morphological criteria referring to vessels of the smallest diameter (4-10 μm) as “capillaries” and to NG2- or PDGFR β -positive spindle-shaped cells that engulf them as “pericytes.” Nevertheless, the collapse of large blood vessels due to the slicing procedure hindered the unequivocal determination of the vascular branching order, leading to the potential inclusion of arterioles and smooth muscle cells in our samples. Although the used fluorescence marker MitoSox is oxidized in different cell types throughout the parenchyma, its colocalization with GFP-positive cells in PDGFR β transgenic mice suggests that MitoSox-accumulating contractile mural cells are actually pericytes, which retain motility and structural requirements to control vascular diameter. It is of note that other cell types, such as oligodendrocyte precursors or fibroblast-like stromal cells, may also express PDGFR β in juvenile tissue or after slicing procedures,¹⁴ which would explain the faint GFP fluorescence in non-mural cells we observed in culture (Figure 11). These cells resembled the fluorescence pattern of NG2, which is in line with the finding that parenchymal PDGFR β immunoreactivity colocalizes with NG2 but is distinct from IBA1⁺ microglia in epileptic specimens.¹⁴

The resting membrane potential of pericytes in culture was close to the reversal potential of potassium, suggesting that potassium conductance dominates in pericytes at rest, in the absence of adrenergic tonus and blood flow. Pericytes were maximally elongated, which necessitated the

application of vasoconstricting thromboxane analogue to restore the vasotonus.²⁹ Moreover, the vascular responses may be underestimated in our preparation, as the high oxygen tension, necessary for maintaining recurrent seizure activity in submerged conditions, does not favor dilation.⁴⁷ The observed resting membrane potential was lower than that reported in freshly isolated retinal capillaries or in acute brain slices,^{11,37} potentially due to the more destructive nature of those preparations or due to alterations in channel expression in culture following the exposure to serum. The effect of U46619 was mediated by a tonic inward current, as clamping the cells to their resting membrane potential prevented vasoconstriction. In line with the known role of moderate rises in extracellular potassium as one of the key mechanisms of vascular responsiveness,^{48,49} seizures led to apparent phasic inward currents associated with each individual clonic discharge. The subsequent reversal of the inward to an outward current, which corresponded to the time of maximal vasodilation of pre-constricted capillaries, may be explained by potassium-dependent activation of inward-rectifying potassium channels, as described for endothelial⁵⁰ and smooth muscle⁴⁸ cells. Unfortunately, pericytic constriction/dilation hindered stable current clamp recordings during recurrent seizures. Future studies are awaited to determine the relationship between recurrent seizures, pericytic membrane potentials, and contractility.

Although depletion of high-energy phosphates and increased lactate levels are frequently observed during status epilepticus,⁵¹ whether this solely points to increased neuronal energy demand or restricted oxidative metabolism remained unclear. Our *in vitro* findings demonstrate that the gradual decrease in capillary responsiveness occurs in the presence of ample oxygen and constant seizure-associated respiration enhancement. Thus, disturbances in neurometabolic coupling and subsequent shifts in pH or tissue redox potential are unlikely to underlie neurovascular decoupling.^{30,31} Conversely, despite the seizure-induced neurovascular decoupling, we never observed tissue oxygenation below the normoxic range (>20 mm Hg) during recurrent seizures *in vivo*. These results are in apparent contradiction to previous studies reporting local postictal hypoxia and vasoconstriction^{24,25} with optical methods (for review, see Suh et al⁵²). This discrepancy could be explained by the lower spatial resolution (~60 μm) of the Clark-style microelectrodes used in our study, by the different models of epileptogenesis, or by the use of the open window technique and perfusion with gassed aCSF. However, although reduced vascular responsiveness may yet prove to induce hypoxic neuronal damage, our results indicate that widespread hypoxia is

not a necessary condition for the dysfunction of pericytes. Remarkably, the loss of vascular responsiveness was observed in capillaries *in vitro* and in arterioles *in vivo*. It remains to be clarified whether pericytes and smooth muscle cells undergo similar functional disturbances or whether pericytic injury has a causal connection to neurovascular uncoupling in arterioles. This latter option is supported by studies suggesting that pericytic dilation precedes arteriolar dilation,¹¹ and that gap junction–coupled pericytes contribute to the spread of vasodilatory signaling.⁵³

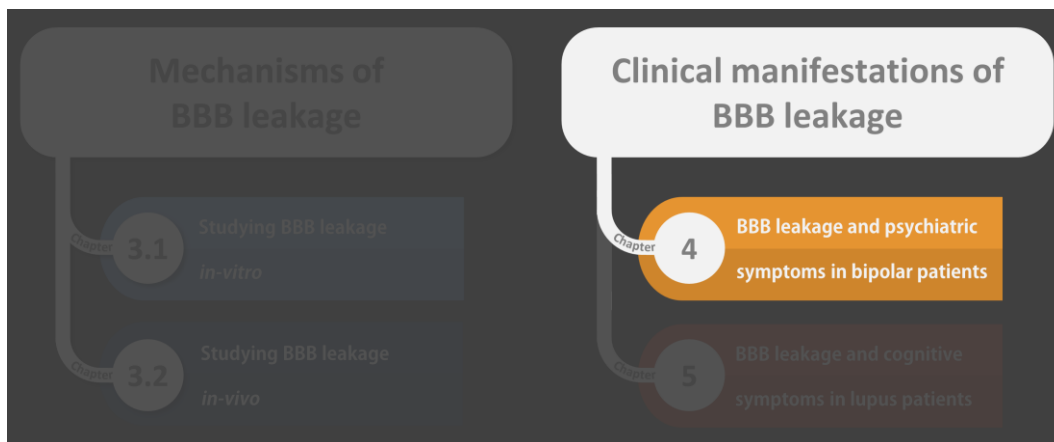
Free radicals are known to have vasoactive effects,⁹ and an increase in their production has been linked to seizures and subsequent cell damage.³¹ However, our experiments do not reflect a seizure-related increase in free radical production in pericytes. The failure of TEMPOL to prevent the cytosolic increase in MitoSox fluorescence suggests that it represents dye leakage from the mitochondria due to loss of mitochondrial integrity, rather than genuine cytosolic oxidation of the probe. Similar to vascular smooth muscle cells, pericyte contraction is controlled by changes in intracellular Ca^{2+} concentration.³⁷ Thus mitochondrial dysfunction leading to cytosolic Ca^{2+} dysregulation may explain the observed terminal rigor of injured pericytes, also described in hypoxia-reperfusion,⁹ and oxygen glucose deprivation.¹¹ Importantly, the observed terminal vasoconstriction and pericytic rigor coincided with a rapid release of intraluminal DCF, pointing to the breakdown of the endothelial diffusion barrier. Although this could be purely coincidental, these results are in accord with recent studies linking pericyte detachment to BBB breakdown.¹³ Mechanisms underlying pericyte-mediated BBB dysfunction may include glutamate-dependent,³ VEGF–dependent,⁵⁴ and matrix metalloproteinase–dependent⁵⁵ pathways. The potential contribution of these mechanisms awaits further investigation.

By studying the longitudinal changes in the hemodynamic responses to seizures, our study reveals a gradual neurovascular decoupling at both the capillary and the arteriolar level and excludes hypoxia as an immediate cause of microvascular dysfunction and cellular injury. Our findings may explain the reported disturbances in blood flow regulation and mural cell remodeling following recurrent seizures.^{20,24,26,27} Furthermore, our *in vitro* evidence of pericytic injury–associated loss of capillary response and increased microvascular permeability highlights pericyte functionality as a potential therapeutic target for seizure disorders.²⁷

Chapter 4 – BBB leakage and psychiatric symptoms in bipolar patients

Chapter Overview

In the second study conducted during my PhD we sought to investigate the clinical relevance of BBB leakage. Specifically, we aimed to examine the potential link between subtle/slow BBB leakage and psychiatric symptoms in living patients. This study was a collaboration with Dr. Cynthia Calkin – the head of the Mood and Metabolism Program at the QEII Health Sciences Center, Halifax, Nova Scotia, and a psychiatrist with an expertise in bipolar disorder.



With the neuroimaging expertise of Dr. Steven Beyea and Dr. Chris Bowen of the Biomedical Translational Imaging Centre (BIOTIC, QEII Hospital, Halifax, Nova Scotia) we established an MRI acquisition protocol suitable for assessing subtle/slow BBB leakage in patients and control volunteers (Figure 9).

This clinical study aimed to test the following hypotheses:

- I. Evidence of subtle/slow BBB leakage can be found in patients with bipolar disorder, despite the absence of gross brain abnormalities (e.g., tumors or ischemic/hemorrhagic lesions).

- II. Subtle/slow BBB leakage may be associated with worse psychiatric symptoms.
- III. BBB leakage may be associated with metabolic dysregulation, i.e., insulin-resistance.

To analyze the MRI data, I developed a fully automatic software that calculates the rate of BBB leakage in every voxel of the brain (Figure 10). A total of 36 patients with bipolar disorder (type I and II) underwent the MRI acquisition protocol, along with 14 volunteers matched in sex, age, and metabolic status to the bipolar cohort. Our findings validated all three hypotheses, showing that:

- I. A subgroup of bipolar patients (~25%) have extensive BBB leakage.
- II. Compared to patients without extensive BBB leakage, this subgroup experiences a significantly more chronic course of illness (more frequent, long-lasting, and severe episodes of mania/depression that do not respond to mood stabilizing treatments), worse depression and anxiety, and lower overall level of functioning.
- III. This subgroup scored significantly higher on scales of metabolic and vascular pathology, and all patients within this subgroup are insulin-resistant.

Our findings highlight the BBB as a likely mediator of bipolar disorder progression, and offer a new mechanistic framework for the severe psychiatric outcomes in bipolar patients with comorbid insulin-resistance. We argue that the long-lasting systemic inflammation associated with insulin-resistance is a likely cause of BBB leakage. We further propose that leakage-mediated neuroinflammation may lead to neuronal dysfunction that underlies the progression of bipolar illness and exacerbation of its neuropsychiatric outcomes. The potential role of altered cross-BBB efflux in bipolar drug-resistance warrants further investigation.

Abstract

Bipolar disorder affects approximately 2% of the population and is typically characterized by recurrent episodes of mania and depression. While some patients achieve remission using mood-stabilizing treatments, a significant proportion of patients show progressive changes in symptomatology over time. Bipolar progression is diverse in nature and may include a treatment-resistant increase in the frequency and severity of episodes, worse psychiatric and functional outcomes, and a greater risk of suicide. The mechanisms underlying bipolar disorder progression remain poorly understood and there are currently no biomarkers for identifying patients at risk. The objective of this study was to explore the potential of blood-brain barrier (BBB) imaging as such a biomarker, by acquiring the first imaging data of BBB leakage in bipolar patients, and evaluating the potential association between BBB dysfunction and bipolar symptoms. To this end, a cohort of 36 bipolar patients and was recruited through the Mood Disorders Clinic (Nova Scotia Health Authority, Canada). All patients, along with 14 control subjects (matched for sex, age, and metabolic status), underwent contrast-enhanced dynamic MRI scanning for quantitative assessment of BBB leakage as well as clinical and psychiatric evaluations. Outlier analysis has identified a group of 10 subjects with significantly higher percentages of brain volume with BBB leakage (labeled the “extensive BBB leakage” group). This group consisted exclusively of bipolar patients, while the “normal BBB leakage” group included the entire control cohort and the remaining 26 bipolar subjects. Among the bipolar cohort, patients with extensive BBB leakage were found to have more severe depression and anxiety, and a more chronic course of illness. Furthermore, all bipolar patients within this group were also found to have co-morbid insulin resistance, suggesting that insulin resistance may increase the risk of BBB dysfunction in bipolar patients. Our findings demonstrate a clear link between BBB leakage and greater psychiatric morbidity in bipolar patients and highlight the potential of BBB imaging as a mechanism-based biomarker for bipolar disorder progression.

4.1. Introduction

Bipolar disorder affects approximately 2% of the population, and is characterized by episodes affecting mood, activity levels, and ability to carry out day-to-day tasks.¹ A growing body of evidence suggests that treatment-resistant disease progression is common in bipolar patients, and may include a shift towards more frequent and severe episodes, worse depression, anxiety, socio/occupational dysfunction and increased risk of suicide.² While the pathophysiology of bipolar disorder remains poorly understood, converging evidence points to the presence of neuroinflammation in bipolar patients.^{3,4} In light of the increasingly recognized role of the brain's microvasculature in neuroinflammation, here we set out to examine the potential link between blood brain barrier (BBB) dysfunction and bipolar disorder progression.

Under normal conditions the BBB restricts the entry of most blood-derived factors into the brain. This tight regulation of the brain's environment is necessary for proper neuronal activity and is performed by the tightly connected membrane of endothelial cells within brain microvessels, and the mural and astrocytic cells engulfing it.⁵ Hence, disruption of this complex interface allows the extravasation of blood-derived factors into the brain, causing neuroinflammatory responses which can initiate various pathways of neural dysfunction and degeneration.⁶

In the past two decades dynamic contrast-enhanced (DCE-) magnetic resonance imaging (MRI) has been gaining popularity as the method of choice for assessing BBB leakage in living subjects.⁷ In this method, repeated scans of the brain are acquired to capture signal changes due to cross-BBB extravasation of an intravenously injected contrast agent. As the current gold standard for BBB assessment still relies on post-mortem tissue analysis, cross-validation of the two methods in the same individuals is not a trivial task. However, DCE-MRI studies have been used to identify BBB dysfunction in disorders such as multiple sclerosis,⁸⁻¹¹ stroke,¹²⁻¹⁴ brain tumors,¹⁵ epilepsy,¹⁶ traumatic brain injury,^{17,18} and dementia^{6,19} — all of which were previously linked to BBB impairment in post-mortem studies. Moreover, while a large-scale validation of this approach is yet to be performed, two recent studies have successfully demonstrated the method's reproducibility²⁰ and biological validity.¹⁰

4.2. Methods

To date DCE-MRI has not been applied to the study of psychiatric disorders and the clinical correlates of BBB dysfunction in these disorders remain unknown. Thus, the goal of the present study was to obtain the first imaging evidence of BBB dysfunction in bipolar patients, and to test the association between BBB pathology and disease severity.

4.2.1. Participants

The study was approved by the Nova Scotia Health Authority Research Ethics Board (1021507). A total of 36 adult patients (over 18 years of age) were recruited to the study through the Mood Disorders Clinic (Nova Scotia Health Authority, Canada). Subjects underwent a detailed psychiatric interview using the schedule for affective disorders and schizophrenia (SADS-L)³⁷ to diagnose bipolar disorder. Diagnoses required a consensus of at least 3 psychiatrists and were based on the DSM-5 criteria.³⁸ As patients with type I versus II bipolar disorder differ primarily in severity of manic episodes, we did not exclude patients based on this criterion. Mood symptoms were rated using the Montgomery-Åsberg depression rating scale (MADRS),²⁴ Hamilton anxiety rating scale (HAM-A),²⁵ and the global assessment of functioning scale (GAF, reflecting illness effects on social, occupational, and psychological functioning).²⁶ Course of illness was determined using the affective morbidity index (AMI, rating the severity and length of manic/depressive episodes),³⁹ patient interviews, detailed review of medical records, and analysis of daily mood ratings. Additional data collection included: blood pressure (BP), body mass index (BMI), the homeostatic model assessment of insulin resistance (HOMA-IR, calculated based on fasting levels of blood glucose and insulin),²³ and Framingham risk scores (heart age and risk of cardiovascular disease).²¹

A group of 14 control subjects was also recruited and was matched for sex, age, and metabolic status to the bipolar cohort. The same schedule used for diagnosing bipolar disorder (SADS-L), was used to confirm a lack of psychiatric history in this group. The control group also underwent the above-mentioned protocol of interviews and assessments.

Participants with diabetes, pregnancy, or contradiction to MRI or contrast-enhancement (estimated glomerular filtration rate < 60) were excluded from the study. All participants provided informed consent prior to enrollment.

4.2.2. BBB Imaging

4.2.2.1. DCE-MRI acquisition and preprocessing

Images were acquired using a 3T MRI scanner (Discovery MR750, GE Healthcare, Waukesha, WI), with a 32-channel MR Instruments head coil. The sequences acquired for BBB assessment included: (1) a T1-weighted 3D sagittal anatomical scan (BRAVO, TE/TR = 2/6ms, TI = 450ms, FOV 22.4cm, acquisition matrix 224x224x168, voxel size 1x1x1 mm, acceleration 2, averages 2, scan time 5min 42s); (2) a T1-weighted 3D tilted axial sequence with variable flip angles (2-10-30°, DESPOT1, TE/TR = 2/10ms, flip angle 15°, averages 2, FOV 24cm, acquisition matrix 192x192x34, voxel size 1.25x1.25x6 mm, scan time 6min 39s) for the calculation of pre-contrast T1 map;⁴⁰ and (3) a T1-weighted 3D axial dynamic scan (LAVA, TE/TR = 2/4ms, FOV 24cm, acquisition matrix: 192x192x34, voxel size 1.25x1.25x6 mm, flip angle 15°, averages 1, $\Delta t = 20$ Sec) acquired between minutes 6 and 20 after intravenous injection enhanced of the magnetic contrast Gadobenate Dimeglumine (0.1 mmol/kg, MultiHance, Bracco Imaging Canada, Montreal, QC). All sequences were registered and normalized to MNI coordinates using SPM12 (University College London, www.fil.ion.ucl.ac.uk/spm).

4.2.2.2. Image analysis

As extravasation of contrast agent due to cross-BBB leakage leads to increased T1 signaling in the affected tissue, it allows quantitative assessment of contrast accumulation in the tissue and hence the contrast leakage rate. To achieve this, T1 intensities are first converted to contrast concentration values,⁴⁰ and concentration-time curves are constructed for every brain voxel. The concentration-time curves can next be fitted to one of several pharmacokinetic models, allowing the calculation of parameters corresponding to leakage rates. Here we used the linear model,^{14,20,27,28} which estimates the leakage rate K_i (mMol/min) by calculating the slope of each concentration-time curve between 6-20 min. To compensate for inter-subject variabilities (due to heart rate, blood flow, or rate of contrast injection), each voxel's leakage rate was normalized to that of the superior sagittal

sinus,^{14,27,28} resulting in a dimensionless measure of leakage rate. Leakage rates were considered pathological when exceeding 0.02, the 95th percentile of all values in a cohort of control subjects.¹⁷ The percent of suprathreshold voxels was used as a measure reflecting overall BBB leakage. To identify subjects with abnormally high overall leakage an outlier analysis was performed (based on the median + two standard deviations of all 50 subjects).

To quantify region-specific BBB leakage, each scan was segmented into 126 anatomically/functionally significant areas in accordance with the MNI brain atlas (<https://github.com/neurodebian/spm12/tree/master/tpm>). The number of voxels with abnormally high leakage rates was quantified within each region and divided by the total of voxels comprising the region. This ratio was used as the measure of region-specific BBB leakage.

4.2.3. Statistical analysis

Continuous variables were compared using the Wilcoxon rank sum test, and categorical variables were compared using either Fisher's or Chi-square test. Corrections for multiple comparisons were performed using the false discovery rate method.

4.3. Results

4.3.1. Participants

A cohort of 36 bipolar patients was recruited for the study (23 bipolar type I and 13 bipolar type II). The average duration of illness among the patients was 28 ± 13 years, with an average onset at 22 ± 10 years of age. Bipolar disorder started with a depressive episode in 76% of patients, and about half (55%) have progressed to a chronic course of illness. The average age of the group was 49.1 ± 11.3 years and 70.6% were females. Control subjects were matched for sex, age, and metabolic syndrome (Table 3). Compared to controls, bipolar patients scored significantly worse on scales of depression (Montgomery-Åsberg depression rating scale), anxiety (Hamilton anxiety rating scale), and capacity of carrying out day-to-day functions (Global Assessment of Functioning, Table 3). No differences in anthropometric or metabolic measures were identified between the groups (Table 3).

4.3.2. A sub-group of bipolar patients have a significantly higher level of BBB dysfunction

All participants underwent DCE-MRI scanning and quantitative maps of leakage rates were calculated for each brain voxel^{27,28} (Figure 17A). The percent of brain tissue with pathological leakage rates was used as an overall measure of BBB dysfunction, revealing a high variability of values among the bipolar cohort (Figure 17B). In order to identify subjects with significantly higher levels of BBB dysfunction, an outlier analysis was performed (based on the median + two standard deviations of all 50 subjects). Ten of the 50 subjects were identified as outliers (subjects with over 12.2% of the brain affected by leakage). The outlier group consisted exclusively of bipolar patients, and was labelled the “extensive BBB leakage” group. The group with the lower level of BBB dysfunction included the entire control cohort as well as the remaining 26 bipolar patients. Since there were no differences between the controls and patients within this group (Figure 17C), it was collectively referred to as the “normal BBB leakage” group. To examine whether the differences between bipolar patients with extensive vs normal leakage were widespread (diffuse) or restricted to specific brain regions (focal), region-specific leakage was quantified in 126 anatomically/functionally significant brain regions and compared between the two groups. The comparison revealed a diffuse rather than focal difference, with 112 of the 126 regions

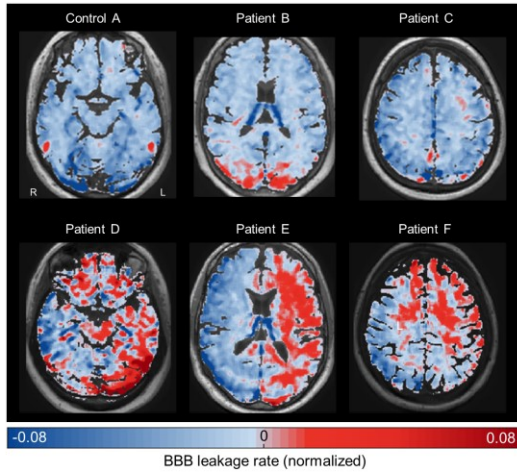
showing significantly higher leakage in the “extensive BBB leakage” group (Figure 17D, $p < 0.05$, corrected for multiple comparisons).

Table 3 – Demographic and clinical features of patients with Bipolar Disorder			
	Bipolar Patients	Controls	P
Demographics			
Age	49.1 (1.9)	47.6 (2.9)	0.666
Sex (% female)	70.6	71.4	1.000
Anthropometric and metabolic measures			
Body mass index (BMI)	30.1 (1.1)	28.2 (1.5)	0.358
Waist-to-hip ratio	0.9 (0.02)	0.9 (0.03)	0.230
Risk of cardiovascular disease (Framingham risk score) ²¹	8.6 (1.5)	4.9 (0.8)	0.469
Framingham heart age ²¹	53.0 (5.3)	47.7 (2)	0.602
Metabolic syndrome ²² (% subjects)	27.8	15.4	0.474
Insulin resistance (HOMA-IR score) ²³	2.7 (0.3)	1.7 (0.2)	0.056
Psychiatric characteristics			
Depression severity (MADRS score) ²⁴	18.1 (2.4)	1.9 (0.4)	<0.001
Anxiety severity (HAM-A score) ²⁵	11.8 (1.5)	2.0 (0.4)	<0.001
Global Assessment of Functioning (GAF score) ²⁶	66.8 (0.5)	92.1 (0.7)	<0.001
Medication use (% patients)			
Lithium	72
Antiepileptics	67
Atypical antipsychotics	56
Antidepressants	44
Benzodiazepines	56
Melatonin	19	0	0.169
Blood pressure medication	14	14	1.000
Cholesterol medication	14	0	0.304

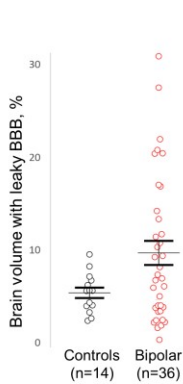
Mean (standard error), unless otherwise indicated. Continuous variables were compared using the Wilcoxon rank sum test, and categorical variables were compared using Fisher’s Exact Test. MADRS, Montgomery-Åsberg depression rating scale; HAM-A, Hamilton anxiety rating scale; HOMA-IR, homeostatic model assessment of insulin resistance.

Figure 17 – A sub-group of bipolar patients have extensive BBB leakage

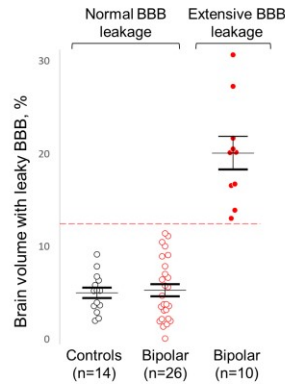
A. Representative maps of BBB leakage



B. Extent of BBB leakage



C. Outlier identification



D. Statistically significant regional differences

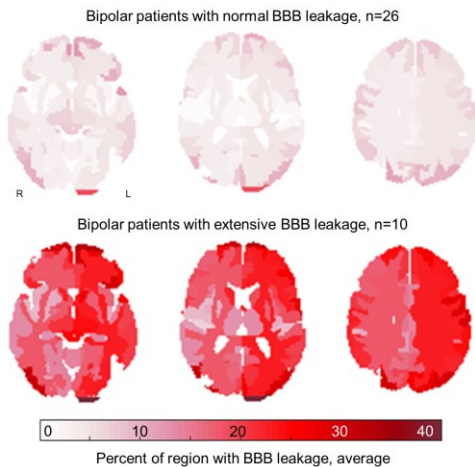


Figure 17. A sub-group of bipolar patients have extensive BBB leakage. A. The rate of BBB leakage was quantified for every brain voxel, with shades of blue representing tissue with non-permeable BBB and shades of red representing contrast agent accumulation due to BBB leakage. Representative leakage maps of five bipolar patients showcase the different extents of leakage among the bipolar cohort (displayed slices were selected to represent maximal BBB leakage in each subject). B. The overall percent of brain tissue with pathological leakage was calculated for all patients and controls, revealing a high variability of values among the bipolar cohort. C. Outlier analysis of all 50 subjects has identified a group with “extensive BBB leakage”, consisting of ten bipolar patients, and a group with “normal BBB leakage”, consisting of 26 patients and 14 controls ($p < 0.0001$). D. Compared to bipolar patients with normal BBB leakage, the “extensive BBB leakage” group had significantly higher levels of leakage in 112 of the 126 regions (Wilcoxon rank sum test with a false discovery rate correction for multiple comparisons).

4.3.3. Extensive BBB leakage in bipolar patients is associated with greater psychiatric morbidity

To examine whether a higher level of BBB dysfunction corresponds to a worse bipolar outcome, we next compared the course of illness among the groups (episodic versus chronic), as well as levels of depression, anxiety, and socio/occupational functioning. Bipolar patients with extensive BBB leakage were found to have higher rates of chronic illness with more frequent and/or severe manic/depressive episodes (as exemplified in Figure 18A and quantified in Figure 18B). Moreover, extensive BBB leakage was found to be associated with greater severity of depression, anxiety, and socio/occupational dysfunction (Figure 18B). No associations between BBB pathology and age or disease duration were found in our cohort.

Figure 18 – Extensive BBB leakage in bipolar patients is associated with a worse neuropsychiatric status

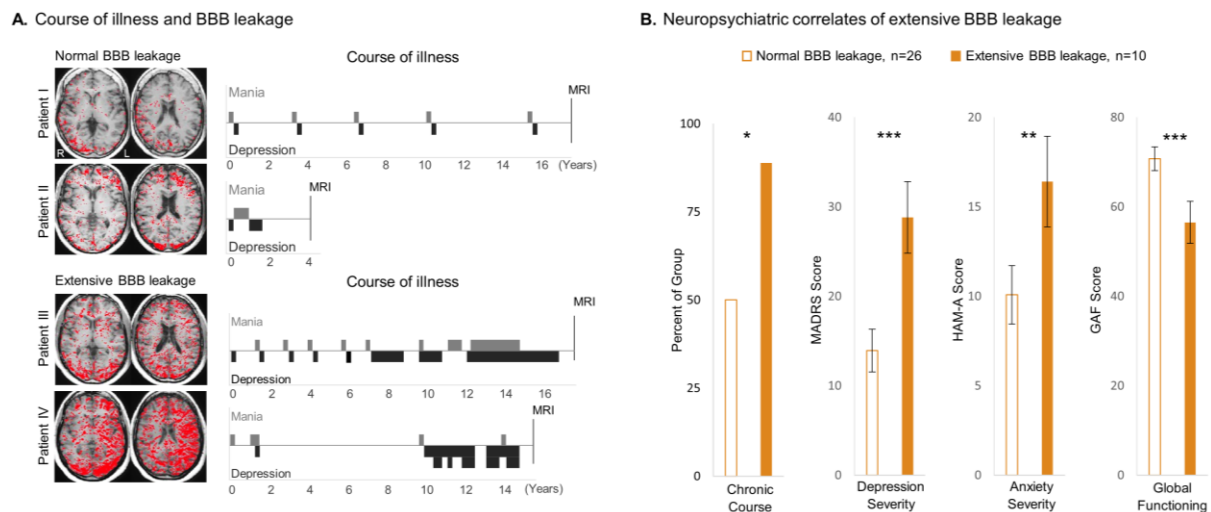


Figure 18. Extensive BBB leakage in bipolar patients is associated with a worse neuropsychiatric status. A. Representative courses of illness show an episodic course in patients with normal BBB leakage (patients I and II, red pixels representing tissue with leaky BBB), and a progression towards a chronic course in patients with extensive BBB leakage (patients III and IV). B. Quantitative analysis confirmed the higher incidence of a chronic (vs episodic) course of illness among patients with extensive BBB leakage. Extensive BBB leakage was also associated with a greater severity of depression (Montgomery-Åsberg Depression Rating Scale, MADRS), elevated anxiety (Hamilton Anxiety Rating Scale, HAM-A), and worse socio/occupational functioning (Global Assessment of Functioning, GAF). Statistical comparisons were conducted using the Wilcoxon rank sum test. Error bars denote standard error of the mean. Asterisks denote level of significance, with * for $p \leq 0.05$, ** for $p \leq 0.01$, and *** for $p \leq 0.001$.

4.3.4. Extensive BBB leakage is associated with metabolic dysregulation, yet not with class of mood-stabilizing drugs

Bipolar patients with extensive BBB leakage were found to have higher body-mass indices, elevated risk of cardiovascular disease, and advanced heart age (Figure 19). Furthermore, all patients within the “extensive BBB leakage” group were also found to have comorbid insulin resistance (homeostatic model assessment of insulin resistance >1.8).²³ Notably, while all subjects with extensive BBB leakage had insulin resistance, not all subjects with insulin resistance had extensive BBB leakage (with four insulin resistant controls and 12 insulin resistant bipolar patients having BBB leakage within the normal range). No patients were receiving anti-diabetic or insulin sensitizing drugs. No differences in the class of mood stabilizing treatments were found between the normal and extensive BBB leakage groups.

Figure 19 – Extensive BBB leakage is associated with metabolic dysregulation.

Metabolic and vascular correlates of extensive BBB leakage

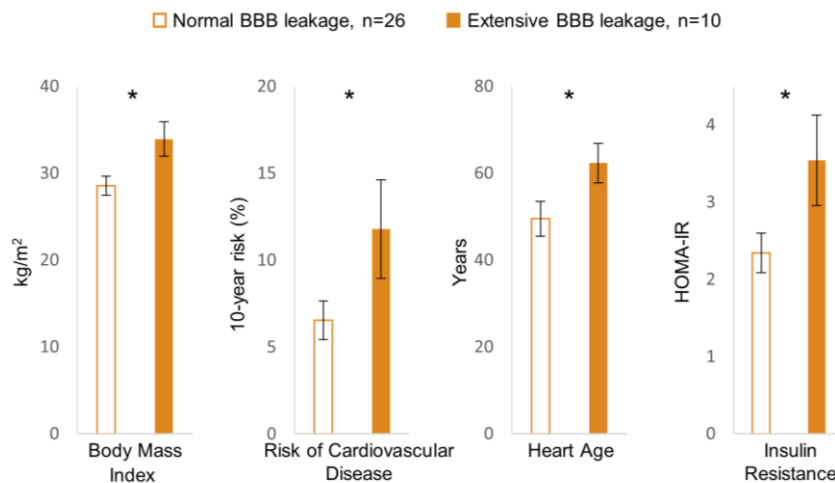


Figure 19. Extensive BBB leakage is associated with metabolic dysregulation. Bipolar patients with extensive BBB leakage were found to have higher body mass indices, increased risk of cardiovascular disease, advanced heart age, and higher levels of insulin resistance. Statistical comparisons were conducted using the Wilcoxon rank sum test. Error bars denote standard error of the mean. Asterisks denote $p \leq 0.05$. HOMA-IR, homeostatic model assessment of insulin resistance.

4.4. Discussion

This study presents the first imaging of BBB leakage in bipolar patients. Using dynamic contrast-enhanced MRI, we show that a higher level of dysfunction (i.e. extensive BBB leakage), affects 28% of the bipolar cohort and none of the controls. The study further shows that patients with extensive BBB leakage experience a more chronic form of illness with greater severity of depression, anxiety, and socio/occupational dysfunction. Our findings suggest that BBB imaging holds potential as a mechanism-based biomarker for the psychiatric deterioration experienced by a sub-group of bipolar patients.

We propose that BBB leakage may impact the functionality of the affected brain regions, leading to region-associated symptomatology. This hypothesis is supported by a recent imaging study in subjects with cognitive decline, linking cognitive impairment to BBB dysfunction in the hippocampus.¹⁹ Larger cohort studies are needed to determine the association between region-specific BBB dysfunction and the diverse symptoms of bipolar progression. Moreover, future large-scale prospective studies are needed for assessing the sensitivity and specificity of DCE-MRI based BBB assessment, before it can become part of routine medical practice.

Our study also links BBB damage in bipolar patients to insulin resistance, in line with recent evidence associating insulin resistance with vascular dysfunction in the brain and increased risk of dementia.²⁹ Insulin resistance is known to be more common in bipolar patients compared to the general population,³⁰⁻³² yet the mechanisms underlying this phenomenon remain poorly understood.³³ While atypical antipsychotics were suggested to cause insulin resistance in patients with bipolar disorder and schizophrenia,³⁴⁻³⁶ we found no association between the use of atypical antipsychotics and insulin resistance or BBB leakage. Future studies are warranted to better understand the high rates of insulin resistance observed in bipolar patients.

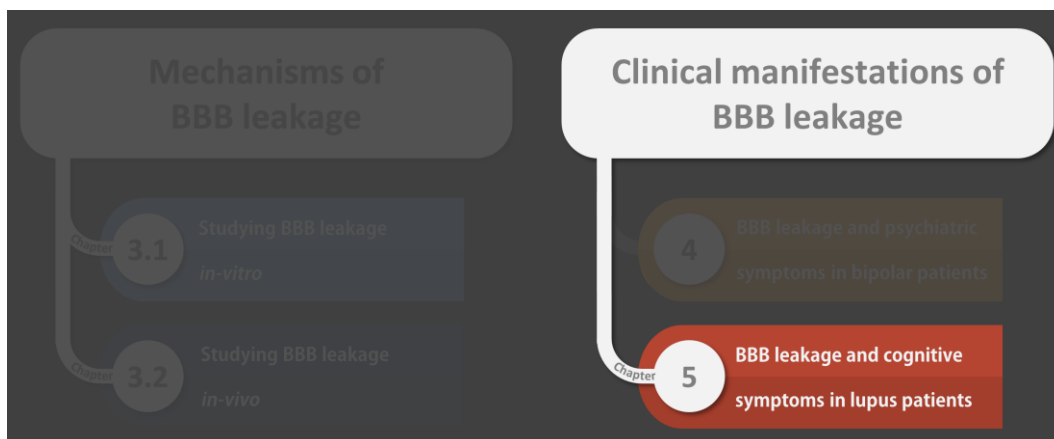
While our study is the first to show direct imaging evidence of BBB dysfunction in psychiatric patients, future studies are needed to fully elucidate the mechanisms mediating the psychiatric decline associated with BBB dysfunction and to determine whether vascular-protecting therapies may prove beneficial for bipolar disorder treatment.

To conclude, our study reveals an association between BBB pathology and worse psychiatric morbidity in bipolar patients. Our findings further suggest that BBB imaging offers promise as a new biomarker for bipolar disorder progression.

Chapter 5 – BBB leakage and cognitive symptoms in lupus patients

Chapter Overview

Our first clinical study has brought forward the hypothesis that the presence or lack of BBB leakage may help explain the stark differences in symptom-severity among patients with similar psychiatric diagnoses. The study's findings also suggested that the observed BBB leakage may be secondary to insulin-resistance-mediated systemic inflammation. The clinical study presented in the current chapter extended these hypotheses to another illness associated with systemic inflammation and differences in the severity of neuropsychiatric symptoms. In a collaboration with Dr. John G Hanly, the director of research at the Division of Rheumatology (QEII Health Sciences Center, Halifax, Nova Scotia), we studied patients with the autoimmune disease lupus.



Lupus patients underwent the same imaging protocol (Figure 9) as the patients and controls of the bipolar study, and a total of 65 lupus patients participated in the study. Nine of the 14 control subjects qualified as controls for this study, and were also matched in sex and age to the lupus cohort. BBB leakage was assessed using the same BBB software pipe-line (Figure 10), with an added data analysis step examining the volume of different brain structures using the [VolBrain](#) freeware.

This clinical study aimed to test the following hypotheses:

- i. Evidence of subtle/slow BBB leakage can be found in patients with lupus, despite the absence of gross brain abnormalities (e.g., tumors or ischemic/hemorrhagic lesions).
- ii. Subtle/slow BBB leakage may be associated with worse cognitive symptoms.
- iii. Subtle/slow BBB leakage may be associated with differences in the volume of specific brain regions.

Excitingly, our findings validated all hypotheses, showing that:

- i. A subgroup of lupus patients (~25%) have extensive BBB leakage.
- ii. This subgroup experiences significantly worse cognitive impairment, compared to patients without extensive BBB leakage.
- iii. This subgroup has significantly smaller gray matter volume, compared to controls.

These findings underscore the potential role of BBB-mediated processes in the cognitive impairment affecting a subgroup of patients with lupus. This study extends the mechanistic framework proposed in the previous chapter to lupus, suggesting that the long-lasting/recurrent systemic inflammation associated with the illness is a likely cause of BBB leakage, subsequent neuroinflammation and development of neuropsychiatric symptomatology.

Manuscript title:

Blood-brain barrier leakage in systemic lupus erythematosus is associated with gray matter loss and cognitive impairment

Annals of the Rheumatic Diseases, 2020

Authors:

Kamintsky L, Beyea SD, Fisk JD, Hashmi JA, Omisade A, Calkin C, Bardouille T, Bowen C, Quraan M, Mitnitsky A, Matheson K, Friedman A, Hanly JG

Abstract

Objectives: To examine the association between blood-brain barrier (BBB) integrity, brain volume and cognitive dysfunction in adult patients with systemic lupus erythematosus (SLE).

Methods: A total of 65 ambulatory SLE patients and 9 healthy controls underwent dynamic contrast-enhanced magnetic resonance imaging (DCE-MRI) scanning, for quantitative assessment of blood-brain barrier (BBB) permeability. Volumetric data was extracted using the VolBrain pipeline. Global cognitive function was evaluated using a screening battery consisting of tasks falling into five broad cognitive domains, and was compared between patients with normal versus extensive BBB leakage.

Results: SLE patients had significantly higher levels of BBB leakage compared to controls ($p=0.04$). Extensive BBB leakage (affecting over $>9\%$ of brain volume) was identified only in SLE patients (16/65; 24.6%), who also had smaller right and left cerebral gray matter volumes compared to controls ($p=0.04$). Extensive BBB leakage was associated with lower global cognitive scores ($p=0.02$), and with the presence of impairment on one or more cognitive tasks ($p=0.01$).

Conclusion: Our findings provide evidence for a link between extensive BBB leakage and changes in both brain structure and cognitive function in SLE patients. Future studies should investigate the mechanisms underlying BBB-mediated cognitive impairment, validate the diagnostic utility of BBB imaging, and determine the potential of targeting the BBB as a therapeutic strategy in SLE patients.

5.1. Introduction

Cognitive impairment is the most commonly reported and most widely studied manifestation of neuropsychiatric SLE (NPSLE),^{1,4} yet its causality remains incompletely understood. Disease mechanisms implicated in NPSLE include thrombotic cerebrovascular ischemia, brain-reactive autoantibodies, and complement activation.³ These pathways may also damage the blood-brain barrier (BBB), and thereby expose the brain to neurotoxic blood components that are normally restricted from entering the brain by the BBB. In animal models, extravasation of plasma proteins (such as albumin, thrombin and activated protein C) and lupus autoantibodies into brain tissue causes neuroinflammation and neurodegeneration.⁵⁻⁹ Recent evidence also suggests that autoimmune antibodies and cytokines can themselves alter the normal function of endothelial cells, breaching the BBB and infiltrating the brain.^{10,11}

Despite a strong rationale for BBB dysfunction playing a role in the pathogenesis of NPSLE,^{12,13} evidence in SLE patients remains scarce and largely circumstantial (e.g. post-mortem findings of vascular lesions).¹⁴ Technical advances in neuroimaging offer a direct, quantitative, and detailed method for BBB assessment.¹⁵ Specifically, the use of dynamic contrast-enhanced MRI (DCE-MRI) allows quantification of contrast extravasation into brain parenchyma, and calculation of cross-BBB leakage-rates for every voxel of the brain.¹⁶⁻¹⁸ While DCE-MRI has been validated in conditions associated with BBB dysfunction (e.g. multiple sclerosis,¹⁹ stroke,²⁰ traumatic brain injury,¹⁸ and dementia),²¹ it has not been well studied in NPSLE.²² Our objective was to measure BBB permeability in a large, unselected adult population of SLE patients, and to examine associations with brain volume and cognitive function.

5.2. Patients and Methods

5.2.1. Patients

Patients fulfilling the revised American College of Rheumatology (ACR) criteria for SLE²³ were consecutively recruited from the Dalhousie Lupus clinic, Division of Rheumatology, Queen Elizabeth II Health Sciences Center, Halifax, Nova Scotia, Canada. All patients were invited to participate unless there were contraindications to contrast-enhanced MRI scanning. Patients were not pre-screened for cognitive impairment prior to study enrollment. The study was approved by the Nova Scotia Health Authority (NSHA) Research Ethics Board, and participants provided written informed consent. Controls were healthy individuals with no neuropsychiatric history, consecutively recruited for another study.²⁴ For the present study, additional exclusion criteria were significant chronic illness (e.g. SLE, diabetes); and age under 35 or over 70 years old.

Demographic and clinical data, disease activity [Systemic Lupus Erythematosus Disease Activity Index-2000 (SLEDAI-2K)]²⁵ and cumulative organ damage [Systemic Lupus International Collaborating Clinics/ACR damage index (SDI)]²⁶ were recorded (Table 4). Other variables included: lupus-related medications such as corticosteroids, antimalarials, immunosuppressive drugs (methotrexate, azathioprine, cyclophosphamide, leflunomide, mycophenolate mofetil and intravenous gamma globulin) and biologic agents (rituximab or belimumab); use of psychoactive medications; lifestyle habits and comorbidities (cigarette smoking, diabetes mellitus and hypertension). Laboratory variables included a complete blood count, serum creatinine, urinalysis, anti-dsDNA, antiphospholipid (anticardiolipin, lupus anticoagulant) antibodies, C3, and C4 levels. Clinical and cognitive assessments, blood collection and DCE-MRI scanning were performed on the same day.

5.2.2. Cognitive function

Clinical neuropsychological tests, based upon ACR recommendations,²⁷ focused on five broad cognitive domains commonly affected in SLE.²⁸ Information processing speed and executive abilities were represented by the Symbol Digit Modalities Test (SDMT)²⁹ and the Design Fluency test (“fixed” generation of designs guided by pre-determined rules),³⁰ respectively. Components of

the California Verbal Learning Test (CVLT-II)³¹ provided indices of attention span (number of words recalled correctly on trial 1), new learning (total words recalled over five list presentations on trials 1-5), and delayed spontaneous recall (number of words recalled spontaneously after a 20-minute delay) for verbal information. Raw scores were standardized based on normative data published for each test, and converted to Z-scores.³⁰ Z-scores ≤ -1.5 were considered to reflect “impaired” performance.

5.2.3. Imaging

5.2.3.1 MRI acquisition

Images were acquired using a 3T MRI scanner (Discovery MR750, GE Healthcare, Waukesha, WI), with a 32-channel MR Instruments head coil. The sequences for BBB assessment included: [1] a T1-weighted 3D sagittal anatomical scan (BRAVO, TE/TR=2/6ms, TI=450ms, FOV 224mm, acquisition matrix 224x224x168, voxel size 1x1x1mm, acceleration 2, averages 2, scan time 5min 42s); [2] a T1-weighted 3D tilted axial sequence with variable flip angles (5-10-30°, DESPOT1, TE/TR=2/10ms, flip angle 15°, averages 2, FOV 240mm, acquisition matrix 192x192x34, voxel size 1.25x1.25x6mm, scan time 6min 39s) for the calculation of pre-contrast T1 map;³² and [3] a T1-weighted 3D axial dynamic scan (LAVA, TE/TR=2/4ms, FOV 240mm, acquisition matrix: 192x192x34, voxel size 1.25x1.25x6mm, flip angle 15°, averages 1, $\Delta t=20$ sec) acquired between minutes 6 and 20 after intravenous injection of the magnetic contrast Gadobenate Dimeglumine (0.1mmol/kg, MultiHance, Bracco Imaging Canada, Montreal, QC).

5.2.3.2. Volume analysis

T1-weighted anatomical images were processed using VolBrain software (<http://volbrain.upv.es>),³³ an online pipeline that registers images to the Montreal Neurological Institute (MNI) space, and reports the volumes of expert-labeled anatomical structures as percentage of total intracranial cavity.³³ We analyzed the volume of the following 23 structures: right/left cerebral gray/white matter, right/left cerebellum gray/white matter, right/left caudate, right/left putamen, right/left thalamus, right/left globus pallidus, right/left hippocampus, right/left amygdala, right/left nucleus accumbens, and the brainstem.

5.2.3.3. BBB leakage analysis

Contrast extravasation due to cross-BBB leakage leads to increased T1-weighted signaling in the affected tissue, allowing the calculation of the contrast leakage-rate. To achieve this, T1-weighted images acquired continuously post contrast-injection are first registered and normalized to MNI coordinates using SPM12 (University College London, www.fil.ion.ucl.ac.uk/spm). The signal magnitudes of the T1-weighted images are then converted to contrast concentration values,³² and concentration-time curves are constructed for every brain voxel. The concentration-time curves can next be fitted to one of several pharmacokinetic models, allowing the calculation of parameters corresponding to leakage-rates. We used the linear model^{17,18,24,34} which estimates the leakage rate K_i (mMol/min) by calculating the slope of each concentration-time curve between 6-20 min. To compensate for inter-subject variabilities (due to heart rate, blood flow, or rate of contrast injection), each voxel's leakage-rate was normalized to that of the superior sagittal sinus, resulting in a dimensionless leakage-rate measure. With each voxel represented by the calculated leakage-rate, 3D maps of BBB leakage were constructed for each subject. Leakage-rates were considered pathological when exceeding 0.02, the 95th percentile of all values in a cohort of control subjects.¹⁸ The percent of suprathreshold voxels was used as a measure reflecting overall BBB leakage.

To identify individuals with overall BBB leakage significantly different from the majority of participants, we applied an outlier analysis. The Median Absolute Deviation (MAD) approach was used for outlier identification, as it is more robust than traditional thresholding using standard deviations around the mean.³⁵ We calculated the median value of all 74 subjects (65 SLE and 9 controls) and the median of absolute deviations from the median. The threshold for abnormal values was defined as the median plus two medians of absolute deviations from the median. Participants with overall BBB leakage above this threshold were considered outliers, and this group was termed “extensive BBB leakage”.

The 3D BBB leakage maps were segmented in accordance with the VolBrain atlas.³³ BBB leakage within the above-detailed 23 structures was calculated as the percent of each structure's voxels with suprathreshold leakage (i.e., leakage-rates exceeding 0.02).

5.2.4. Statistical analysis

Continuous variables were compared using the Wilcoxon rank sum test, and categorical variables using the Chi-square test. The false discovery rate method was used to correct for multiple comparisons.

5.3. Results

5.3.1. Demographic and clinical characteristics

The 65 SLE patients were predominantly Caucasian (89%) and female (87.7%), with a mean age of 48.9 ± 13.3 years (Table 4). The median disease duration was 14 years (1 – 44), with a mean \pm SD of 15.1 ± 10.5 . Cumulative disease manifestations, medication utilization and autoantibodies reflected the general lupus population,³⁹ with low generalized disease activity and modest organ damage.

Prior NP events from all causes occurred in 50/65 (77%) patients and NP events attributable to SLE were present in 15/65 (23%). The latter included transient ischemic attacks (n=4), stroke (n=3), cranial neuropathy (n=3), seizure disorder (n=2), acute confusional state (n=2), psychosis (n=2) and aseptic meningitis (n=1). Neuropsychological testing was omitted in one patient who was not a native English speaker. Impairment in one or more cognitive tests was present in 31/65 (47.7%) patients. This included deficits in information processing speed (11%), attention span (22%), new learning (4.7%), delayed recall (12.5%) and executive abilities (22%).

5.3.2. A sub-group of SLE patients have extensive BBB leakage

3D maps of BBB leakage-rates were calculated for all SLE patients and controls (Figure 20A). Compared to controls, SLE patients had significantly higher brain volumes with pathological BBB leakage ($p=0.04$, Figure 20B). Outlier analysis was applied to identify subjects with abnormally high overall BBB leakage, termed “extensive BBB leakage”. Notably, all sixteen individuals identified as outliers were SLE patients. Those with lower levels of BBB leakage included all controls and 49 SLE patients. As SLE patients within this group had BBB leakage comparable to controls ($p=0.3$, Figure 20B), SLE patients within this group were considered to have normal BBB function.

Table 4 – Demographic and clinical features of SLE patients			
	SLE (n=65)	Controls (n=9)	P
Female (%)	87.7	66.7	0.1
Age (years) (mean ± SD)	48.9 ± 13.3	51.8 ± 9.4	0.4
Race/Ethnicity			0.4
Caucasian (%)	89	100	
Other (%)	11	0	
Years of education (mean ± SD)	15.3 ± 3.1	20.9 ± 2.8	3·10 ⁻⁴
Smokers (%): Current/Ever	11/37	0/22.2	0.3/0.4
Disease duration (yr) (mean ± SD)	15.1 ± 10.5	-	
Cumulative ACR manifestations (%)			
Malar rash	43	-	
Discoid rash	7.7	-	
Photosensitivity	49	-	
Oral/nasal ulcers	57	-	
Serositis	31	-	
Arthritis	77	-	
Renal disorder	31	-	
Neurological disorder	11	-	
Hematologic disorder	86	-	
Immunologic disorder	85	-	
Antinuclear antibody	100	-	
Prior NP events (%)	77	0	
Prior NP events attributed to SLE (%)	23	-	
SLEDAI-2K score (mean ± SD) with/without NP variables	2.8 ± 3.4/2.8 ± 3.4	-	
*SLICC/ACR damage index score (mean ± SD) with/without NP variables	1.1 ± 1.2 /0.8 ± 1	-	
Medications (%)			
Corticosteroids	9.2	-	
Antimalarials	72.3	-	
Immunosuppressants	47.7	-	
ASA/clopidogrel	15.4	-	
Warfarin	10.8	-	
Psychoactive drugs	40	-	
Autoantibody positivity N (%)			
Lupus anticoagulant	27.7	-	
Anticardiolipin	17	-	
Co-morbidities (%):			
Hypertension	13.8	33.3	0.14
Diabetes	4.6	0	-

The Wilcoxon rank sum test and Fisher test were used for comparison of continuous and categorical data, respectively. NP, Neuropsychiatric; SLEDAI-2K, Systemic Lupus Erythematosus Disease Activity Index 2000; SLICC/ACR, Systemic Lupus International Collaborating Clinics/American College of Rheumatology.

Figure 20 – A sub-group of SLE patients have extensive BBB leakage

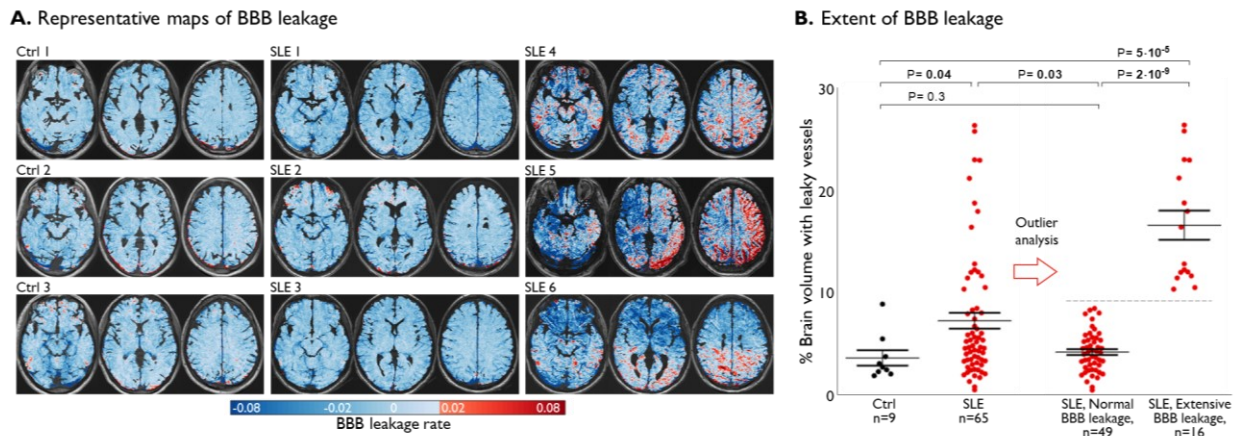


Figure 20. A sub-group of SLE patients have extensive BBB leakage. A. The rate of BBB leakage was quantified for every brain voxel, with shades of blue representing tissue with non-permeable BBB and shades of red representing contrast agent accumulation due to BBB leakage. A qualitative review of leakage maps in these selected cases illustrates that some SLE patients are visually comparable to controls, while others exhibit visibly higher number of voxels with BBB leakage. B. The percent of brain volume with BBB leakage was quantified for each subject, revealing a significant difference between SLE patients and controls ($p=0.04$). Outlier analysis of all 74 participants identified a group with “extensive BBB leakage”, consisting of 16 SLE patients; and a group termed “normal BBB leakage”, consisting of 9 controls and 49 SLE patients.

5.3.3. Extensive BBB leakage in SLE patients is associated with smaller gray matter volume

Volumetric comparison of 23 brain structures revealed that SLE patients with extensive BBB leakage had significantly smaller cerebral gray matter volumes compared to controls (right and left, $p=0.04$, corrected for multiple comparisons, Figure 21A). To examine whether the decrease in cerebral gray matter volume was associated with structure-specific BBB leakage, we compared the extent of BBB leakage within the 23 structures between the two SLE groups and controls. While the volumetric differences were restricted to cortical gray matter, differences in BBB leakage were present in all 23 structures ($p<0.001$, corrected for multiple comparisons, Figure 21B).

Figure 21 – Extensive BBB leakage in SLE patients is associated with smaller gray matter volume

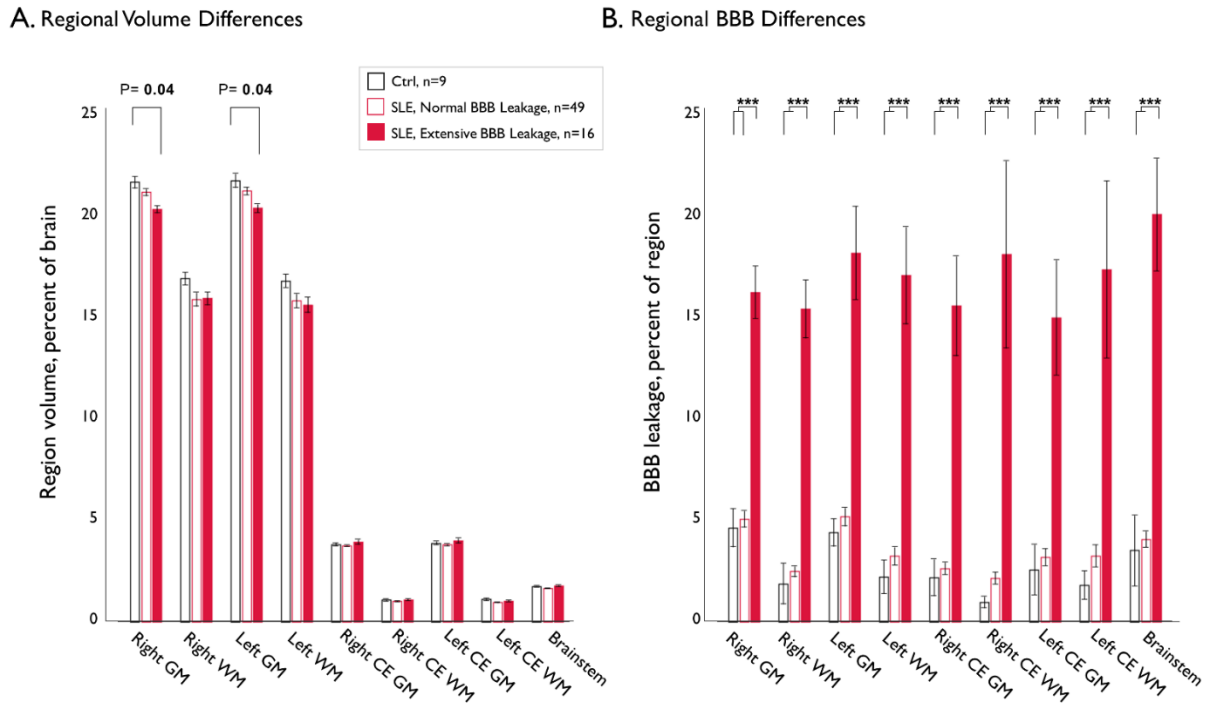


Figure 21. Extensive BBB leakage in SLE patients is associated with smaller gray matter volume. **A.** Depiction of the nine largest brain structures (of the 23 regions compared between the groups) illustrates the reduced right- and left- gray matter volumes in patients with extensive BBB leakage compared to controls ($p=0.04$, corrected for multiple comparisons). There were no volumetric differences in any other regions. **B.** Comparison of BBB leakage in the same 23 brain structures revealed that the ‘extensive BBB leakage group’ had higher levels of leakage in all regions (the same nine regions are depicted in B and A), compared to patients with normal BBB leakage and controls ($p\leq 0.001$, corrected for multiple comparisons). The Wilcoxon rank sum test was used to compare between the groups, and the false discovery rate algorithm was used to correct for multiple comparisons. Error bars denote standard error of the mean. Asterisks denote level of significance, with $***p\leq 0.001$. GM, gray matter; WM, white matter; CE, cerebellum.

5.3.4. Extensive BBB leakage in SLE patients is associated with cognitive impairment

Compared to patients with normal BBB leakage, patients with extensive BBB leakage had poorer delayed recall ($p=0.034$, Figure 22A) and worse overall cognitive test performance (averaged Z-score of five cognitive tasks, $p=0.02$). Impairment in ≥ 1 cognitive task was present in 47.7% of the total SLE sample, but occurred in 75% of patients with extensive BBB leakage, compared to only 38.8% of patients with normal BBB leakage ($p=0.01$, Figure 22B). Testing for potential

confounders (Table 5) revealed that the groups were similar in age, use of medications, prior NP events due to any cause and those attributed to SLE, disease activity (SLEDAI-2K), cumulative organ damage (SDI), and rates of hypertension and diabetes mellitus, but that patients with extensive BBB leakage were more likely to be active smokers ($p=0.03$).

Figure 22 – Extensive BBB leakage in SLE patients is associated with cognitive impairment

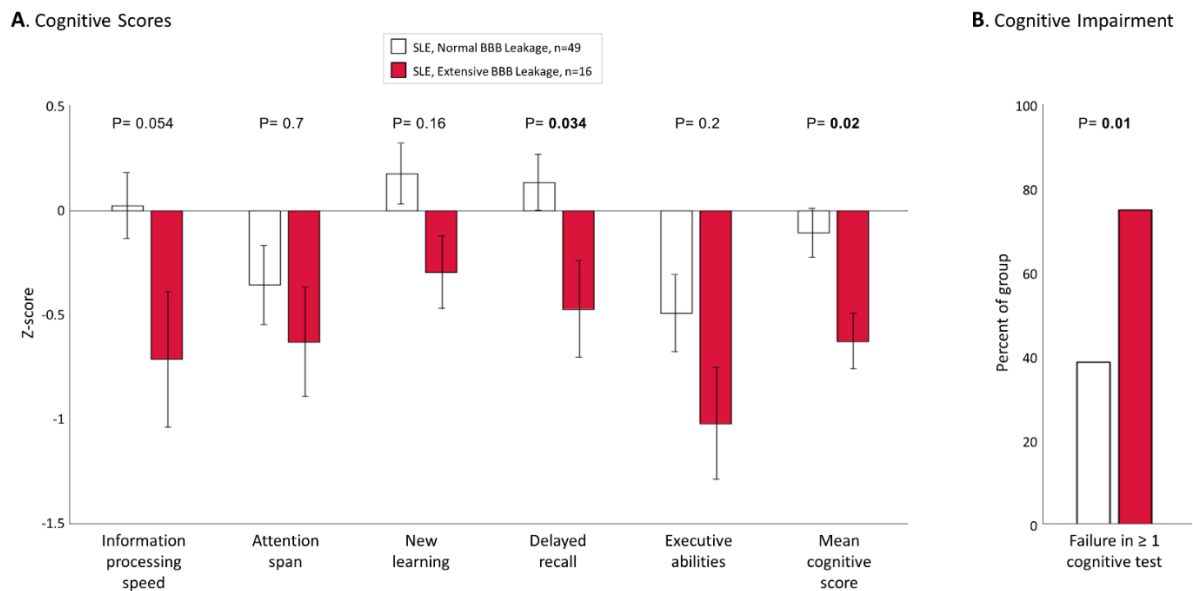


Figure 22. Extensive BBB leakage in SLE patients is associated with cognitive impairment. A. SLE patients with extensive BBB leakage had worse delayed recall and lower mean cognitive scores (averaged Z-scores of the selected test scores representing each broad cognitive domain) compared to patients with normal BBB leakage ($p=0.02$, Wilcoxon rank sum test). B. The extensive BBB leakage group also had a significantly higher percent of subjects failing at least one cognitive test ($p=0.01$, chi-square test). Error bars denote standard error of the mean.

Table 5 – Comparison between SLE patients with extensive versus normal BBB leakage			
	Normal BBB Leakage (n=49)	Extensive BBB Leakage (n=16)	P Value
Percent of brain volume with pathological leakage	4.2 ± 2	16.5 ± 5.7	2·10 ⁻⁹
Female (%)	87.8	87.5	1
Age (years) (mean ± SD)	48.7 ± 13.4	49.5 ± 13.6	0.8
Race/Ethnicity			0.8
Caucasian (%)	89.8	87.5	
Other (%)	10.2	12.5	
Years of education	15.5 ± 3.2	14.9 ± 3	0.5
Smokers (%): Current/Ever	6.1/30.6	25/56.3	0.03/0.06
Disease duration (yr) (mean ± SD)	16.5 ± 10.5	11 ± 9.8	0.052
Prior NP events (%)	79.6	68.8	0.40
Prior NP events attributed to SLE (%)	22.4	25	0.8
SLEDAI-2K score (mean ± SD) with/without NP variables	2.4 ± 2.4 / 2.4 ± 2.4	4 ± 5.4 / 4 ± 5.4	0.6/0.6
SLICC/ACR damage index score (mean ± SD) with/without NP variables	1 ± 1.1 / 0.9 ± 1	1.1 ± 1.5 / 0.8 ± 1.1	0.8 / 0.6
Medications (%)			
Corticosteroids	10.2	6.25	0.6
Antimalarials	71.4	75	0.8
Immunosuppressants	42.9	62.5	0.2
ASA/clopidogrel	18.4	6.25	0.2
Warfarin	10.2	12.5	0.8
Psychoactive drugs	42.9	31.3	0.4
Autoantibody positivity N (%)			
Lupus anticoagulant	26.5	31.25	0.7
Anticardiolipin	14.3	25	0.3
Co-morbidities (%):			
Hypertension	14.3	12.5	0.9
Diabetes	6.1	0	0.3

The Wilcoxon rank sum test and Chi square test were used for comparison of continuous and categorical data, respectively. NP, Neuropsychiatric; SLEDAI-2K, Systemic Lupus Erythematosus Disease Activity Index 2000; SLICC/ACR, Systemic Lupus International Collaborating Clinics/American College of Rheumatology.

5.4. Discussion

The proposed pathogenesis of NPSLE involves variable autoimmune-mediated pro-thrombotic and pro-inflammatory mechanisms.^{3,4,36} Micro-vascular damage is common in many organs affected by SLE³⁷ and has been found in brains of SLE patients examined postmortem.¹⁴ While impairment of the BBB may be a core component of the pathogenesis of NPSLE^{12,13} the evidence for this remains indirect and circumstantial,^{14,38,39} as clinical tools for diagnosing BBB dysfunction are lacking. In the current study we employed DCE-MRI to quantify BBB permeability directly and objectively in 65 ambulatory SLE patients. We found associations of extensive BBB leakage with reduced cortical gray matter and with concurrent cognitive impairment. These findings are a key step in establishing the role of BBB dysfunction in the pathogenesis of NPSLE and highlight the BBB as a potential diagnostic and therapeutic target.

The BBB provides the major physical interface between the circulation and the brain,¹³ regulating the passage of substances in and out of brain neuropil and maintaining the chemical environment needed for normal neuronal function. This control occurs through tightly connected endothelial cells, and the pericytes and astrocytes surrounding the endothelium. Dysfunction of the BBB allows leakage of blood components into the brain neuropil, triggering inflammatory processes that alter glial function, extracellular-matrix composition, neuronal connectivity, and neuronal function. One widely studied example is the inflammatory cascade initiated when albumin, a large serum protein, enters the brain. Albumin binds to astrocytes and activates the pro-inflammatory TGF- β cascade, resulting in neuronal hyperexcitability and delayed neurodegeneration.⁶ Similarly, thrombin and activated protein C enhance neuronal excitability in the brain.⁵

In SLE, autoantibodies and inflammatory mediators may be responsible for BBB leakage.⁴⁰ Anti-ribosomal P and anti-NR2 autoantibodies,¹¹ associated with NPSLE, were shown to bind the surface of cultured endothelial cells, causing endothelial activation, upregulation of adhesion molecules, and increased production of cytokines such as IL-6. Complement activation products, including C5a generated by immune complexes, can cause in vitro BBB disruption and apoptosis of

endothelial cells in an animal model of SLE.¹⁰ Once the BBB is breached, circulating autoantibodies (including anti-ribosomal P⁷ and anti-NR2 antibodies)⁸ can access the brain and bind to neuronal cells, causing apoptotic cell death,^{7,8} as well as microglial activation, synaptic pruning and reduced synaptic density.⁹

Non-SLE specific mechanisms such as hypertension, systemic infection and cigarette smoking can also injure endothelial cells and increase BBB permeability.^{41,42} More frequent in SLE patients, these variables may be viewed as modifiable risk factors for BBB dysfunction. Our data revealed an association between current cigarette smoking and extensive BBB leakage in our SLE cohort. This finding is supported by experimental evidence that tobacco smoke disrupts endothelial tight-junctions,⁴³ and generates highly reactive oxygen species that cause oxidative damage.⁴⁴

Our study focused on cognitive impairment as a clinical phenotype of NPSLE. Neuropsychological testing permitted a standardized and objective determination of cognitive impairment, which can be regarded as both a subset of NPSLE and an indicator of overall brain health. A recent review reported 38% point prevalence (95% CI: 33-43) of cognitive impairment in SLE patients.¹ Our study identified a comparable prevalence of 47.7% that is similar to previously reported studies.² Our patients were ambulatory with stable SLE and participated regardless of cognitive symptoms. It is, therefore, striking that extensive BBB leakage was found in 24.6% of patients, and one might anticipate an even higher prevalence in SLE patients with more overt NPSLE manifestations. The fact that not all patients with cognitive impairment had extensive BBB leakage is not surprising, since impaired cognition can result from a variety of factors, including many unrelated to SLE. However, patients with extensive BBB leakage were twice as likely to have cognitive impairment compared to those with normal BBB function, suggesting that the BBB plays an important role in this NPSLE manifestation. Notably, while 77% of patients had a history of NP events, none had clinically active NP events during the study which may account for the lack of association between extensive BBB leakage and NP events in our cohort.

In early BBB studies, evidence for BBB leakage was inferred from CSF proteins that are normally restricted to the peripheral circulation (e.g. albumin¹³ and immunoglobulin G⁴⁵). However, the presence of these proteins in the CSF can result from BBB-unrelated factors, such as blood-CSF barrier dysfunction (i.e. damaged choroid plexus epithelium) or meningeal barrier dysfunction (i.e. damaged arachnoid epithelium).¹³ These barriers differ significantly from the BBB, the capillaries of

which penetrate deep into the brain parenchyma. To address the limitations of CSF markers, BBB studies have evolved to MRI-based BBB assessment that allows calculation of cross-BBB contrast leakage in every voxel of the brain. Such studies have already demonstrated BBB dysfunction in patients with multiple sclerosis,¹⁹ stroke,²⁰ traumatic brain injury¹⁸ and dementia.²¹ Two recent pilot studies demonstrated the proof-of-concept of MRI-based BBB assessment in 6 adult SLE patients (focusing on 5 regions of interest),²² and in 11 children with SLE (using arterial spin labeling).⁴⁶ While limited by small sample sizes, both studies reported increased BBB leakage in SLE patients compared to controls (finding lower cognitive performance in the 6 adult patients and normal cognition in the 11 children with SLE). Here we studied BBB leakage in a cohort of 65 patients, confirming higher levels of leakage compared to controls, and revealing that this difference is driven by a sub-group of SLE patients. Our results further demonstrate that compared to the rest of the SLE cohort, this sub-group had worse cognitive performance, and smaller cortical gray matter volumes, a finding commonly associated with neurodegenerative dementias. These findings support the hypothesis that BBB leakage may mediate neurodegeneration in SLE, leading to loss of gray matter and cognitive impairment. Our findings also highlight the potential of BBB imaging as a biomarker for identifying SLE patients at risk of cognitive decline.

Strengths of our study include the lack of explicit recruitment bias, and the temporal proximity between clinical and neuroimaging protocols, usually within 6 hours. Longitudinal studies of cognition in SLE indicate that impairments can be subtle and evanescent.⁴⁷ Thus, the short interval between neuroimaging and cognitive-testing increases the biological plausibility of the observed associations. Our study reflects the demographic characteristics of SLE patients in our clinic⁴⁸ but may not be applicable to younger SLE patients with more diverse race/ethnicity and shorter disease duration. The small number of controls and the sample size of our SLE cohort were additional limitations, precluding a more detailed examination of associations between BBB permeability in specific brain regions and scores in specific cognitive tests. A more comprehensive cognitive battery (allowing precise distinction between cognitive domains) and a larger sample size are needed to address this important question. Additionally, our imaging protocol required a gadolinium-based contrast that may be a concern in patients with substantial renal impairment. The use of contrast-free BBB imaging (e.g. arterial spin labeling), or identification of reliable serum-based markers of BBB dysfunction, may allow wider applicability of BBB pathology as a screening biomarker.

The current study provides the first compelling evidence for a link between extensive BBB leakage and cognitive impairment within a sample of SLE patients. Future longitudinal studies are needed to examine changes in BBB permeability over time and whether concurrent presence of circulating autoantibodies increases the risk of cognitive impairment or other NPSLE features. Our findings also highlight the need to clarify the exact mechanisms underlying BBB damage and subsequent neuronal dysfunction in SLE, and the therapeutic potential of treatments targeting these mechanisms.

Chapter 6 – Discussion

Chapter Overview

The research presented in this thesis adds to the current understanding of altered BBB influx – termed BBB leakage, and its role in human neuro-pathologies. The three peer-reviewed studies that comprise the results chapters targeted several unknowns in the mechanisms mediating BBB leakage, the changes triggered by BBB leakage, clinical diagnosis of BBB leakage, and clinical symptoms associated with BBB leakage. As each of the results chapters presented a detailed discussion of our findings, their interpretation and significance, here I will focus on positioning the findings in the broader context of BBB research. I will revisit the open questions presented in section 1.1.5.1 of the introduction chapter, and discuss the insights added by the current work and other relevant studies in the field. In Figure 23, I provide an overview of the proposed mechanistic framework for clinical symptoms associated with BBB leakage.

6.1. What is BBB leakage?

6.1.1. How does endothelial selectivity change?

Altered endothelial selectivity may involve changes in the function of any one of the selectivity mechanisms reviewed in section 1.1.4.1 (and Figure 3), including tight junctions, specific and non-specific influx transporters/vesicles, efflux transporters, and enzymes. In this thesis I studied the pathological role of increased cross-BBB influx from the bloodstream into the brain, and will use the term ‘BBB leakage’ to refer to this aspect of altered endothelial selectivity. Mechanisms related to modified cross-BBB efflux will be discussed later in this chapter (section 6.6.3).

Until recently, the prevailing hypothesis in BBB research presumed that BBB leakage occurs when the gaps between endothelial cells are no longer sealed by tight junctions. This hypothesis is reflected in the early term used to describe BBB pathology – ‘BBB breakdown’. First appearing in literature in 1975, the term suggests that leakage across the BBB is a result of structural break-down of its components, creating robust diffusion from the capillary to the extra-capillary space. Notably, this assumption shaped the Tofts pharmacokinetic model of BBB leakage,¹ developed by Paul Tofts

in the 1990s and still widely used today. The approach characterizes fast and robust leakage occurring during bolus wash-in of contrast into the brain (first ~3 or 5 minutes following contrast injection), and has been shown to be highly useful for the detection of brain tumors (supplied by newly-formed blood vessels that lack a functional BBB), and the identification of BBB leakage in the core of ischemic/traumatic lesions.²⁻⁴ However, accumulating evidence suggests that this method fails to detect leakage in neurological disorders that are not associated with clear anatomical abnormalities or in non-lesion tissue.⁵

The present thesis used the Veksler pharmacokinetic model to examine whether it can detect subtle BBB leakage in patients without gross anatomical abnormalities. Using this approach, we characterized BBB leakage occurring during the slow phase of contrast washout from the brain (6-20 minutes following contrast injection) in patients with lupus and bipolar disorder. Our results revealed slow BBB leakage in ~25% of patients in each cohort.^{6,7} As the time scale of the observed leakage is likely to reflect the temporal properties of trans-endothelial trafficking,⁵ our findings suggest that BBB leakage does not necessarily equate structural BBB breakdown, and may in fact, involve altered endothelial function. Not only do we show that this approach is sensitive to BBB leakage in brains lacking overt anatomical abnormalities; but we also report a link between subtle leakage and neuropsychiatric symptoms.^{6,7}

The modifiable nature of trans-endothelial selectivity is supported by several animal studies. Early experimental evidence came from a 2013 collaboration between our group and Dr. Jens Dreier.⁸ The study demonstrated that the large protein albumin (normally absent from the brain) can cross the leaky BBB of live rats, while the passage of smaller molecules remains barred and tight-junctions remain intact.⁸ More recent support for these findings comes from rodent studies showing that increased trans-endothelial influx underlies BBB leakage in the aging brain,⁹ and following traumatic brain injury.¹⁰ This transport was further shown to involve the trafficking of plasma proteins across the endothelium via non-specific caveolin vesicles – the expression of which is suggested to be upregulated in pathological conditions.⁹⁻¹¹ In a parallel study by our group (Swissa et al., in preparation), we too show increased trans-endothelial trafficking of proteins across the leaky BBB, likely mediated by caveolin vesicles. Together, these results disprove the earlier assumptions equating all BBB leakage to free diffusion between broken-down junctions. These findings further suggest that subtle trans-endothelial BBB leakage involves altered expression of endothelial

transport mechanisms, and underscore the importance of future research into the role of altered trans-endothelial selectivity to blood-borne molecules.

The potential role of fast/para-endothelial leakage in neuropsychiatric symptomatology also requires in-depth characterization. Reports that support this hypothesis include studies in stress⁹⁵ and schizophrenia,⁹⁶ showing downregulated expression of the tight-junction protein Claudin-5.^{95,96} Notably, accumulating evidence suggests that schizophrenia is associated with genes that regulate both trans- and para- endothelial leakage.⁹⁷⁻⁹⁹ A better understanding of alterations in both leakage mechanisms in different neuropsychiatric disorders may allow the development of new mechanism-specific treatments.

6.1.2. What transformations take place in non-endothelial neurovascular unit elements?

In the previous section I discussed the endothelial transformation associated with BBB leakage. Here, I will focus on the transformation of the other cellular elements of the neurovascular unit (NVU) – astrocytes, microglia, pericytes and neurons.

Thus far, the most extensively studied NVU cells in the context of BBB leakage have been the glial cells – astrocytes and microglia. A plethora of studies have linked BBB leakage to the activation of astrocytes and microglia, and subsequent initiation of a neuroinflammatory response (secretion of cytokines and chemokines, and recruitment of other immune cells).¹²⁻¹⁵ However, the causal link between these events is far from trivial, with evidence showing that neuroinflammation is both secondary to BBB leakage and can cause BBB leakage. In fact, the current consensus in the field is that BBB leakage and neuroinflammation act in a self-reinforcing feedback loop,¹⁶ that amplifies both processes (Figure 23). Hence, whether glial activation triggers the initial leakage or is triggered by it – is likely to be case-dependent.

Pericytes and neurons are critical for proper embryonic development of the BBB,¹⁷⁻¹⁹ however, their role in BBB leakage in the adult brain remains incompletely understood. The experimental part of this thesis was the first to reveal that neuronal hyperexcitation leads to injury of pericytic mitochondria and subsequent pericyte rigor.²⁰ Pericytic injury is then followed by BBB leakage and reduced dilation of capillaries/arterioles in response to neuronal activation – i.e., impaired neurovascular coupling.²⁰ These results suggest that a transformation in pericyte function is likely to contribute to the altered selectivity of the brain's endothelium. The mechanisms underlying pericyte

injury may involve neuronal release of glutamate,^{21–23} while pericyte-mediated changes in endothelial selectivity may involve the vascular endothelial growth factor (VEGF) pathway²⁶ and matrix-metalloproteinase activation.²⁷ The exact mechanistic chain of events requires further research.

6.2. What causes BBB leakage?

While our animal study focused on the mechanisms underlying BBB leakage following seizures, BBB leakage can result from various types of brain pathologies and systemic immune-diseases:

- a) Brain pathologies that have been associated with BBB leakage can be further subdivided into:
 - Acute brain insults, such as seizures, ischemic/hemorrhagic stroke, tumors, brain infection, and traumatic brain injury.²⁸
 - Neuro-inflammatory disorders, such as multiple sclerosis, dementia, Alzheimer's disease, aging, amyotrophic lateral sclerosis (ALS) and Parkinson's disease.²⁹
- b) Systemic immune-diseases that have been suggested to induce BBB leakage include sepsis,³⁰ lupus,⁶⁹ insulin resistance,³¹ and diabetes melitus.³²

The studies conducted in this thesis explored mechanisms of BBB leakage following seizures (in animals) and clinical correlates of BBB leakage in patients with lupus and bipolar disorder. Here, I will discuss the current understanding of mechanisms causing BBB leakage in these disorders.

6.2.1. How do seizures cause BBB leakage?

Seizures have long been on the list of brain insults that result in BBB leakage,^{33,94} however, the mechanisms underlying seizure-induced BBB leakage remain largely unknown. The animal experiments conducted in this thesis were the first to directly explore how seizures cause BBB leakage both in-vitro and in-vivo. Our findings suggest that seizures trigger pericyte injury that, in turn, leads to BBB leakage.²⁰ Our study has also examined whether increased production of free radicals (reactive oxygen species – ROS) contributes to the observed pericytic damage. Notably, our data did not support the involvement of this mechanism, highlighting the potential mechanistic-role of alternative processes, such as increased neuronal release of glutamate.^{21,22} While neurogenic inflammation has also been suggested to contribute to seizure-induced cellular damage,^{24,25} whether neuronal inflammatory signaling can be fast enough to underlie the rapid pericytic injury observed

in our experiments remains to be examined. As stated in the previous section, how pericytes alter BBB selectivity also requires further exploration.

6.2.2. How does lupus cause BBB leakage?

In lupus, autoimmune antibodies circulate the bloodstream, interacting with different organ tissues and inducing inflammatory responses.^{34,35} Hence, the prevailing hypothesis in lupus research states that inflammatory factors interact with the BBB and cause increase in its permeability.³⁴ However, while there is general consensus regarding the role of inflammation in causing BBB leakage, there is an ongoing debate regarding the site of the inflammatory interaction with the BBB.¹⁰⁰ Some experimental evidence suggests that immune factors in the bloodstream interact with the BBB at the endothelial lumen;^{34,35} other studies suggest that immune cells migrate into the brain's CSF via the lymphatic system³⁶ or the choroid plexus³⁷ and interact with the BBB at the abluminal space (in the network of clearance channels formed by astroglial cells around medium-sized blood vessels).³⁷ Further research is needed to better understand the inflammatory interactions resulting in BBB leakage in lupus patients, and whether they take place at the luminal and/or abluminal BBB surface.

6.2.3. How does insulin-resistant bipolar disorder cause BBB leakage?

Our study in patients with bipolar disorder revealed that all patients with extensive BBB leakage were also insulin resistant. This finding highlights the likelihood of a causal link between insulin resistance and BBB leakage. Indirect support for this hypothesis comes in several forms: a) shared inflammatory profiles that have been separately identified in BBB leakage and insulin resistance (e.g., the VEGF pathway and protein kinase C signaling);³¹ b) animal studies showing that high levels of serum glucose (hyperglycemia) trigger inflammation and BBB leakage;³⁸⁻⁴⁰ and c) studies in type 2 diabetes implicating chronic inflammation as a cause of BBB leakage.³¹ However, despite the probable role of inflammation in mediating BBB leakage in patients with insulin resistance, this inflammatory cascade and its effect on BBB selectivity is only partially understood. Future studies are needed to elucidate how systemic inflammation transforms BBB function.

6.3. How does BBB leakage mediate changes in brain function?

As discussed in section 6.2, BBB leakage can be a result of brain insults, neuro-inflammatory disorders, and systemic immune diseases. Accumulating evidence suggests that BBB leakage is not

only a consequence of these conditions, but may also play a critical role in their pathophysiology and progression.^{28,41,42} Animal studies by our group and others demonstrate that BBB leakage, in itself, mediates changes in neuronal function and connectivity that can result in seizures and neurodegeneration.^{13,43} These findings have been confirmed in animal models of brain insults such as traumatic brain injury, stroke and seizures, showing that mechanisms triggered by BBB leakage play key roles in the sequela of these neuropathologies.^{28,41,42} While the exact underlying mechanisms are not fully known, existing literature in this field converges on the role of BBB-triggered inflammation.⁴⁴⁻⁴⁶ For simplicity, from here on, I will use the terms ‘neuro-inflammation’ and ‘systemic inflammation’ to distinguish between inflammation in the brain and peripheral inflammation.

Notably, the interplay between neuro-inflammation and BBB leakage is complex and multifaceted. The two processes can cause and amplify each other in a feedback-loop analogous to the chicken-and-the-egg conundrum.⁴⁷ Altered BBB function has been shown to trigger neuro-inflammation in several ways, including: a) failure to restrict blood-to-brain influx of neurotoxic macromolecules (e.g., serum albumin) that trigger astroglial activation,⁴⁴⁻⁴⁶ b) failure to expel noxious waste products,^{48,49} and c) recruitment of systemic pro-inflammatory cells.^{37,50}

Neuro-inflammatory signaling can, in turn, lead to neuronal damage either directly,²⁴ or by first altering the connectivity of the neuronal network.⁵² In 2009, the Friedman group has identified the pathogenic role of the neuro-inflammatory TGF- β pathway (transforming growth factor beta) in neuronal damage triggered by BBB leakage.^{45,51} The pathway was found to be activated by the interaction of extravasated albumin with astrocytes,^{45,51} leading to astrocytic transformation,^{45,51} secretion of pro-inflammatory cytokines (including interleukin-6, interleukin-1 β and TNF α),^{12,24} modified expression of astrocytic transporters,⁵¹ and altered ionic homeostasis.⁴⁵ In 2015, we revealed that the TGF- β cascade also re-organizes the neural network (by stimulating the growth of new excitatory neuronal synapses), shifts the network balance toward excitation versus inhibition, and lowers the threshold for seizure activity.⁵² The increased propensity to seizures may then result in further cellular damage via increased glutamatergic neuronal signaling.²¹⁻²³

The experimental chapter of this thesis explored another major hypothesis linking BBB leakage and neuronal injury. Specifically, we tested whether BBB leakage mediates neuronal damage by causing oxygen deficiency. This hypothesis assumed that BBB leakage is associated with impaired

neurovascular coupling and subsequent inability of the vasculature to supply sufficient oxygen to meet neuronal energy demands.^{53–55} Our *in-vivo* and *in-vitro* results confirmed the first part of the hypothesis: BBB leakage is, indeed, associated with impaired neurovascular coupling and gradual decrease in the responsiveness of both capillaries and arterioles to neuronal activity.²⁰ Notably, contrary to the second part of the hypothesis, we found that focal loss of neurovascular coupling did not result in hypoxia, suggesting that widespread hypoxia may not be a primary mediator of tissue damage associated with BBB leakage. These results can be explained by what is referred to as the ‘oxygen paradox of neurovascular coupling’, arguing that oxygen supply to neuronal tissue evolved to surpass even extreme increases in energy demands.⁵⁶ According to this hypothesis, the blood-flow responses to neuronal activation normally overshoot the required levels of oxygen, as a safeguard protecting brain tissue against fluctuations in oxygen supply and neurovascular coupling.^{56,57} Together these results suggest that BBB leakage is indeed associated with impaired neurovascular coupling, yet not necessarily hypoxia, due to protective oversupply of oxygen to the brain. However, the effects of long-term neurovascular un-coupling on tissue oxygenation are yet to be examined, and the full scope of mechanisms contributing to neuronal dysfunction following BBB leakage requires further investigation.

6.4. Is BBB leakage always bad?

Mounting evidence implicates BBB leakage in the development and exacerbation of brain pathologies.^{6,7,20,52,58,59} However, the tight link between BBB leakage and inflammation suggests that BBB leakage may also have physiologically-beneficial effects. Here, like in the rest of the body, the difference may lie in the distinction between transient and chronic inflammation: transient/acute inflammation fights invaders and heals injured tissue, while chronic inflammation may – in itself – cause tissue damage. For instance, the growth of new synapses we have demonstrated following leakage-induced neuro-inflammatory TGF- β signaling is thought to have evolved as a compensatory repair mechanism.⁵² Yet if the neuro-inflammatory activation persists, this repair process may result in overly-connected excitatory neuronal-networks that increase the susceptibility to seizures.⁵²

Additional evidence supporting an adaptive role of transient induction of BBB-leakage and neuro-inflammation comes from studies of white blood cells. White blood cells (mainly lymphocytes T and B) have been shown to regularly enter the brain to provide additional immunosurveillance for

pathogens.^{50,61,62} Upon detection of a pathogen these cells stimulate BBB-mediated signaling that recruits a large number of additional lymphocytes circulating the bloodstream.^{50,61,62} The recruited lymphocytes are trafficked trans-cellularly across the BBB's endothelium and help quell infection and repair injured tissue.^{50,61,62} However, this response can be a double-edged sword: if migration persists it can turn into chronic neuro-inflammation, edema and neuronal damage,⁶² yet blocking this trafficking altogether increases patients' susceptibility to fatal CNS infections.⁶²

Together, these studies emphasize the importance of distinguishing between acute and chronic changes in BBB selectivity. Preliminary results from our lab suggest that adaptive increase in trans-endothelial transport may play a role in strengthening synaptic connections (Swissa et al., in preparation) via an NMDA-dependent pathway.²¹ Swissa et al., show that neuronal stimulation induces a transient increase in trans-endothelial trafficking of sodium fluorescein (a dye that normally does not cross the BBB), and that this transport does not involve lymphocytes. Notably, the trafficking of sodium fluorescein has recently been shown to be carried out by transporters of thyroid hormones involved in synaptic plasticity and angiogenesis.^{63,64} Together, these results suggest that there might be separate mechanisms of adaptive/transient changes in BBB selectivity, the details of which require further characterization.

While animal studies support the pathogenic role of the shift from acute to chronic BBB leakage,^{28,65} whether the leakage we observed in patients with lupus and bipolar disorder reflects an analogous mal-adaptive transition remains unclear. However, if our hypothesis is valid, it may help explain why neurological symptoms do not affect all patients with these disorders equally. We hypothesize that a subset of patients develop long-lasting/recurrent BBB leakage, coupled with neuro-inflammation and subsequent neuronal dysfunction (Figure 23). Future research is needed to delineate the mechanisms involved in acute and chronic BBB leakage, and their physiological/pathological roles.

6.5. Can BBB leakage be diagnosed in living patients and what are the clinical features of BBB leakage?

In the introduction chapter, I have reviewed the existing methods allowing BBB assessment in living patients. These include indirect indicators of BBB leakage, such as serum/CSF markers,⁶⁶⁻⁶⁹ or direct visualization of the human BBB using neuroimaging modalities. While non-imaging markers

have the potential of offering accessible preliminary screening for BBB leakage, the existing markers are considered unreliable,^{70,71} and call for the development of more effective alternatives. As demonstrated in Figure 4, the past several decades have seen a marked increase in the popularity of MRI-based BBB assessment, likely due to its use of non-ionizing radiation (unlike SPECT, CT, and PET imaging), minimal invasiveness (as apposed to intra-operative fluorescence microscopy), and competitive spatial resolution. The introduction also reviewed the important distinction between the approaches currently used for quantifying BBB leakage, with the Tofts method characterizing fast and robust leakage during contrast wash-in and the Veksler method characterizing slow and subtle leakage during contrast wash-out. The Patlak model is not specific to either types of leakages, and has been suggested to capture both.⁷²⁻⁷⁴

To understand the role of subtle BBB leakage in human neuropathology this thesis applied the Veksler approach to the exploration of a two-part hypothesis:

- I. Subtle/slow BBB leakage can be detected in disorders not associated with gross brain abnormalities (e.g., tumors or ischemic/hemorrhagic lesions).
- II. Subtle/slow BBB leakage may be associated with neuropsychiatric complications.

The two clinical chapters of this thesis provided the first concrete evidence of subtle/slow BBB leakage in patients with lupus and patients with bipolar disorder, validating the first part of the hypothesis. Moreover, we discovered that ~25% of patients in each cohort have widespread or ‘extensive’ BBB leakage affecting over 10% of brain tissue. The second part of the hypothesis was also confirmed separately in each cohort, when the neuropsychiatric symptoms of patients with extensive BBB leakage were found to be significantly more severe than of patients without extensive leakage.^{6,7} These results suggest that extensive BBB leakage does not affect all patients, but rather characterizes a sub-population of individuals with worse neuropsychiatric outcomes. Notably, brain volume examination of patients with lupus revealed that extensive BBB leakage is also associated with reduced gray matter volume – suggestive of neurodegeneration commonly found in patients with neurodegenerative dementias.

Our findings emphasize the importance of examining both fast/robust and slow/subtle BBB leakage, as they may represent different leakage mechanisms (para-cellular vs trans-cellular) and phases (severe vs mild).⁵ As all studied patients have been diagnosed with lupus or bipolar disease

for a minimum of a year prior to MRI scanning, these results suggest that the observed leakage is likely to represent either a long-lasting or recurrent change in cross-BBB influx. We suggest that chronic BBB leakage may affect a sub-population of patients, and contribute to the pathogenesis of neurological symptoms, even when the leakage is subtle and trans-endothelial.

We further argue that the nature of the neuropsychiatric symptoms is likely to depend on the specific brain regions and brain networks affected by leakage. This hypothesis is supported by a recent study in patients with dementia, linking BBB leakage in the hippocampus to memory impairment.⁷⁵ We extend this hypothesis to suggest that cognitive impairment may be mediated by BBB leakage in regions/networks associated with executive function and memory, and that mood symptoms (depression/anxiety) may result from leakage in regions/networks associated with reward/affective processing and self-reflection (Figure 23). Larger scale clinical studies are needed to determine the association between specific neuropsychiatric symptoms and region-specific BBB leakage, and further animal studies are required to better understand the molecular mechanisms involved.

Figure 23 – Summary of proposed disease mechanisms

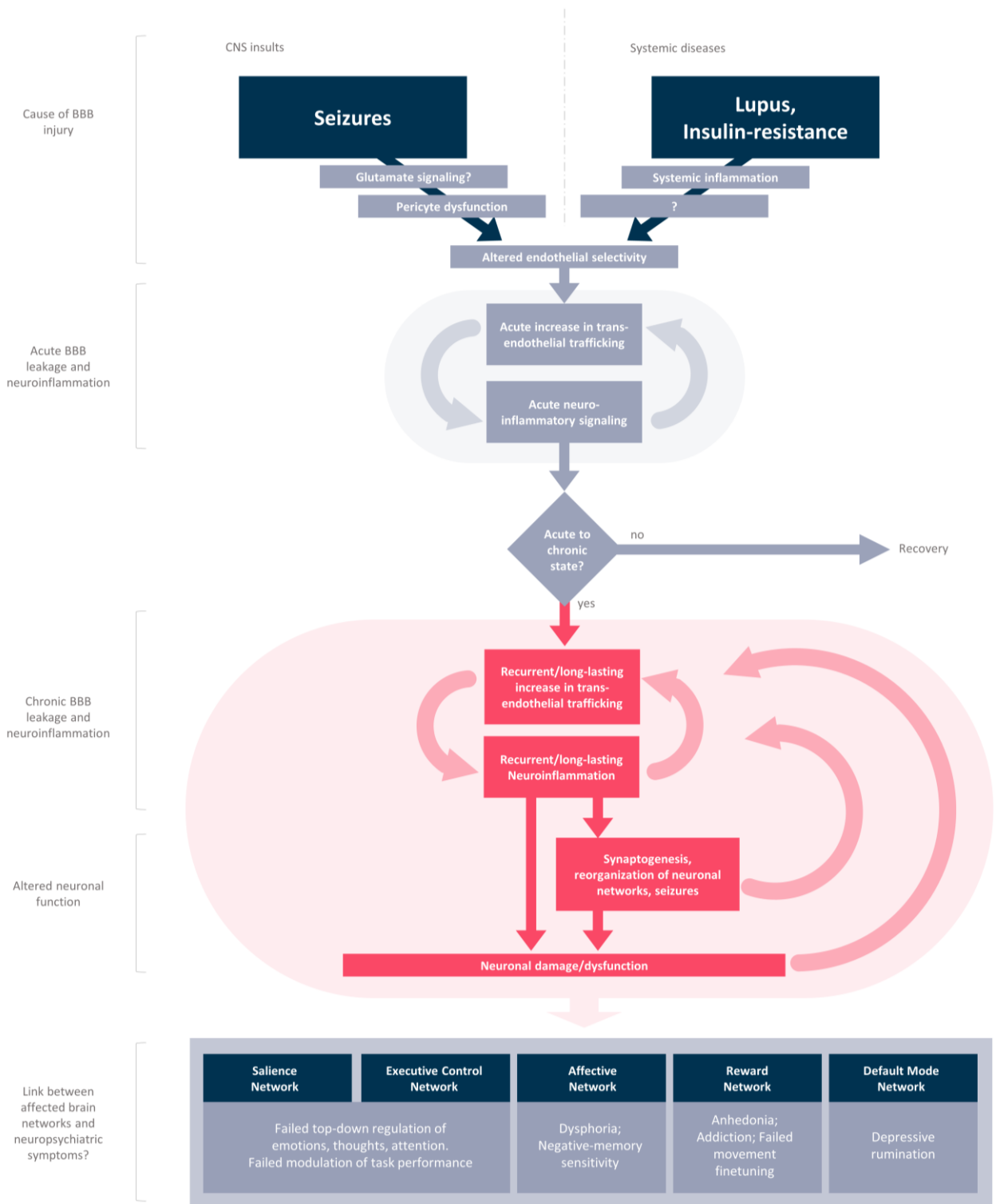


Figure 23. Summary of proposed disease mechanisms. Our findings add several insights to the current framework of BBB-associated pathogenesis. Our animal study has shown that the excessive neural activity during seizures causes pericytic injury (potentially mediated by increased release of glutamate),^{21–23} and subsequent BBB leakage.²⁰ Our clinical studies suggest that BBB leakage can also be caused by systemic inflammation, and that the associated leakage is likely to be mediated by increased trans-endothelial transport.^{6,7} How exactly systemic inflammation causes BBB leakage remains a matter of ongoing debate, with some groups implicating immune interactions at the endothelial lumen,³⁴ while others suggesting that immune cells migrate to the CNS via the lymphatic system and interact with the endothelium at its abluminal side.³⁷ We further propose that BBB-leakage/neuroinflammation may have adaptive roles,^{50,63,64} that can become maladaptive if the processes persist or frequently reoccur. We argue that in a subset of patients, systemic inflammation may underlie a shift from transient/acute to long-lasting/recurrent BBB-leakage/neuroinflammation, creating a chronic amplification loop between leakage and neuroinflammatory signaling (including TGF β , IL6, IL1 β , TNF α),^{12,24,52} that damages neurons directly²⁴ or via excitatory network-reorganization.⁵² Lastly, we hypothesize that the clinical symptoms of affected patients may correspond to the brain regions/networks affected by BBB leakage, and its duration and extent. Testing this hypothesis will require larger cohorts of patients, and will be the focus of future research.

6.6. Future directions

6.6.1. Diagnosing BBB leakage in clinical settings

A large portion of this research was dedicated to the development of a software for DCE-MRI based quantification of BBB leakage. Notably, the software allows the characterization of both fast/robust leakage using the Tofts approach and slow/subtle leakage based on the Veksler method. While the current thesis focused on subtle leakage, we acknowledge the need to provide a comprehensive comparison between the two approaches.

Additionally, the threshold used for distinguishing between normal and abnormal leakage stands to be optimized. At present, the upper threshold for ‘normal’ BBB leakage is based on a control study of 50 healthy individuals.⁷⁶ The study examined the distribution of all leakage values in the control cohort and calculated the 95th percentile as the threshold separating ‘normal’ and ‘abnormal’ leakage. However, we have yet to explore whether the thresholding approach can be optimized to account for innate region-specific differences in cross-BBB influx,⁷⁷ and the effects of age and sex.⁹ As argued earlier, the duration of BBB leakage in different neuro-pathologies also needs to be understood. These questions need to be investigated in comprehensive – and potentially multi-center – studies of healthy volunteers of different ages and sexes, and patients with different pathologies.

Moreover, the thresholding approach classifies leakage rates solely into two categories: normal and abnormal. This division binarizes the continuous values of leakage intensity, disregarding potentially valuable information. Future studies should examine whether nuanced differences in leakage intensity bear physiological and/or diagnostic significance. Future research should also explore whether machine learning algorithms can allow the detection/prediction of specific symptoms/diagnoses based on BBB leakage patterns.

Importantly, the translation potential of the Veksler approach stands to greatly benefit from a simplified MRI acquisition protocol. At present the approach images the brain for 14 minutes (6 to 20 minutes post contrast injection), significantly increasing the duration of routine clinical MRI scans. A shortened protocol would reduce the costs of the procedure and increase the appeal of the approach to clinical centers. This issue may be addressed via analysis of real and simulated data, examining the correlation between the output of the current gold standard and the output of scans with less data points.

The software's computation of T1 relaxation times also stands to be optimized (methods section 2.2.2.2). The current calculation uses the variable flip angle approach, which derives the baseline T1 relaxation times from three scans – each acquired at a different flip angle.¹⁰²⁻¹⁰³ As this approach relies on accurate knowledge of the excitation flip angle, it is sensitive to potential flip angle errors and/or non-uniformities.¹⁰⁴⁻¹⁰⁶ Recent years have seen the emergence of T1 mapping approaches that account for potential flip angle inaccuracies,¹⁰⁴⁻¹⁰⁶ and the incorporation of these techniques into the BBB acquisition protocol and software should be considered.

Lastly, the translation of BBB diagnosis into clinical practice may also be facilitated by the development of contrast-free BBB imaging (e.g., arterial spin labelling),⁷⁸ eliminating the DCE-MRI requirement for the injection of gadolinium-based contrast agents that can exacerbate kidney damage in patients with existing renal pathology.⁷⁹

6.6.2. Understanding the neuro-functional correlates of BBB dysfunction

In the present thesis, I used DCE-MRI to explore the link between imaging evidence of BBB leakage and clinical symptoms in living patients. The next step of this research should characterize the neuro-functional changes that may correspond to the observed symptoms. Specifically, assessment of neuronal activity – using modalities such as EEG (electroencephalogram), MEG

(magnetoencephalogram), and fMRI (functional MRI) – may reveal activation patterns associated with both BBB leakage and clinical disease manifestations. A recent study by our group examined the EEG recordings of patients with epilepsy and Alzheimer’s disease, and showed that regions with BBB leakage are associated with slower neuronal activity.⁸⁰ In an ongoing extension of our lupus study, we are also characterizing BBB-associated changes in network functionality and connectivity using MEG and fMRI data. Additional studies are warranted to determine the effects of BBB leakage on neuronal activity in humans, and to understand the clinical relevance of mechanisms identified in animal studies.

6.6.3. Understanding changes in BBB efflux

My research examined changes in altered transport of substances from the bloodstream to the brain – a.k.a. cross-BBB influx/leakage. However, the BBB has several important functions beyond limiting entry into the brain. The BBB also plays critical roles in regulating homeostatic levels of ions, hormones and peptides in the brain, and removal of waste products from brain tissue into the bloodstream. The most abundant BBB efflux transporters are the P-glycoprotein and breast cancer resistance protein. Notably, in Alzheimer’s disease decreased expression of the P-glycoprotein efflux transporter is suggested to contribute to the accumulation of amyloid beta ($A\beta$) complexes in the brain, along with failure to remove other neurotoxic elements from the brain’s environment.⁸¹ Conversely, epilepsy and amyotrophic lateral sclerosis (ALS) have been linked to overexpression of P-glycoprotein transport^{82,83} and the breast cancer resistance protein.⁸⁴ While this overexpression is thought to have evolved as a protective mechanism (pumping out invaders/drugs from the brain), it was shown to contribute to drug resistance in both epilepsy and ALS.^{82,84} Together, these studies suggest that altered BBB efflux may also contribute to the development and progression of neuropathologies, and call for a comprehensive characterization of the associated mechanisms.

6.6.4 . Coupling BBB diagnosis with targeted treatments

As the understanding of BBB-mediated pathology matures, it opens an exciting avenue for the development of novel mechanism-specific treatments. Such treatment-strategies will require: a) tools for accurate diagnosis of BBB-leakage; b) precise interpretation of the observed leakage (i.e., transient/adaptive or chronic/pathogenic); and c) risk analysis of treatment side-effects.

At present two treatments targeting mechanisms triggered by BBB leakage are being developed in our lab. The first is the off-label use of the FDA-approved drug Losartan (Cozaar). In 2014, we showed that Losartan blocks the TGF- β pathway (triggered by albumin influx), and inhibits the TGF- β neuroinflammatory cascade.⁸⁵ Inhibition of neuroinflammation in turn, prevents the seizures and neuronal damage linked to BBB leakage.⁸⁵ More recently, our group has tested another antagonist of the TGF- β pathway, the smaller molecule IPW.⁸⁶ The study revealed that IPW can reverse neurological symptoms of aging in mice, such as hyperexcitability and memory impairment.⁸⁶ However, while animal studies present encouraging results, the therapeutic potential of these treatments in patients with BBB-related pathologies awaits clinical validation.

Other groups are examining treatments that inhibit alternative neuroinflammatory pathways, including the IL-6 signaling axis and the prostanoid cascade.¹⁰¹ Notably, studies in mice suggest that co-treatment with drugs that block different neuroinflammatory pathways is more effective than treatment with each drug individually.¹⁰¹ The discovered role of increased BBB efflux in drug-resistant neuro-pathologies has also led to experimental exploration of therapies that inhibit the involved efflux transporters.^{87,88}

Another exciting treatment path is being studied by our collaborator Dr. Cynthia Calkin – the head of the Mood and Metabolism Program (QEII Health Sciences Center, Halifax, Nova Scotia). Dr. Calkin is examining whether metformin – an insulin-sensitizing drug – can treat refractory bipolar disorder symptoms in patients with co-morbid insulin-resistance. Remarkably, preliminary results suggest that once the treatment reverses insulin-resistance, patients experience improvement in affective symptoms, such as depression and anxiety. We hypothesize, that metformin reduces systemic inflammation, and subsequent BBB leakage and neuro-inflammatory signaling. Notably, previous clinical studies of metformin support its role in reducing systemic inflammation,^{89–91} and animal studies have demonstrated that metformin reduces both neuroinflammation⁹² and BBB leakage.⁹³ Our collaboration with Dr. Calkin will be the first to test whether metformin reduces BBB leakage in humans, and whether BBB repair mediates the therapeutic effects of metformin.

6.7. Chapter Summary

Many aspects of BBB function in health in disease remain unknown, however, there is little doubt that BBB pathology contributes to the development of neurological dysfunction. This thesis adds

insights regarding: a) etiologies that can cause BBB leakage, b) mechanisms that mediate BBB leakage, c) clinical diagnosis of trans-cellular BBB leakage, and d) clinical symptoms of trans-cellular BBB leakage. Our animal study suggests that pericytic injury is likely to play a role in BBB leakage, and our clinical studies demonstrate that systemic immune diseases can lead to subtle BBB leakage, likely representative of altered trans-endothelial selectivity. Our findings raise the hypothesis that a sub-group of patients may develop recurrent and/or long-lasting BBB leakage and neuroinflammation that can lead to damage and reorganization of neuronal networks. This work has also involved the development of a completely automatic software for quantifying BBB leakage in living patients, and discussed the future steps required for translating MRI-based BBB imaging into routine clinical care. Together, the studies of this thesis serve as a stepping-stone towards the development of diagnosis-coupled treatment strategies, that target BBB-mediated mechanisms in patients with BBB pathology.

References, Chapter 1

1. Gould, I. G., Tsai, P., Kleinfeld, D. & Linninger, A. The capillary bed offers the largest hemodynamic resistance to the cortical blood supply. doi:10.1177/0271678X16671146
2. Abbott, N. J. & Friedman, A. Overview and introduction: the blood-brain barrier in health and disease. *Epilepsia* 53 Suppl 6, 1–6 (2012).
3. Graham, R. C. & Karnovsky, M. J. The early stages of absorption of injected horseradish peroxidase in the proximal tubules of mouse kidney: ultrastructural cytochemistry by a new technique. *J Histochem Cytochem* (1966).
4. Reese, T. S. & Karnovsky, M. J. Fine structural localization of a blood-brain barrier to exogenous peroxidase. *J. Cell Biol.* 34, 207–217 (1967).
5. Mathiisen, T. M., Lehre, K. P., Danbolt, N. C. & Ottersen, O. P. The perivascular astroglial sheath provides a complete covering of the brain microvessels: An electron microscopic 3D reconstruction. *Glia* 58, (2010).
6. Janzer, R. C. & Raff, M. C. Astrocytes induce blood-brain barrier properties in endothelial cells. *Nature* 10, 1347–1353 (1987).
7. Tao-Cheng, J.-H., Nagy, Z. & Brightman, M. W. Tight Junctions of Brain Endothelium in vitro Are Enhanced by Astroglia. *The Journal of Neuroscience* 7, (1987).
8. Alvarez, J. I., Katayama, T. & Prat, A. Glial influence on the blood brain barrier. *Glia* 61, 1939–1958 (2013).
9. Abbott, N. J., Ronnback, L. & Hansson, E. Astrocyte-endothelial interactions at the blood-brain barrier. *Nat Rev Neurosci* 7, 41–53 (2006).
10. Lukes, A., Mun-Bryce, S., Lukes, M. & Rosenberg, G. A. Extracellular matrix degradation by metalloproteinases and central nervous system diseases. *Mol. Neurobiol.* 19, 267–284 (1999).
11. Thomsen, M. S., Routhe, L. J. & Moos, T. The vascular basement membrane in the healthy and pathological brain. *J. Cereb. Blood Flow Metab.* 37, 3300–3317 (2017).
12. Halder, S. K. & Milner, R. A critical role for microglia in maintaining vascular integrity in the hypoxic spinal cord. *PNAS* (2019). doi:10.1073/pnas.1912178116/-/DCSupplemental
13. Rosenberg, G. A. Matrix metalloproteinases in neuroinflammation. *Glia* 39, 279–291 (2002).
14. Könnecke, H. & Bechmann, I. The role of microglia and matrix metalloproteinases involvement in neuroinflammation and gliomas. *Clin. Dev. Immunol.* 2013, (2013).
15. Jolivel, V. et al. Perivascular microglia promote blood vessel disintegration in the ischemic penumbra. *Acta Neuropathol* 3, 279–295 (2015).

16. Liebner, S. et al. Wnt/ β -catenin signaling controls development of the blood - brain barrier. *J. Cell Biol.* 183, 409–417 (2008).
17. Roy, C. S. & Sherrington, C. S. On the Regulation of the Blood-Supply of the Brain. *J. Physiol.* (1890).
18. Attwell, D. et al. Glial and neuronal control of brain blood flow. *Nature* 468, 232–243 (2010).
19. Pulido, R. S. et al. Neuronal Activity Regulates Blood-Brain Barrier Efflux Transport through Endothelial Circadian Genes. *Neuron* 108, 937-952.e7 (2020).
20. Vazana, U. et al. Neurobiology of Disease Glutamate-Mediated Blood-Brain Barrier Opening: Implications for Neuroprotection and Drug Delivery. (2016). doi:10.1523/JNEUROSCI.0587-16.2016
21. Vazana, U. et al. pharmaceuticals TMS-Induced Controlled BBB Opening: Preclinical Characterization and Implications for Treatment of Brain Cancer. doi:10.3390/pharmaceutics12100946
22. Xhima, K., Weber-Adrian, D. & Silburt, J. Glutamate induces blood–brain barrier permeability through activation of N-methyl-D-aspartate receptors. *J. Neurosci.* 36, 12296–12298 (2016).
23. Armulik, A. et al. Pericytes regulate the blood-brain barrier. *Nature* 468, 557–561 (2010).
24. Daneman, R., Zhou, L., Kebede, A. A. & Barres, B. A. Pericytes are required for blood–brain barrier integrity during embryogenesis. *Nature* 468, (2010).
25. Abbott, N. J., Patabendige, A. A. K., Dolman, D. E. M., Yusof, S. R. & Begley, D. J. Structure and function of the blood-brain barrier. *Neurobiol. Dis.* 37, 13–25 (2010).
26. Pardridge, W. M. Molecular Biology of the Blood–Brain Barrier. *Mol. Biotechnol.* 30, 057–070 (2005).
27. Obermeier, B., Daneman, R. & Ransohoff, R. M. Development, maintenance and disruption of the blood-brain barrier. *Nat. Med.* 19, 1584–1596 (2013).
28. Xu, L., Nirwane, A. & Yao, Y. Basement membrane and blood-brain barrier. *Stroke and Vascular Neurology* 4, 78–82 (2019).
29. Crouch, E. E., Liu, C., Silva-Vargas, V. & Doetsch, F. Regional and stage-specific effects of prospectively purified vascular cells on the adult V-SVZ neural stem cell lineage. *J. Neurosci.* 35, 4528–4539 (2015).
30. Vandenhaute, E. et al. Modelling the Neurovascular Unit and the Blood-Brain Barrier with the Unique Function of Pericytes. *Curr. Neurovasc. Res.* 8, 258–269 (2011).
31. Herculano-Houzel, S. The glia/neuron ratio: How it varies uniformly across brain structures and species and what that means for brain physiology and evolution. *Glia* 62, 1377–1391 (2014).
32. Kabba, J. A. et al. Microglia: Housekeeper of the Central Nervous System. *Cell. Mol. Neurobiol.* 38, 53–71 (2018).

33. Sá-Pereira, I., Brites, D. & Brito, M. A. Neurovascular unit: A focus on pericytes. *Molecular Neurobiology* 45, 327–347 (2012).
34. Abbott, N. J., Rönnbäck, L. & Hansson, E. Astrocyte-endothelial interactions at the blood-brain barrier. *Nat. Rev. Neurosci.* 7, 41–53 (2006).
35. Coomber, B. L. & Stewart, P. A. Three-dimensional reconstruction of vesicles in endothelium of blood-brain barrier versus highly permeable microvessels. *Anat. Rec.* 215, 256–261 (1986).
36. Anderson, J. M. Molecular structure of tight junctions and their role in epithelial transport. *News Physiol. Sci.* 16, 126–130 (2001).
37. Liebner, S., Kniesel, U., Kalbacher, H. & Wolburg, H. Correlation of tight junction morphology with the expression of tight junction proteins in blood-brain barrier endothelial cells. *Eur. J. Cell Biol.* 79, 707–717 (2000).
38. Castro Dias, M. et al. Claudin-12 is not required for blood-brain barrier tight junction function. *Fluids Barriers CNS* 16, 1–17 (2019).
39. Varadarajan, S., Stephenson, R. E. & Miller, A. L. Multiscale dynamics of tight junction remodeling. *J. Cell Sci.* 132, (2019).
40. Vermette, D. et al. Tight junction structure, function, and assessment in the critically ill: a systematic review. *Intensive Care Med. Exp.* 6, 37 (2018).
41. Dickie, B. R., Parker, G. J. M. & Parkes, L. M. Measuring water exchange across the blood-brain barrier using MRI. *Progress in Nuclear Magnetic Resonance Spectroscopy* 116, 19–39 (2020).
42. De Bock, M. et al. Endothelial calcium dynamics, connexin channels and blood-brain barrier function. *Prog. Neurobiol.* 108, 1–20 (2013).
43. Daneman, R. & Prat, A. The blood–brain barrier. *Cold Spring Harb. Perspect. Biol.* 7, (2015).
44. Orthmann, A., Fichtner, I. & Zeisig, R. Improving the transport of chemotherapeutic drugs across the blood-brain barrier. *Expert Rev. Clin. Pharmacol.* 4, 477–490 (2011).
45. Yang, A. C. et al. Physiological blood–brain transport is impaired with age by a shift in transcytosis. *Nature* 583, 425–430 (2020).
46. Vink, R., Gabrielian, L. & Thornton, E. The role of substance P in secondary pathophysiology after traumatic brain injury. *Frontiers in Neurology* 8, 304–304 (2017).
47. Ohtsuki, S. & Terasaki, T. Contribution of carrier-mediated transport systems to the blood-brain barrier as a supporting and protecting interface for the brain; importance for CNS drug discovery and development. *Pharmaceutical Research* 24, 1745–1758 (2007).
48. Demeule, M. et al. Drug transport to the brain: Key roles for the efflux pump P-glycoprotein in the blood-brain barrier. *Vascul. Pharmacol.* 38, 339–348 (2002).
49. Wang, W., M. Bodles-Brakhop, A. & W. Barger, S. A Role for P-Glycoprotein in Clearance of Alzheimer Amyloid β -Peptide from the Brain. *Curr. Alzheimer Res.* 13, 615–620 (2016).

50. Van Vliet, E. A. et al. Expression and Cellular Distribution of P-Glycoprotein and Breast Cancer Resistance Protein in Amyotrophic Lateral Sclerosis Patients. *J. Neuropathol. Exp. Neurol.* 79, 266–276 (2020).
51. Ilyas-Feldmann, M. et al. P-glycoprotein overactivity in epileptogenic developmental lesions measured in vivo using (R)-[11C]verapamil PET. *Epilepsia* 61, 1472–1480 (2020).
52. Van Assema, D. M. E. et al. P-glycoprotein function at the blood-brain barrier: Effects of age and gender. *Mol. Imaging Biol.* 14, 771–776 (2012).
53. Montagne, A., Zhao, Z. & Zlokovic, B. V. Alzheimer's disease: A matter of blood-brain barrier dysfunction? *Journal of Experimental Medicine* 214, 3151–3169 (2017).
54. Ghosh, C. Blood-Brain Barrier P450 Enzymes and Multidrug Transporters in Drug Resistance: A Synergistic Role in Neurological Diseases. *Curr. Drug Metab.* 999, 1–10 (2011).
55. Wimmer, I. et al. PECAM-1 stabilizes blood-brain barrier integrity and favors paracellular T-cell diapedesis across the blood-brain barrier during neuroinflammation. *Front. Immunol.* 10, 711 (2019).
56. Engelhardt, B. T cell migration into the central nervous system during health and disease: Different molecular keys allow access to different central nervous system compartments. *Clin. Exp. Neuroimmunol.* 1, 79–93 (2010).
57. Wraith, D. C. & Nicholson, L. B. The adaptive immune system in diseases of the central nervous system. *Journal of Clinical Investigation* 122, 1172–1179 (2012).
58. Abadier, M. et al. Cell surface levels of endothelial ICAM-1 influence the transcellular or paracellular T-cell diapedesis across the blood-brain barrier. *Eur. J. Immunol.* 45, 1043–1058 (2015).
59. Di Piero, V. et al. Sequential assessment of regional cerebral blood flow, regional cerebral blood volume, and blood-brain barrier in focal cerebral ischemia: A case report. *J. Cereb. Blood Flow Metab.* 6, 379–384 (1986).
60. Barzó, P., Marmarou, A., Fatouros, P., Corwin, F. & Dunbar, J. Magnetic resonance imaging-monitored acute blood-brain barrier changes in experimental traumatic brain injury. *J. Neurosurg.* 85, 1113–21 (1996).
61. Tofts, P. S. Modeling tracer kinetics in dynamic Gd-DTPA MR imaging. *J. Magn. Reson. Imaging* 7, 91–101 (1997).
62. Kang, E. J. et al. Blood-brain barrier opening to large molecules does not imply blood-brain barrier opening to small ions. *Neurobiol. Dis.* 52, 204–218 (2013).
63. Zhang, S. L., Yue, Z., Arnold, D. M. & Artushin, G. A Circadian Clock in the Blood-Brain Barrier Regulates Xenobiotic Efflux. *Cell* 173, 130-139.e10 (2018).
64. Abbott, N. J. & Friedman, A. Overview and introduction: the blood-brain barrier in health and disease. *Epilepsia* 53 Suppl 6, 1–6 (2012).

65. Prager, O. Kamintsky, L. et al. Seizure-induced microvascular injury is associated with impaired neurovascular coupling and blood–brain barrier dysfunction. *Epilepsia* 60, 322–336 (2019).
66. Kamintsky, L. et al. Blood-brain barrier leakage in systemic lupus erythematosus is associated with gray matter loss and cognitive impairment. *Ann. Rheum. Dis.* annrheumdis-2020-218004 (2020). doi:10.1136/annrheumdis-2020-218004
67. Kamintsky, L. et al. Blood-brain barrier imaging as a potential biomarker for bipolar disorder progression. *NeuroImage Clin.* 102049 (2019). doi:10.1016/j.nicl.2019.102049
68. Larsson, H. B. W., Courivaud, F., Rostrup, E. & Hansen, A. E. Measurement of brain perfusion, blood volume, and blood-brain barrier permeability, using dynamic contrast-enhanced T₁-weighted MRI at 3 tesla. *Magn. Reson. Med.* 62, 1270–1281 (2009).
69. Aksoy, D. et al. Magnetic resonance imaging profile of blood-brain barrier injury in patients with acute intracerebral hemorrhage. *J. Am. Heart Assoc.* 2, e000161 (2013).
70. Yang, X. & Knopp, M. V. Quantifying Tumor Vascular Heterogeneity with Dynamic Contrast-Enhanced Magnetic Resonance Imaging: A Review. *J. Biomed. Biotechnol.* 2011, 1–12 (2011).
71. Veksler, R. et al. Slow blood-to-brain transport underlies enduring barrier dysfunction in American football players. *Brain* 1–17 (2020). doi:10.1093/brain/awaa140
72. MOORE, G. E. & PEYTON, W. T. The clinical use of fluorescein in neurosurgery; the localization of. *J. Neurosurg.* 5, (1948).
73. Moore, G. E., Hunter, S. W. & Hubbard, T. B. Clinical And Experimental Studies Of Fluorescein Dyes With Special Reference To Their Use For The Diag-Nosis Of Central Nervous System Tumors*. *Ann. Surg.* (1949).
74. Hägerstrand, I. Vascular Changes In Cerebral Metastases. *Acta Pathol. Microbiol. Scand.* 51, (1961).
75. NYSTROM, S. Pathological changes in blood vessels of human glioblastoma multiforme. Comparative studies using plastic casting, angiography, light microscopy and electron microscopy, and with reference to some other brain tumours. *Acta Pathol. Microbiol. Scand. Suppl.* 49, (1960).
76. Long, D. M. Capillary ultrastructure and the blood-brain barrier in human malignant brain tumors. *J. Neurosurg.* 32, 127–144 (1970).
77. Wahl, M., Unterberg, A. & Baethmann, A. Intravital fluorescence microscopy for the study of blood-brain-barrier function. *Int. J. Microcirc. Clin. Exp.* 4, (1985).
78. Prager, O. et al. Dynamic in vivo imaging of cerebral blood flow and blood-brain barrier permeability. *Neuroimage* 49, 337–44 (2010).
79. Levi, H. et al. Stimulation of the sphenopalatine ganglion induces reperfusion and blood-brain barrier protection in the photothrombotic stroke model. *PLoS One* 7, e39636 (2012).
80. Prager, O. Kamintsky, L. et al. Pericyte-dependent impairment of neurovascular coupling in status epilepticus. *Prep.*

81. Acerbi, F. et al. The role of indocyanine green videoangiography with FLOW 800 analysis for the surgical management of central nervous system tumors: An update. *Neurosurg. Focus* 44, 1–11 (2018).
82. Schoknecht, K. et al. Monitoring stroke progression: in vivo imaging of cortical perfusion, blood-brain barrier permeability and cellular damage in the rat photothrombosis model. *J. Cereb. Blood Flow Metab.* (2014). doi:10.1038/jcbfm.2014.147
83. Coste, A., Oktay, M. H., Condeelis, J. S. & Entenberg, D. Intravital Imaging Techniques for Biomedical and Clinical Research. *Cytometry Part A* 97, (2020).
84. Rosenthal, L., Ambhanwong, S. & Traford, J. Observations on the effect of contrast material on normal and abnormal brain tissue using radiopertechetate. *Radiology* 92, 1467–1472 (1969).
85. Fazio F.; Lenzi, G. L.; Gerundini, P.; Collice, M.; Gilardi, M. C.; Colombo, R.; Taddei, G.; Del Maschio, A.; Piacentini, M.; Kung, H. F.; Blau, M. Fazio F.; Lenzi, G. L.; Gerundini, P.; Collice, M.; Gilardi, M. C.; Colombo, R.; Taddei, G.; Del Maschio, A., M. *Tomographic_Assessment_of_Regional_Cerebral*. *J. Comput. Assist. Tomogr.* p 911-921 (1984).
86. Andersen, A. R. et al. Extraction of [⁹⁹ fffTc]-d,l-HM-PAO Across the Blood-Brain Barrier. *J. Cereb. Blood Flow Metab.* (1988).
87. Jeppsson, P. G. & Olin, T. Neurotoxicity of Roentgen Contrast Media. *Acta Radiol. Diagnosis* 10, 17–34 (1970).
88. Gado, M. H., Phelps, M. E. & Coleman, R. E. An extravascular component of contrast enhancement in cranial computed tomography. Part I: The tissue blood ratio of contrast enhancement. *Radiology* 117, 589–593 (1975).
89. Riding, M., Bergstrom, M., Bergvall, U. & Greitz, T. Computer intravenous angiography. *Acta Radiologica - Series Diagnosis* 16, 82–90 (1975).
90. Frackowiak. *Quantitative_Measurement_of_Regional_Cerebral*. *J. Comput. Assist. Tomogr.* (1980).
91. Hendrikse, N. H. et al. Complete in vivo reversal of P-glycoprotein pump function in the blood-brain barrier visualized with positron emission tomography. *Br. J. Pharmacol.* 124, 1413–1418 (1998).
92. Patel, J. P. & Frey, B. N. Disruption in the blood-brain barrier: The missing link between brain and body inflammation in bipolar disorder? *Neural Plast.* 2015, (2015).
93. Marie Caille, J., Lemanceau, B. & Bonnemain, B. Gadolinium as a contrast agent for NMR. *Am. J. Neuroradiol.* 4, 1041–1042 (1983).
94. Carr, D. H. et al. Gadolinium-DTPA as a Contrast Agent in MRI. *Am. J. Roentgenol.* 143, 215–224 (1984).
95. Runge, V. M. et al. The use of GD DTPA as a perfusion agent and marker of blood-brain barrier disruption. *Magn. Reson. Imaging* 3, 43–55 (1985).

96. Larsson, H. B. W. et al. Quantitation of blood-brain barrier defect by magnetic resonance imaging and gadolinium-DTPA in patients with multiple sclerosis and brain tumors. *Magn. Reson. Med.* 16, 117–131 (1990).
97. Kermodé, A. G. et al. Breakdown of the blood-brain barrier precedes symptoms and other MRI signs of new lesions in multiple sclerosis: Pathogenetic and clinical implications. *Brain* 113, 1477–1489 (1990).
98. Edelman, R. R. et al. Cerebral blood flow: Assessment with dynamic contrast-enhanced T2*-weighted MR imaging at 1.5 T. *Radiology* 176, (1990).
99. Heiland, S. et al. Simultaneous assessment of cerebral hemodynamics and contrast agent uptake in lesions with disrupted blood-brain-barrier. *Magn. Reson. Imaging* 17, (1999).
100. Emerson, J. F., Chen, P. C., Shankle, W. R., Haier, R. J. & Nalcioglu, O. Data analysis for dynamic contrast-enhanced MRI-based cerebral perfusion measurements: correcting for changing cortical CSF volumes. *Magma Magn. Reson. Mater. Physics, Biol. Med.* 3, (1995).
101. Deoni, S. C. L., Rutt, B. K. & Peters, T. M. Rapid combined T1 and T2 mapping using gradient recalled acquisition in the steady state. *Magn. Reson. Med.* 49, 515–526 (2003).
102. Deoni, S. C. L., Peters, T. M. & Rutt, B. K. High-Resolution T1 and T2 Mapping of the Brain in a Clinically Acceptable Time with DESPOT1 and DESPOT2. 241, 237–241 (2005).
103. Tofts, P. S. et al. Contrast-Enhanced T1-Weighted MRI of a Diffusible Tracer: Standardized Quantities and Symbols. *Imaging* 232, 223–232 (1999).
104. Brix G, Semmler W, Port R, Schad LR, Layer G, L. W. Pharmacokinetic parameters in CNS Gd-DTPA enhanced MR imaging. 621–8. (1991).
105. Blyth, B. J. et al. Validation of serum markers for blood-brain barrier disruption in traumatic brain injury. *J. Neurotrauma* 26, 1497–1507 (2009).
106. Marchi, N. et al. Peripheral markers of blood-brain barrier damage. *Clin. Chim. Acta* (2004). doi:10.1016/j.cccn.2003.12.008
107. Gudmundsson, P. et al. The relationship between cerebrospinal fluid biomarkers and depression in elderly women. *Am. J. Geriatr. Psychiatry* 15, 832–838 (2007).
108. Stock, A. D., Gelb, S., Pasternak, O., Ben-zvi, A. & Putterman, C. The blood brain barrier and neuropsychiatric lupus: new perspectives in light of advances in understanding the neuroimmune interface. *Autoimmun. Rev.* 16, 612–619 (2017).
109. Steiner, J. et al. S100B serum levels are closely correlated with body mass index: An important caveat in neuropsychiatric research. *Psychoneuroendocrinology* 35, 321–324 (2010).
110. Pollak, T. A. et al. The blood-brain barrier in psychosis. *The Lancet Psychiatry* 0366, 1–14 (2017).
111. Patlak, C. S., Blasberg, R. G. & Fenstermacher, J. D. Graphical Evaluation of Blood-to-Brain Transfer Constants from Multiple-Time Uptake Data. 1–7 (1983).

112. Cramer, S. P. & Larsson, H. B. W. Accurate determination of blood-brain barrier permeability using dynamic contrast-enhanced T1-weighted MRI: A simulation and in vivo study on healthy subjects and multiple sclerosis patients. *J. Cereb. Blood Flow Metab.* 34, 1655–1665 (2014).
113. Heye, A. K., Culling, R. D., Hernández, C. V., Thrippleton, M. J. & Wardlaw, J. M. Assessment of blood – brain barrier disruption using dynamic contrast-enhanced MRI . A systematic review. *NeuroImage Clin.* 6, 262–274 (2014).
114. Heye, A. K. et al. NeuroImage Tracer kinetic modelling for DCE-MRI quanti fi cation of subtle blood – brain barrier permeability. *Neuroimage* 125, 446–455 (2016).
115. Levi, H. et al. Stimulation of the sphenopalatine ganglion induces reperfusion and blood-brain barrier protection in the photothrombotic stroke model. *PLoS One* 7, e39636 (2012).
116. Chassidim, Y. et al. Quantitative imaging assessment of blood-brain barrier permeability in humans. *Fluids Barriers CNS* 10, 9 (2013).
117. Veksler, R., Shelef, I. & Friedman, A. Blood-brain barrier imaging in human neuropathologies. *Arch. Med. Res.* 45, 646–652 (2014).
118. Serlin, Y. et al. Blood-Brain Barrier Leakage in TIA. 1266–1269 (2019). doi:10.1161/Stroke.AHA.119.025247
119. Ohene, Y. et al. Increased blood–brain barrier permeability to water in the aging brain detected using noninvasive multi-TE ASL MRI. *Magn. Reson. Med.* 85, 326–333 (2021).
120. Kane, G. C. et al. Comparison between gadolinium and iodine contrast for percutaneous intervention in atherosclerotic renal artery stenosis: Clinical outcomes. *Nephrol. Dial. Transplant.* 23, 1233–1240 (2008).

References, Chapter 2

1. Mathiisen, T. M., Lehre, K. P., Danbolt, N. C. & Ottersen, O. P. The perivascular astroglial sheath provides a complete covering of the brain microvessels: An electron microscopic 3D reconstruction. *Glia* 58, (2010).
2. Abbott, N. J. & Friedman, A. Overview and introduction: the blood-brain barrier in health and disease. *Epilepsia* 53 Suppl 6, 1–6 (2012).
3. Goodall, E. F. et al. Age-associated changes in the blood-brain barrier: Comparative studies in human and mouse. *Neuropathol. Appl. Neurobiol.* 328–340 (2017). doi:10.1111/nan.12408
4. Schoknecht, K. et al. Monitoring stroke progression: in vivo imaging of cortical perfusion, blood-brain barrier permeability and cellular damage in the rat photothrombosis model. *J. Cereb. Blood Flow Metab.* (2014). doi:10.1038/jcbfm.2014.147
5. Bar-Klein, G. Cacheaux, LP. Kamintsky. et al. Losartan prevents acquired epilepsy via TGF-beta signaling suppression. *Ann. Neurol.* 75, 864–875 (2014).
6. Daneman, R., Zhou, L., Kebede, A. A. & Barres, B. A. Pericytes are required for blood-brain barrier integrity during embryogenesis. *Nature* 468, (2010).
7. Ketzeff, M. Compensatory network alterations upon onset of epilepsy in synapsin triple knock-out mice. *Neuroscience* 189, 108–122 (2011).
8. Van Vliet, E. A. et al. Blood-brain barrier leakage after status epilepticus in rapamycin-treated rats I: Magnetic resonance imaging. *Epilepsia* 57, 59–69 (2016).
9. Mendes, N. F. et al. The Blood-Brain Barrier Breakdown During Acute Phase of the Pilocarpine Model of Epilepsy Is Dynamic and Time-Dependent. *Front. Neurol.* 10, 1–13 (2019).
10. Ketzeff, M. et al. Compensatory network alterations upon onset of epilepsy in synapsin triple knock-out mice. *Neuroscience* 189, 108–122 (2011).
11. Kovács, R., Papageorgiou, I. & Heinemann, U. Slice cultures as a model to study neurovascular coupling and blood brain barrier in vitro. *Cardiovasc. Psychiatry Neurol.* 2011, (2011).
12. Schuchmann, S., Buchheim, K., Meierkord, H. & Heinemann, U. A relative energy failure is associated with low-Mg²⁺ but not with 4-aminopyridine induced seizure-like events in entorhinal cortex. *J. Neurophysiol.* 81, 399–403 (1999).
13. Castilho, R. F., Ward, M. W. & Nicholls, D. G. Oxidative stress, mitochondrial function, and acute glutamate excitotoxicity in cultured cerebellar granule cells. *J. Neurochem.* 72, 1394–1401 (1999).
14. Manjón, J. V. & Coupé, P. volBrain: An Online MRI Brain Volumetry System. *Front. Neuroinform.* 10, (2016).
15. Tofts, P. S. Modeling tracer kinetics in dynamic Gd-DTPA MR imaging. *J. Magn. Reson. Imaging* 7, 91–101 (1997).

16. Veksler, R., Shelef, I. & Friedman, A. Blood-brain barrier imaging in human neuropathologies. *Arch. Med. Res.* 45, 646–652 (2014).
17. Chassidim, Y. et al. Quantitative imaging assessment of blood-brain barrier permeability in humans. *Fluids Barriers CNS* 10, 9 (2013).
18. A Brief History of Medical Image Registration: Part 1 | by Kris Huang | Pymedix | Medium. Available at: <https://medium.com/pymedix/a-brief-history-of-medical-image-registration-part-1-45b29867d7dd>. (Accessed: 22nd December 2020)
19. Muhei-aladin, O. et al. An investigation of fMRI time series stationarity during motor sequence learning foot tapping tasks. *J. Neurosci. Methods* 227, 75–82 (2014).
20. Yucel, M. et al. Hemispheric and Gender-related Differences in the Gross Morphology of the Anterior Cingulate/Paracingulate Cortex in Normal Volunteers: An MRI Morphometric Study. *Cereb. Cortex* 11, 17–25 (2001).
21. Armitage, P. A., Farrall, A. J., Carpenter, T. K., Doubal, F. N. & Wardlaw, J. M. Use of dynamic contrast-enhanced MRI to measure subtle blood-brain barrier abnormalities ☆. (2011). doi:10.1016/j.mri.2010.09.002
22. Deoni, S. C. L. Quantitative relaxometry of the brain. *Top. Magn. Reson. Imaging* 21, 101–113 (2010).
23. Look, D. C. & Locker, D. R. Time saving in measurement of NMR and EPR relaxation times. *Rev. Sci. Instrum.* 41, 250–251 (1970).
24. Deoni, S. C. L., Rutt, B. K. & Peters, T. M. Rapid combined T1 and T2 mapping using gradient recalled acquisition in the steady state. *Magn. Reson. Med.* 49, 515–526 (2003).
25. Deoni, S. C. L., Peters, T. M. & Rutt, B. K. High-Resolution T 1 and T 2 Mapping of the Brain in a Clinically Acceptable Time with DESPOT1 and DESPOT2. 241, 237–241 (2005).
26. Jackson, A., Buckley, D. L. & Parker, G. J. M. *Dynamic Contrast-Enhanced Magnetic Resonance Imaging in Oncology (Medical Radiology / Diagnostic Imaging)*. Springer-Verlag Berlin Heidelberg (2005).
27. Gowland, P. et al. Dynamic studies of gadolinium uptake in brain tumors using inversion-recovery echo-planar imaging. *Magn. Reson. Med.* 26, 241–258 (1992).
28. Tofts, P. S. et al. Contrast-Enhanced T 1 -Weighted MRI of a Diffusible Tracer : Standardized Quantities and Symbols. *Imaging* 232, 223–232 (1999).
29. Veksler, R. et al. Slow blood-to-brain transport underlies enduring barrier dysfunction in American football players. *Brain* 143, 1826–1842 (2020).
30. Serlin, Y. et al. Blood-Brain Barrier Leakage in TIA. 1266–1269 (2019). doi:10.1161/STROKEAHA.119.025247
31. Hui Poon, S., Sim, K. & J. Baldessarini, R. Pharmacological Approaches for Treatment-resistant Bipolar Disorder. *Curr. Neuropharmacol.* 13, 592–604 (2015).
32. Leslie, B. & Crowe, S. F. Cognitive functioning in systemic lupus erythematosus: a meta-analysis. *Lupus* 961203317751859 (2018). doi:10.1177/0961203317751859

33. American Psychiatric Association. American Psychiatric Association: Diagnostic and Statistical Manual of Mental Disorders. (American Psychiatric Association, 2013).
34. Hawley, C. J., Gale, T. M. & Sivakumaran, T. Defining remission by cut off score on the MADRS: selecting the optimal value. *J. Affect. Disord.* 72, 177–184 (2002).
35. Leentjens, A. F. et al. Anxiety rating scales in Parkinson's disease: a validation study of the Hamilton anxiety rating scale, the Beck anxiety inventory, and the hospital anxiety and depression scale. *Mov. Disord.* 26, 407–415 (2011).
36. Hall, R. C. Global Assessment of Functioning. *Psychosomatics* 36, 267–275 (1995).
37. Berghofer, A. et al. Long-term effectiveness of lithium in bipolar disorder: a multicenter investigation of patients with typical and atypical features. *J. Clin. Psychiatry* 69, 1860–1868 (2008).
38. Hochberg, M. C. Updating the American College of Rheumatology revised criteria for the classification of systemic lupus erythematosus. *Arthritis and rheumatism* (1997). doi:10.1002/art.1780400928
39. Smith, A. Symbol Digit Modalities Test. 9th ed: Western Psychological Services. (2002).
40. Walker, L. A. S. et al. Canadian Normative Data for Minimal Assessment of Cognitive Function in Multiple Sclerosis. *Can. J. Neurol. Sci.* 44, 547–555 (2017).
41. Delis, D. C., Kramer, J. H., Kaplan, E. & Ober, B. A. California Verbal Learning Test – second edition. Adult version. Manual. (Psychological Corporation, 2000).
42. Leys, C., Ley, C., Klein, O., Bernard, P. & Licata, L. Detecting outliers: Do not use standard deviation around the mean, use absolute deviation around the median. (2013). doi:10.1016/j.jesp.2013.03.013

References, Chapter 3

1. Keezer MR, Sisodiya SM, Sander JW. Comorbidities of epilepsy: current concepts and future perspectives. *Lancet Neurol.* 2016; 15(1):106–15.
2. Friedman A. Blood-brain barrier dysfunction, status epilepticus, seizures, and epilepsy: a puzzle of a chicken and egg? *Epilepsia.* 2011;52(Suppl 8):19–20.
3. Vazana U, Veksler R, Pell GS, et al. Glutamate-mediated blood-brain barrier opening: implications for neuroprotection and drug delivery. *J Neurosci.* 2016;36(29):7727–39.
4. van Vliet EA, Aronica E, Gorter JA. Role of blood–brain barrier in temporal lobe epilepsy and pharmacoresistance. *Neuroscience.* 2014;277:455–73.
5. Ivens S, Kaufer D, Flores LP, et al. TGF- β receptor-mediated albumin uptake into astrocytes is involved in neocortical epileptogenesis. *Brain.* 2007;130(Pt 2):535–47.
6. Weissberg I, Wood L, Kamintsky L, et al. Albumin induces excitatory synaptogenesis through astrocytic TGF- β /ALK5 signaling in a model of acquired epilepsy following blood–brain barrier dysfunction. *Neurobiol Dis.* 2015;78:115–25.
7. Tomkins O, Friedman O, Ivens S, et al. Blood-brain barrier disruption results in delayed functional and structural alterations in the rat neocortex. *Neurobiol Dis.* 2007;25(2):367–77.
8. Armulik A, Genové G, Mäe M, et al. Pericytes regulate the blood–brain barrier. *Nature.* 2010;468(7323):557–61.
9. Yemisci M, Gursoy-Ozdemir Y, Vural A, et al. Pericyte contraction induced by oxidative-nitrative stress impairs capillary reflow despite successful opening of an occluded cerebral artery. *Nat Med.* 2009;15(9):1031–7.
10. Kisler K, Nelson AR, Rege SV, et al. Pericyte degeneration leads to neurovascular uncoupling and limits oxygen supply to brain. *Nat Neurosci.* 2017;20(3):406–16.
11. Hall CN, Reynell C, Gesslein B, et al. Capillary pericytes regulate cerebral blood flow in health and disease. *Nature.* 2014;508 (7494):55–60.
12. Klement W, Garbelli R, Zub E, et al. Seizure progression and inflammatory mediators promote pericytosis and pericyte-microglia clustering at the cerebrovasculature. *Neurobiol Dis.* 2018;113:70–81.
13. Milesi S, Boussadia B, Plaud C, et al. Redistribution of PDGFR β cells and NG2DsRed pericytes at the cerebrovasculature after status epilepticus. *Neurobiol Dis.* 2014;71:151–8.
14. Garbelli R, de Bock F, Medici V, et al. PDGFR β (+) cells in human and experimental neuro-vascular dysplasia and seizures. *Neuroscience.* 2015;306:18–27.
15. Fernández-Klett F, Priller J. Diverse functions of pericytes in cerebral blood flow regulation and ischemia. *J Cereb Blood Flow Metab.* 2015;35(6):883–7.
16. Hill RA, Tong L, Yuan P, et al. Regional blood flow in the normal and ischemic brain is controlled by arteriolar smooth muscle cell contractility and not by capillary pericytes. *Neuron.* 2015;87(1):95–110.

17. Attwell D, Mishra A, Hall CN, et al. What is a pericyte? *J Cereb Blood Flow Metab.* 2016;36(2):451–5.
18. Zlokovic BV. Neurovascular mechanisms of Alzheimer’s neurodegeneration. *Trends Neurosci.* 2005;28(4):202–8.
19. Piilgaard H, Lauritzen M. Persistent increase in oxygen consumption and impaired neurovascular coupling after spreading depression in rat neocortex. *J Cereb Blood Flow Metab.* 2009;29(9):1517–27.
20. Parfenova H, Carratu P, Tcheranova D, et al. Epileptic seizures cause extended postictal cerebral vascular dysfunction that is prevented by HO-1 overexpression. *Am J Physiol Heart Circ Physiol.* 2005;288(6):H2843–50.
21. Harris S, Bruyns-Haylett M, Kennerley A, et al. The effects of focal epileptic activity on regional sensory-evoked neurovascular coupling and postictal modulation of bilateral sensory processing. *J Cereb Blood Flow Metab.* 2013;33(10):1595–604.
22. Zhao M, Nguyen J, Ma H, et al. Preictal and ictal neurovascular and metabolic coupling surrounding a seizure focus. *J Neurosci.* 2011;31(37):13292–300.
23. Harris SS, Boorman LW, Kennerley AJ, et al. Seizure epicenter depth and translaminal field potential synchrony underlie complex variations in tissue oxygenation during ictal initiation. *Neuroimage.* 2018;171:165–75.
24. Farrell JS, Gaxiola-Valdez I, Wolff MD, et al. Postictal behavioural impairments are due to a severe prolonged hypoperfusion/hypoxia event that is COX-2 dependent. *Elife.* 2016;5:e19352.
25. Farrell JS, Colangeli R, Wolff MD, et al. Postictal hypoperfusion/ hypoxia provides the foundation for a unified theory of seizure- induced brain abnormalities and behavioral dysfunction. *Epilepsia.* 2017;58(9):1493–501.
26. Leal-Campanario R, Alarcon-Martinez L, Rieiro H, et al. Abnormal capillary vasodynamics contribute to ictal neurodegeneration in epilepsy. *Sci Rep.* 2017;7:43276.
27. Arango-Lievano M, Boussadia B, De Terdonck LDT, et al. Topographic reorganization of cerebrovascular mural cells under seizure conditions. *Cell Rep.* 2018;23(4):1045–59.
28. Kovács R, Papageorgiou I, Heinemann U. Slice cultures as a model to study neurovascular coupling and blood brain barrier in vitro. *Cardiovasc Psychiatry Neurol.* 2011;2011:1–9.
29. Fernández-Klett F, Offenhauser N, Dirnagl U, et al. Pericytes in capillaries are contractile in vivo, but arterioles mediate functional hyperemia in the mouse brain. *Proc Natl Acad Sci USA.* 2010;107(51):22290–5.
30. Schuchmann S, Buchheim K, Meierkord H, et al. A relative energy failure is associated with low-Mg²⁺ but not with 4-aminopyridine induced seizure-like events in entorhinal cortex. *J Neurophysiol.* 1999;81(1):399–403.
31. Kovács R, Schuchmann S, Gabriel S, et al. Free radical-mediated cell damage after experimental status epilepticus in hippocampal slice cultures. *J Neurophysiol.* 2002;88(6):2909–18.
32. Schoknecht K, Berndt N, Rösner J, et al. Event-associated oxygen consumption rate increases ca. five-fold when interictal activity transforms into seizure-like events in vitro. *Int J Mol Sci.* 2017;18(9):1925.

33. Schoknecht K, Prager O, Vazana U, et al. Monitoring stroke progression: in vivo imaging of cortical perfusion, blood-brain barrier permeability and cellular damage in the rat photothrombosis model. *J Cereb Blood Flow Metab.* 2014;34(11):1791–801.
34. Prager O, Chassidim Y, Klein C, et al. Dynamic in vivo imaging of cerebral blood flow and blood–brain barrier permeability. *Neuroimage.* 2010;49(1):337–44.
35. Bar-Klein G, Cacheaux LP, Kamintsky L, et al. Losartan prevents acquired epilepsy via TGF- β signaling suppression. *Ann Neurol.* 2014;75(6):864–75.
36. Levi H, Schoknecht K, Prager O, et al. Stimulation of the sphenopalatine ganglion induces reperfusion and blood-brain barrier protection in the photothrombotic stroke model. *PLoS One.* 2012;7(6):e39636.
37. Kawamura H, Sugiyama T, Wu DM, et al. ATP: a vasoactive signal in the pericyte-containing microvasculature of the rat retina. *J Physiol.* 2003;551(3):787–99.
38. Castilho RF, Ward MW, Nicholls DG. Oxidative stress, mitochondrial function, and acute glutamate excitotoxicity in cultured cerebellar granule cells. *J Neurochem.* 1999;72 (4):1394–401.
39. Daneman R, Zhou L, Kebede AA, et al. Pericytes are required for blood-brain barrier integrity during embryogenesis. *Nature.* 2010;468(7323):562–6.
40. Bénar CG, Gross DW, Wang Y, et al. The BOLD response to interictal epileptiform discharges. *Neuroimage.* 2002;17(3):1182–92.
41. Nersesyan H, Hyder F, Rothman DL, et al. Dynamic fMRI and EEG recordings during spike-wave seizures and generalized tonic-clonic seizures in WAG/Rij rats. *J Cereb Blood Flow Metab.* 2004;24(6):589–99.
42. Ingvar M. Cerebral blood flow and metabolic rate during seizures. Relationship to epileptic brain damage. *Ann N Y Acad Sci.* 1986;462:194–206.
43. Thompson JK, Peterson MR, Freeman RD. Single-neuron activity and tissue oxygenation in the cerebral cortex. *Science.* 2003;299 (5609):1070–2.
44. Ingram J, Zhang C, Cressman JR, et al. Oxygen and seizure dynamics: I. Experiments. *J Neurophysiol.* 2014;112(2):205–12.
45. Camenzind RS, Chip S, Gutmann H, et al. Preservation of transendothelial glucose transporter 1 and P-glycoprotein transporters in a cortical slice culture model of the blood-brain barrier. *Neuroscience.* 2010;170(1):361–71.
46. Morin-Brureau M, Lebrun A, Rousset M-C, et al. Epileptiform activity induces vascular remodeling and zonula occludens 1 downregulation in organotypic hippocampal cultures: role of VEGF signaling pathways. *J Neurosci.* 2011;31(29):10677–88.
47. Gordon GRJ, Choi HB, Rungta RL, et al. Brain metabolism dictates the polarity of astrocyte control over arterioles. *Nature.* 2008;456(7223):745–9.
48. Filosa JA, Bonev AD, Straub SV, et al. Local potassium signaling couples neuronal activity to vasodilation in the brain. *Nat Neurosci.* 2006;9(11):1397–403.
49. Girouard H, Bonev AD, Hannah RM, et al. Astrocytic endfoot Ca²⁺ and BK channels determine both arteriolar dilation and constriction. *Proc Natl Acad Sci USA.* 2010;107(8):3811–6.

50. Longden TA, Dabertrand F, Koide M, et al. Capillary K⁺-sensing initiates retrograde hyperpolarization to increase local cerebral blood flow. *Nat Neurosci.* 2017;20(5):717–26.
51. Ingvar M, Söderfeldt B, Folbergrová J, et al. Metabolic, circulatory, and structural alterations in the rat brain induced by sustained pentylenetetrazole seizures. *Epilepsia.* 1984;25(2):191–204.
52. Suh M, Ma H, Zhao M, et al. Neurovascular coupling and oximetry during epileptic events. *Mol Neurobiol.* 2006;33(3):181–97.
53. Ivanova E, Kovacs-Oller T, Sagdullaev BT. Vascular pericyte impairment and connexin43 gap junction deficit contribute to vasomotor decline in diabetic retinopathy. *J Neurosci.* 2017; 37(32):7580–94.
54. Bai Y, Zhu X, Chao J, et al. Pericytes contribute to the disruption of the cerebral endothelial barrier via increasing VEGF expression: implications for stroke. *PLoS One.* 2015;10(4):e0124362.
55. Underly RG, Levy M, Hartmann DA, et al. Pericytes as inducers of rapid, matrix metalloproteinase-9-dependent capillary damage during ischemia. *J Neurosci.* 2017;37(1):129–40.

References, Chapter 4

1. Kessler, R. C. et al. Lifetime prevalence and age-of-onset distributions of DSM-IV disorders in the National Comorbidity Survey Replication. *Arch. Gen. Psychiatry* 62, 593–602 (2005).
2. Hui, S., Sim, K. & Baldessarini, R. J. Pharmacological Approaches for Treatment-resistant Bipolar Disorder. 592–604 (2015).
3. Naaldijk, Y. M., Bittencourt, M. C., Sack, U. & Ulrich, H. Kinins and microglial responses in bipolar disorder: a neuroinflammation hypothesis. *Biol. Chem.* 397, 283–96 (2016).
4. Patel, J. P. & Frey, B. N. Disruption in the blood-brain barrier: The missing link between brain and body inflammation in bipolar disorder? *Neural Plast.* 2015, (2015).
5. Abbott, N. J., Patabendige, A. A. K., Dolman, D. E. M., Yusof, S. R. & Begley, D. J. Structure and function of the blood-brain barrier. *Neurobiol Dis* 37, 13–25 (2010).
6. Sweeney, M. D., Sagare, A. P. & Zlokovic, B. V. Blood-brain barrier breakdown in Alzheimer disease and other neurodegenerative disorders. *Nat. Rev. Neurol.* 14, 133–150 (2018).
7. Heye, A. K., Culling, R. D., Hernández, C. V., Thrippleton, M. J. & Wardlaw, J. M. NeuroImage : Clinical Assessment of blood – brain barrier disruption using dynamic contrast-enhanced MRI . A systematic review. *YNICL* 6, 262–274 (2014).
8. Ingrisch, M., Sourbron, S., Morhard, D., Ertl-wagner, B. & Ku, T. Quantification of Perfusion and Permeability in Multiple Sclerosis. (2012).
9. Cramer, S. P., Simonsen, H., Frederiksen, J. L., Rostrup, E. & Larsson, H. B. W. NeuroImage : Clinical Abnormal blood – brain barrier permeability in normal appearing white matter in multiple sclerosis investigated by MRI ☆ , ☆☆. *NeuroImage Clin.* 4, 182–189 (2014).
10. Varatharaj, A., Liljeroth, M., Darekar, A., Larsson, H. B. W. & Galea, I. Blood – brain barrier permeability measured using dynamic contrast-enhanced magnetic resonance imaging : 3, 699–709 (2019).
11. Haider, L., Naismith, R. T. & Rovira, A. Use of gadolinium for MRI diagnostic or surveillance studies in patients with MS. 239–240 (2019). doi:10.1212/WNL.0000000000007891
12. Merali, Z., Huang, K., Mikulis, D., Silver, F. & Kassner, A. Evolution of blood-brain-barrier permeability after acute ischemic stroke. *PLoS One* 12, 1–11 (2017).
13. Kassner, A., Roberts, T. P. L., Moran, B., Silver, F. L. & Mikulis, D. J. Increases Blood-Brain Barrier Disruption in Acute Ischemic Stroke : An MR Imaging Permeability. (2009). doi:10.3174/ajnr.A1774
14. Serlin, Y. et al. Blood-Brain Barrier Leakage in TIA. 1266–1269 (2019). doi:10.1161/STROKEAHA.119.025247

15. Bergamino, M. et al. Measurement of blood-brain barrier permeability with t1-weighted dynamic contrast-enhanced MRI in brain tumors: a comparative study with two different algorithms. *ISRN Neurosci.* 2013, 905279 (2013).
16. Bar-Klein, G. et al. Imaging blood–brain barrier dysfunction as a biomarker for epileptogenesis. *Brain* 140, 1692–1705 (2017).
17. Weissberg, I. Veksler R. Kamintsky L. et al. Imaging blood-brain barrier dysfunction in football players. *JAMA Neurol.* 71, (2014).
18. Tomkins, O. et al. Blood-brain barrier disruption in post-traumatic epilepsy. *J. Neurol. Neurosurg. Psychiatry* 79, 774–7 (2008).
19. Nation, D. et al. Blood-brain barrier breakdown is an early biomarker of human cognitive dysfunction. *Nat. Med.* in press, (2018).
20. Wong, S. M. et al. Measuring Subtle Leakage of the Blood – Brain Barrier in Cerebrovascular Disease with DCE-MRI : Test – Retest Reproducibility and Its Influencing Factors. 159–166 (2017). doi:10.1002/jmri.25540
21. Wilson, P. W. F. et al. Prediction of Coronary Heart Disease Using Risk Factor Categories. (1998).
22. Alberti, K. G. M. M. et al. Harmonizing the metabolic syndrome: A joint interim statement of the International Diabetes Federation Task Force on Epidemiology and Prevention; National Heart, Lung, and Blood Institute; American Heart Association; World Heart Federation; International . *Circulation* 120, 1640–1645 (2009).
23. Esteghamati, A. et al. Optimal cut-off of homeostasis model assessment of insulin resistance (HOMA-IR) for the diagnosis of metabolic syndrome: third national surveillance of risk factors of non-communicable diseases in Iran (SuRFNCD-2007). *Nutr. Metab. (Lond).* 7, 26 (2010).
24. Hawley, C. J., Gale, T. M. & Sivakumaran, T. Defining remission by cut off score on the MADRS: selecting the optimal value. *J. Affect. Disord.* 72, 177–184 (2002).
25. Leentjens, A. F. et al. Anxiety rating scales in Parkinson’s disease: a validation study of the Hamilton anxiety rating scale, the Beck anxiety inventory, and the hospital anxiety and depression scale. *Mov. Disord.* 26, 407–415 (2011).
26. Hall, R. C. Global Assessment of Functioning. *Psychosomatics* 36, 267–275 (1995).
27. Veksler, R., Shelef, I. & Friedman, A. Blood-brain barrier imaging in human neuropathologies. *Arch. Med. Res.* 45, 646–652 (2014).
28. Chassidim, Y. et al. Quantitative imaging assessment of blood-brain barrier permeability in humans. *Fluids Barriers CNS* 10, 9 (2013).
29. Hughes, T. M. & Craft, S. The role of insulin in the vascular contributions to age-related dementia. *Biochim. Biophys. Acta - Mol. Basis Dis.* 1862, 983–991 (2016).
30. Brietzke, E. et al. Insulin dysfunction and allostatic load in bipolar disorder. *Expert Rev. Neurother.* 11, 1017–1028 (2011).
31. Calkin, C. V. et al. Insulin resistance and outcome in bipolar disorder. *Br. J. Psychiatry* 206, 52–57 (2015).
32. Kretschmer, E. Physique and Character. *Int. Libr. Psychol.* (1931).

33. Calkin, C. V. *Annals of Medicine* Insulin resistance takes center stage : a new paradigm in the progression of bipolar disorder. *Ann. Med.* 0, 1–13 (2019).
34. Vancampfort, D. et al. Diabetes mellitus in people with schizophrenia, bipolar disorder and major depressive disorder: a systematic review and large scale meta-analysis. *World Psychiatry* 15, 166–74 (2016).
35. Burghardt, K. J. et al. Atypical antipsychotics, insulin resistance and weight; a meta-analysis of healthy volunteer studies. *Prog. Neuro-Psychopharmacology Biol. Psychiatry* 83, 55–63 (2018).
36. Correll, C. U., Frederickson, A. M., Kane, J. M. & Manu, P. Equally increased risk for metabolic syndrome in patients with bipolar disorder and schizophrenia treated with second-generation antipsychotics. *Bipolar Disord.* 10, 788–797 (2008).
37. Endicott, J. & Spitzer, R. L. A diagnostic interview: the schedule for affective disorders and schizophrenia. *Arch. Gen. Psychiatry* 35, 837–844 (1978).
38. American Psychiatric Association. *American Psychiatric Association: Diagnostic and Statistical Manual of Mental Disorders.* (American Psychiatric Association, 2013).
39. Berghofer, A. et al. Long-term effectiveness of lithium in bipolar disorder: a multicenter investigation of patients with typical and atypical features. *J. Clin. Psychiatry* 69, 1860–1868 (2008).
40. Deoni, S. C. L., Peters, T. M. & Rutt, B. K. High-Resolution T 1 and T 2 Mapping of the Brain in a Clinically Acceptable Time with DESPOT1 and DESPOT2. 241, 237–241 (2005).

References, Chapter 5

1. Leslie B, Crowe SF. Cognitive functioning in systemic lupus erythematosus: a meta-analysis. *Lupus*. 2018;961203317751859.
2. Rayes HA, Tani C, Kwan A, Marzouk S, Colosimo K, Medina-Rosas J, et al. What is the prevalence of cognitive impairment in lupus and which instruments are used to measure it? A systematic review and meta-analysis. *Semin Arthritis Rheum*. 2018;48(2):240-55.
3. Hanly JG, Kozora E, Beyea SD, Birnbaum J. Review: Nervous System Disease in Systemic Lupus Erythematosus: Current Status and Future Directions. *Arthritis & rheumatology*. 2019;71(1):33-42.
4. Schwartz N, Stock AD, Putterman C. Neuropsychiatric lupus: new mechanistic insights and future treatment directions. *Nat Rev Rheumatol*. 2019;15(3):137-52.
5. De Luca C, Virtuoso A, Maggio N, Papa M. Neuro-Coagulopathy: Blood Coagulation Factors in Central Nervous System Diseases. *International journal of molecular sciences*. 2017;18(10).
6. Heinemann U, Kaufer D, Friedman A. Blood-brain barrier dysfunction, TGFbeta signaling, and astrocyte dysfunction in epilepsy. *Glia*. 2012;60(8):1251-7.
7. Bravo-Zehnder M, Toledo EM, Segovia-Miranda F, Serrano FG, Benito MJ, Metz C, et al. Anti-ribosomal p protein autoantibodies from patients with neuropsychiatric lupus impair memory in mice. *Arthritis & rheumatology*. 2015;67(1):204-14.
8. Faust TW, Chang EH, Kowal C, Berlin R, Gazaryan IG, Bertini E, et al. Neurotoxic lupus autoantibodies alter brain function through two distinct mechanisms. *Proc Natl Acad Sci U S A*. 2010;107(43):18569-74.
9. Nestor J, Arinuma Y, Huerta TS, Kowal C, Nasiri E, Kello N, et al. Lupus antibodies induce behavioral changes mediated by microglia and blocked by ACE inhibitors. *J Exp Med*. 2018;215(10):2554-66.
10. Mahajan SD, Parikh NU, Woodruff TM, Jarvis JN, Lopez M, Hennon T, et al. C5a alters blood-brain barrier integrity in a human in vitro model of systemic lupus erythematosus. *Immunology*. 2015;146(1):130-43.
11. Yoshio T, Okamoto H, Hirohata S, Minota S. IgG anti-NR2 glutamate receptor autoantibodies from patients with systemic lupus erythematosus activate endothelial cells. *Arthritis Rheum*. 2013;65(2):457-63.
12. Abbott NJ, Mendonca LL, Dolman DE. The blood-brain barrier in systemic lupus erythematosus. *Lupus*. 2003;12(12):908-15.
13. Stock AD, Gelb S, Pasternak O, Ben-Zvi A, Putterman C. The blood brain barrier and neuropsychiatric lupus: new perspectives in light of advances in understanding the neuroimmune interface. *Autoimmun Rev*. 2017;16(6):612-9.
14. Cohen D, Rijnink EC, Nabuurs RJ, Steup-Beekman GM, Versluis MJ, Emmer BJ, et al. Brain histopathology in patients with systemic lupus erythematosus: identification of lesions associated

- with clinical neuropsychiatric lupus syndromes and the role of complement. *Rheumatology (Oxford)*. 2017;56(1):77-86.
15. Mackay M, Tang CC, Vo A. Advanced neuroimaging in neuropsychiatric systemic lupus erythematosus. *Current opinion in neurology*. 2020;33(3):353-61.
 16. Heye AK, Culling RD, Valdes Hernandez Mdel C, Thrippleton MJ, Wardlaw JM. Assessment of blood-brain barrier disruption using dynamic contrast-enhanced MRI. A systematic review. *NeuroImage Clinical*. 2014;6:262-74.
 17. Weissberg I, Veksler R, Kamintsky L, Saar-Ashkenazy R, Milikovsky DZ, Shelef I, et al. Imaging blood-brain barrier dysfunction in football players. *JAMA neurology*. 2014;71(11):1453-5.
 18. Veksler R VU, Serlin Y, Prager O, Ofer J, Shemen N, Fisher AM, Minaeva O, Hua N, Saar-Ashkenazy R, Benou I, Riklin-Raviv T, Parker E, Mumby G, Kamintsky L, Beyea S, Bowen CV, Shelef I, O'Keefe E, Campbell M, Kaufer D, Goldstein LE, Friedman A. . Slow blood-to-brain transport underlies enduring barrier dysfunction in American football players *Brain*. 2020;(in press).
 19. Cramer SP, Simonsen H, Frederiksen JL, Rostrup E, Larsson HB. Abnormal blood-brain barrier permeability in normal appearing white matter in multiple sclerosis investigated by MRI. *NeuroImage Clinical*. 2014;4:182-9.
 20. Merali Z, Huang K, Mikulis D, Silver F, Kassner A. Evolution of blood-brain-barrier permeability after acute ischemic stroke. *PLoS One*. 2017;12(2):e0171558.
 21. Sweeney MD, Sagare AP, Zlokovic BV. Blood-brain barrier breakdown in Alzheimer disease and other neurodegenerative disorders. *Nature reviews Neurology*. 2018;14(3):133-50.
 22. Chi JM, Mackay M, Hoang A, Cheng K, Aranow C, Ivanidze J, et al. Alterations in Blood-Brain Barrier Permeability in Patients with Systemic Lupus Erythematosus. *AJNR Am J Neuroradiol*. 2019;40(3):470-7.
 23. Hochberg MC. Updating the American College of Rheumatology revised criteria for the classification of systemic lupus erythematosus. *Arthritis Rheum*. 1997;40(9):1725.
 24. Kamintsky L, Cairns KA, Veksler R, Bowen C, Beyea SD, Friedman A, et al. Blood-brain barrier imaging as a potential biomarker for bipolar disorder progression. *NeuroImage Clinical*. 2019:102049.
 25. Gladman DD, Ibanez D, Urowitz MB. Systemic lupus erythematosus disease activity index 2000. *J Rheumatol*. 2002;29(2):288-91.
 26. Gladman DD, Urowitz MB, Goldsmith CH, Fortin P, Ginzler E, Gordon C, et al. The reliability of the Systemic Lupus International Collaborating Clinics/American College of Rheumatology Damage Index in patients with systemic lupus erythematosus. *Arthritis Rheum*. 1997;40(5):809-13.
 27. The American College of Rheumatology nomenclature and case definitions for neuropsychiatric lupus syndromes. *Arthritis Rheum*. 1999;42(4):599-608.
 28. Kozora E, Ellison MC, West S. Reliability and validity of the proposed American College of Rheumatology neuropsychological battery for systemic lupus erythematosus. *Arthritis Rheum*. 2004;51(5):810-8.
 29. Smith A. Symbol Digit Modalities Test. 9th ed: Western Psychological Services; 2002.

30. Walker LAS, Marino D, Berard JA, Feinstein A, Morrow SA, Cousineau D. Canadian Normative Data for Minimal Assessment of Cognitive Function in Multiple Sclerosis. *Can J Neurol Sci.* 2017;44(5):547-55.
31. Delis DC JHK, Kaplan E, Ober BA. . California Verbal Learning Test Second Edition Adult Version Manual:. In: Corporation TP, editor. 2000.
32. Deoni SC, Peters TM, Rutt BK. High-resolution T1 and T2 mapping of the brain in a clinically acceptable time with DESPOT1 and DESPOT2. *Magn Reson Med.* 2005;53(1):237-41.
33. Manjon JV, Coupe P. volBrain: An Online MRI Brain Volumetry System. *Frontiers in neuroinformatics.* 2016;10:30.
34. Wong SM, Jansen JFA, Zhang CE, Staals J, Hofman PAM, van Oostenbrugge RJ, et al. Measuring subtle leakage of the blood-brain barrier in cerebrovascular disease with DCE-MRI: Test-retest reproducibility and its influencing factors. *J Magn Reson Imaging.* 2017;46(1):159-66.
35. Leys C, Ley C, Klein O, Bernard P, Licata L. Detecting outliers: Do not use standard deviation around the mean, use absolute deviation around the median. *Journal of Experimental Social Psychology.* 2013;49:764-6.
36. Hanly JG. Diagnosis and management of neuropsychiatric SLE. *Nat Rev Rheumatol.* 2014;10(6):338-47.
37. Belmont HM, Abramson SB, Lie JT. Pathology and pathogenesis of vascular injury in systemic lupus erythematosus. Interactions of inflammatory cells and activated endothelium. *Arthritis Rheum.* 1996;39(1):9-22.
38. Brooks WM, Sibbitt WL, Jr., Kornfeld M, Jung RE, Bankhurst AD, Roldan CA. The histopathologic associates of neurometabolite abnormalities in fatal neuropsychiatric systemic lupus erythematosus. *Arthritis Rheum.* 2010;62(7):2055-63.
39. Sarbu N, Alobeidi F, Toledano P, Espinosa G, Giles I, Rahman A, et al. Brain abnormalities in newly diagnosed neuropsychiatric lupus: systematic MRI approach and correlation with clinical and laboratory data in a large multicenter cohort. *Autoimmun Rev.* 2015;14(2):153-9.
40. Duarte-Delgado NP, Vasquez G, Ortiz-Reyes BL. Blood-brain barrier disruption and neuroinflammation as pathophysiological mechanisms of the diffuse manifestations of neuropsychiatric systemic lupus erythematosus. *Autoimmun Rev.* 2019;18(4):426-32.
41. Mayhan WG. Regulation of blood-brain barrier permeability. *Microcirculation.* 2001;8(2):89-104.
42. Mazzone P, Tierney W, Hossain M, Puvenna V, Janigro D, Cucullo L. Pathophysiological impact of cigarette smoke exposure on the cerebrovascular system with a focus on the blood-brain barrier: expanding the awareness of smoking toxicity in an underappreciated area. *International journal of environmental research and public health.* 2010;7(12):4111-26.
43. Abbruscato TJ, Lopez SP, Mark KS, Hawkins BT, Davis TP. Nicotine and cotinine modulate cerebral microvascular permeability and protein expression of ZO-1 through nicotinic acetylcholine receptors expressed on brain endothelial cells. *Journal of pharmaceutical sciences.* 2002;91(12):2525-38.

44. Tsuchiya M, Asada A, Kasahara E, Sato EF, Shindo M, Inoue M. Smoking a single cigarette rapidly reduces combined concentrations of nitrate and nitrite and concentrations of antioxidants in plasma. *Circulation*. 2002;105(10):1155-7.
45. Asano T, Ito H, Kariya Y, Hoshi K, Yoshihara A, Ugawa Y, et al. Evaluation of blood-brain barrier function by quotient alpha2 macroglobulin and its relationship with interleukin-6 and complement component 3 levels in neuropsychiatric systemic lupus erythematosus. *PLoS One*. 2017;12(10):e0186414.
46. Gulati G, Jones JT, Lee G, Altaye M, Beebe DW, Meyers-Eaton J, et al. Altered Blood-Brain Barrier Permeability in Patients With Systemic Lupus Erythematosus: A Novel Imaging Approach. *Arthritis Care Res (Hoboken)*. 2017;69(2):299-305.
47. Ceccarelli F, Perricone C, Pirone C, Massaro L, Alessandri C, Mina C, et al. Cognitive dysfunction improves in systemic lupus erythematosus: Results of a 10 years prospective study. *PLoS One*. 2018;13(5):e0196103.
48. Legge A, Doucette S, Hanly JG. Predictors of Organ Damage Progression and Effect on Health-related Quality of Life in Systemic Lupus Erythematosus. *J Rheumatol*. 2016;43(6):1050-6.

References, Chapter 6

1. Brix G, Semmler W, Port R, Schad LR, Layer G, L. W. Pharmacokinetic parameters in CNS Gd-DTPA enhanced MR imaging. 621–8. (1991).
2. Larsson, H. B. W., Courivaud, F., Rostrup, E. & Hansen, A. E. Measurement of brain perfusion, blood volume, and blood-brain barrier permeability, using dynamic contrast-enhanced T₁-weighted MRI at 3 tesla. *Magn. Reson. Med.* 62, 1270–1281 (2009).
3. Aksoy, D. et al. Magnetic resonance imaging profile of blood-brain barrier injury in patients with acute intracerebral hemorrhage. *J. Am. Heart Assoc.* 2, e000161 (2013).
4. Yang, X. & Knopp, M. V. Quantifying Tumor Vascular Heterogeneity with Dynamic Contrast-Enhanced Magnetic Resonance Imaging: A Review. *J. Biomed. Biotechnol.* 2011, 1–12 (2011).
5. Veksler, R. et al. Slow blood-to-brain transport underlies enduring barrier dysfunction in American football players. *Brain* 1–17 (2020). doi:10.1093/brain/awaa140
6. Kamintsky, L. et al. Blood-brain barrier leakage in systemic lupus erythematosus is associated with gray matter loss and cognitive impairment. *Ann. Rheum. Dis.* annrheumdis-2020-218004 (2020). doi:10.1136/annrheumdis-2020-218004
7. Kamintsky, L. et al. Blood-brain barrier imaging as a potential biomarker for bipolar disorder progression. *NeuroImage Clin.* 102049 (2019). doi:10.1016/j.nicl.2019.102049
8. Kang, E. J. et al. Blood-brain barrier opening to large molecules does not imply blood-brain barrier opening to small ions. *Neurobiol. Dis.* 52, 204–218 (2013).
9. Yang, A. C. et al. Physiological blood–brain transport is impaired with age by a shift in transcytosis. *Nature* 583, 425–430 (2020).
10. Vink, R., Gabrielian, L. & Thornton, E. The role of substance P in secondary pathophysiology after traumatic brain injury. *Frontiers in Neurology* 8, 304–304 (2017).
11. Dickie, B. R., Parker, G. J. M. & Parkes, L. M. Measuring water exchange across the blood-brain barrier using MRI. *Progress in Nuclear Magnetic Resonance Spectroscopy* 116, 19–39 (2020).
12. Levy, N. et al. Differential TGF- β signaling in glial subsets underlies IL-6-mediated epileptogenesis in mice. *J. Immunol.* 195, (2015).
13. Seiffert, E. et al. Lasting blood-brain barrier disruption induces epileptic focus in the rat somatosensory cortex. *J Neurosci* 24, 7829–7836 (2004).
14. Ivens, S. et al. TGF-beta receptor-mediated albumin uptake into astrocytes is involved in neocortical epileptogenesis. *Brain* 130, 535–47 (2007).
15. Abbott, N. J., Ronnback, L. & Hansson, E. Astrocyte-endothelial interactions at the blood-brain barrier. *Nat Rev Neurosci* 7, 41–53 (2006).

16. Löscher, W. & Friedman, A. Structural, molecular, and functional alterations of the blood-brain barrier during epileptogenesis and epilepsy: A cause, consequence, or both? *International Journal of Molecular Sciences* 21, (2020).
17. Liebner, S. et al. Wnt/ β -catenin signaling controls development of the blood - brain barrier. *J. Cell Biol.* 183, 409–417 (2008).
18. Armulik, A. et al. Pericytes regulate the blood-brain barrier. *Nature* 468, 557–561 (2010).
19. Daneman, R., Zhou, L., Kebede, A. A. & Barres, B. A. Pericytes are required for blood–brain barrier integrity during embryogenesis. *Nature* 468, (2010).
20. Prager, O. Kamintsky L. et al. Seizure-induced microvascular injury is associated with impaired neurovascular coupling and blood–brain barrier dysfunction. *Epilepsia* 60, (2019).
21. Vazana, U. et al. Neurobiology of Disease Glutamate-Mediated Blood-Brain Barrier Opening: Implications for Neuroprotection and Drug Delivery. (2016). doi:10.1523/JNEUROSCI.0587-16.2016
22. Vazana, U. et al. pharmaceuticals TMS-Induced Controlled BBB Opening: Preclinical Characterization and Implications for Treatment of Brain Cancer. doi:10.3390/pharmaceutics12100946
23. Xhima, K., Weber-Adrian, D. & Silburt, J. Glutamate induces blood–brain barrier permeability through activation of N-methyl-D-aspartate receptors. *J. Neurosci.* 36, 12296–12298 (2016).
24. Vezzani, A., Balosso, S. & Ravizza, T. Neuroinflammatory pathways as treatment targets and biomarkers in epilepsy. *Nature Reviews Neurology* 15, 459–472 (2019).
25. Xanthos, D. N. & Sandkühler, J. Neurogenic neuroinflammation: Inflammatory CNS reactions in response to neuronal activity. *Nature Reviews Neuroscience* 15, 43–53 (2014).
26. Bai, Y. et al. Pericytes contribute to the disruption of the cerebral endothelial barrier via increasing VEGF expression: Implications for stroke. *PLoS One* 10, (2015).
27. Underly, R. G. et al. Pericytes as inducers of rapid, matrix metalloproteinase-9-dependent capillary damage during ischemia. *J. Neurosci.* 37, 129–140 (2017).
28. Shlosberg, D., Benifla, M., Kaufer, D. & Friedman, A. Blood-brain barrier breakdown as a therapeutic target in traumatic brain injury. *Nat. Rev. Neurol.* 6, 393–403 (2010).
29. Sweeney, M. D., Zhao, Z., Montagne, A., Nelson, A. R. & Zlokovic, B. V. Blood-brain barrier: From physiology to disease and back. *Physiological Reviews* 99, 21–78 (2019).
30. Nwafor, D. C. et al. Targeting the Blood-Brain Barrier to Prevent Sepsis-Associated Cognitive Impairment. *J. Cent. Nerv. Syst. Dis.* 11, 117957351984065 (2019).
31. Van Dyken, P. & Lacoste, B. Impact of Metabolic Syndrome on Neuroinflammation and the Blood–Brain Barrier. *Front. Neurosci.* 12, 930 (2018).

32. Bogush, M., Heldt, N. A. & Persidsky, Y. Blood Brain Barrier Injury in Diabetes: Unrecognized Effects on Brain and Cognition. *J. Neuroimmune Pharmacol.* 12, 593–601 (2017).
33. Abbott, N. J. & Friedman, A. Overview and introduction: the blood-brain barrier in health and disease. *Epilepsia* 53 Suppl 6, 1–6 (2012).
34. Duarte-Delgado, N. P., Vásquez, G. & Ortiz-Reyes, B. L. Blood-brain barrier disruption and neuroinflammation as pathophysiological mechanisms of the diffuse manifestations of neuropsychiatric systemic lupus erythematosus. *Autoimmun. Rev.* 18, 426–432 (2019).
35. Varatharaj, A. & Galea, I. The blood-brain barrier in systemic inflammation. *Brain, Behavior, and Immunity* 60, 1–12 (2017).
36. Esposito, E. et al. Brain-to-cervical lymph node signaling after stroke. *Nat. Commun.* 10, (2019).
37. Stock, A. D. et al. Tertiary lymphoid structures in the choroid plexus in neuropsychiatric lupus. *JCI Insight* 4, (2019).
38. Blake, R. & Trounce, I. A. Mitochondrial dysfunction and complications associated with diabetes. *Biochimica et Biophysica Acta - General Subjects* 1840, 1404–1412 (2014).
39. Mapanga, R. F. & Essop, M. F. Damaging effects of hyperglycemia on cardiovascular function: Spotlight on glucose metabolic pathways. *American Journal of Physiology - Heart and Circulatory Physiology* 310, H153–H173 (2016).
40. Ennis, S. R. & Keep, R. F. Effect of sustained-mild and transient-severe hyperglycemia on ischemia-induced blood-brain barrier opening. *J. Cereb. Blood Flow Metab.* 27, 1573–1582 (2007).
41. Abbott, N. J., Patabendige, A. A. K., Dolman, D. E. M., Yusof, S. R. & Begley, D. J. Neurobiology of Disease Structure and function of the blood – brain barrier. *Neurobiol. Dis.* 37, 13–25 (2010).
42. Sweeney, M. D., Kisler, K., Montagne, A., Toga, A. W. & Zlokovic, B. V. The role of brain vasculature in neurodegenerative disorders. *Nature Neuroscience* 21, 1318–1331 (2018).
43. Schoknecht, K. et al. Monitoring stroke progression: In vivo imaging of cortical perfusion, blood-brain barrier permeability and cellular damage in the rat photothrombosis model. *J. Cereb. Blood Flow Metab.* 34, (2014).
44. Cacheaux, L. P. et al. Transcriptome profiling reveals TGF-beta signaling involvement in epileptogenesis. *J Neurosci* 29, 8927–8935 (2009).
45. David, Y. et al. Astrocytic dysfunction in epileptogenesis: consequence of altered potassium and glutamate homeostasis? *J. Neurosci.* 29, 10588–99 (2009).
46. Schoknecht, K. et al. Monitoring stroke progression: in vivo imaging of cortical perfusion, blood-brain barrier permeability and cellular damage in the rat photothrombosis model. *J. Cereb. Blood Flow Metab.* (2014). doi:10.1038/jcbfm.2014.147
47. Friedman, A. Blood-brain barrier dysfunction, status epilepticus, seizures, and epilepsy: a puzzle of a chicken and egg? *Epilepsia* 52 Suppl 8, 19–20 (2011).

48. Bevan-Jones, W. R. et al. Neuroinflammation and protein aggregation co-localize across the frontotemporal dementia spectrum. *Brain* 143, 1010–1026 (2020).
49. Sweeney, M. D., Sagare, A. P. & Zlokovic, B. V. Blood-brain barrier breakdown in Alzheimer disease and other neurodegenerative disorders. *Nat. Rev. Neurol.* 14, 133–150 (2018).
50. Wimmer, I. et al. PECAM-1 stabilizes blood-brain barrier integrity and favors paracellular T-cell diapedesis across the blood-brain barrier during neuroinflammation. *Front. Immunol.* 10, 711 (2019).
51. Cacheaux, L. P. et al. Transcriptome profiling reveals TGF- β signaling involvement in epileptogenesis. *J. Neurosci.* 29, 8927–8935 (2009).
52. Weissberg, I. Wood, L. Kamintsky, L. et al. Albumin induces excitatory synaptogenesis through astrocytic TGF- β /ALK5 signaling in a model of acquired epilepsy following blood-brain barrier dysfunction. *Neurobiol. Dis.* 78, (2015).
53. INGVAR, M. Cerebral Blood Flow and Metabolic Rate during Seizures: Relationship to Epileptic Brain Damage. *Ann. N. Y. Acad. Sci.* 462, 194–206 (1986).
54. Fernández-Klett, F., Offenhauser, N., Dirnagl, U., Priller, J. & Lindauer, U. Pericytes in capillaries are contractile in vivo, but arterioles mediate functional hyperemia in the mouse brain. *Proc. Natl. Acad. Sci. U. S. A.* 107, 22290–22295 (2010).
55. Piilgaard, H. & Lauritzen, M. Persistent increase in oxygen consumption and impaired neurovascular coupling after spreading depression in rat neocortex. *J. Cereb. Blood Flow Metab.* 29, 1517–1527 (2009).
56. Leithner, C. & Royl, G. The oxygen paradox of neurovascular coupling. *Journal of Cerebral Blood Flow and Metabolism* 34, 19–29 (2014).
57. Devor, A. et al. ‘Overshoot’ of O₂ is required to maintain baseline tissue oxygenation at locations distal to blood vessels. *J. Neurosci.* 31, 13676–13681 (2011).
58. Abbott, N. J. & Friedman, A. Overview and introduction: the blood-brain barrier in health and disease. *Epilepsia* 53 Suppl 6, 1–6 (2012).
59. Weissberg, I. Veksler, R. Kamintsky, L. et al. Imaging blood-brain barrier dysfunction in football players. *JAMA Neurol.* 71, (2014).
60. Weissberg, I. Wood L. Kamintsky L. et al. Albumin induces excitatory synaptogenesis through astrocytic TGF- β /ALK5 signaling in a model of acquired epilepsy following blood-brain barrier dysfunction. *Neurobiol. Dis.* 78, (2015).
61. Engelhardt, B. T cell migration into the central nervous system during health and disease: Different molecular keys allow access to different central nervous system compartments. *Clin. Exp. Neuroimmunol.* 1, 79–93 (2010).
62. Wraith, D. C. & Nicholson, L. B. The adaptive immune system in diseases of the central nervous system. *Journal of Clinical Investigation* 122, 1172–1179 (2012).

63. Talhada, D., Santos, C. R. A., Gonçalves, I. & Ruscher, K. Thyroid hormones in the brain and their impact in recovery mechanisms after stroke. *Frontiers in Neurology* 10, (2019).
64. Patik, I. et al. Functional expression of the 11 human Organic Anion Transporting Polypeptides in insect cells reveals that sodium fluorescein is a general OATP substrate. *Biochem. Pharmacol.* 98, 649–658 (2015).
65. Bar-Klein, G. Lublinsky, S. Kamintsky, L et al. Imaging blood-brain barrier dysfunction as a biomarker for epileptogenesis. *Brain* 140, (2017).
66. Blyth, B. J. et al. Validation of serum markers for blood-brain barrier disruption in traumatic brain injury. *J. Neurotrauma* 26, 1497–1507 (2009).
67. Marchi, N. et al. Peripheral markers of blood-brain barrier damage. *Clin. Chim. Acta* (2004). doi:10.1016/j.cccn.2003.12.008
68. Gudmundsson, P. et al. The relationship between cerebrospinal fluid biomarkers and depression in elderly women. *Am. J. Geriatr. Psychiatry* 15, 832–838 (2007).
69. Stock, A. D., Gelb, S., Pasternak, O., Ben-zvi, A. & Putterman, C. The blood brain barrier and neuropsychiatric lupus : new perspectives in light of advances in understanding the neuroimmune interface. *Autoimmun. Rev.* 16, 612–619 (2017).
70. Steiner, J. et al. S100B serum levels are closely correlated with body mass index: An important caveat in neuropsychiatric research. *Psychoneuroendocrinology* 35, 321–324 (2010).
71. Pollak, T. A. et al. The blood-brain barrier in psychosis. *The Lancet Psychiatry* 0366, 1–14 (2017).
72. Cramer, S. P. & Larsson, H. B. W. Accurate determination of blood-brain barrier permeability using dynamic contrast-enhanced T1-weighted MRI: A simulation and in vivo study on healthy subjects and multiple sclerosis patients. *J. Cereb. Blood Flow Metab.* 34, 1655–1665 (2014).
73. Heye, A. K., Culling, R. D., Hernández, C. V., Thrippleton, M. J. & Wardlaw, J. M. Assessment of blood – brain barrier disruption using dynamic contrast-enhanced MRI . A systematic review. *NeuroImage Clin.* 6, 262–274 (2014).
74. Heye, A. K. et al. NeuroImage Tracer kinetic modelling for DCE-MRI quanti fi cation of subtle blood – brain barrier permeability. *Neuroimage* 125, 446–455 (2016).
75. Nation, D. et al. Blood-brain barrier breakdown is an early biomarker of human cognitive dysfunction. *Nat. Med.* in press, (2018).
76. Serlin, Y. et al. Blood-Brain Barrier Leakage: A New Biomarker in Transient Ischemic Attacks. *Stroke* 50, 1266–1269 (2019).
77. Wilhelm, I., Nyúl-Tóth, Á., Suciú, M., Hermenean, A. & Krizbai, I. A. Heterogeneity of the blood-brain barrier. *Tissue Barriers* 4, (2016).
78. Ohene, Y. et al. Increased blood–brain barrier permeability to water in the aging brain detected using noninvasive multi-TE ASL MRI. *Magn. Reson. Med.* 85, 326–333 (2021).

79. Kane, G. C. et al. Comparison between gadolinium and iodine contrast for percutaneous intervention in atherosclerotic renal artery stenosis: Clinical outcomes. *Nephrol. Dial. Transplant.* 23, 1233–1240 (2008).
80. Milikovsky, D. Z. et al. Paroxysmal slow cortical activity in Alzheimer’s disease and epilepsy is associated with blood-brain barrier dysfunction. *Sci. Transl. Med.* 11, 1–12 (2019).
81. Montagne, A., Zhao, Z. & Zlokovic, B. V. Alzheimer’s disease: A matter of blood-brain barrier dysfunction? *Journal of Experimental Medicine* 214, 3151–3169 (2017).
82. Feldmann, M. & Koepp, M. ABC Transporters and Drug Resistance in Patients with Epilepsy. *Curr. Pharm. Des.* 22, (2016).
83. Ilyas-Feldmann, M. et al. P-glycoprotein overactivity in epileptogenic developmental lesions measured in vivo using (R)-[11C]verapamil PET. *Epilepsia* 61, 1472–1480 (2020).
84. Van Vliet, E. A. et al. Expression and Cellular Distribution of P-Glycoprotein and Breast Cancer Resistance Protein in Amyotrophic Lateral Sclerosis Patients. *J. Neuropathol. Exp. Neurol.* 79, 266–276 (2020).
85. Bar-Klein, G. Cacheaux, LP. Kamintsky, L. et al. Losartan prevents acquired epilepsy via TGF- β signaling suppression. *Ann. Neurol.* 75, 864–75 (2014).
86. Senatorov, V. V. et al. Blood-brain barrier dysfunction in aging induces hyperactivation of TGF β signaling and chronic yet reversible neural dysfunction. *Sci. Transl. Med.* 11, (2019).
87. Brandt, C., Bethmann, K., Gastens, A. M. & Löscher, W. The multidrug transporter hypothesis of drug resistance in epilepsy: Proof-of-principle in a rat model of temporal lobe epilepsy. *Neurobiol. Dis.* 24, 202–211 (2006).
88. Jablonski, M. R. et al. Inhibiting drug efflux transporters improves efficacy of ALS therapeutics. *Ann. Clin. Transl. Neurol.* 1, 996–1005 (2014).
89. Lashen, H. Role of metformin in the management of polycystic ovary syndrome. *Ther. Adv. Endocrinol. Metab.* 1, 117–28 (2010).
90. Abdelgadir, E., Ali, R., Rashid, F. & Bashier, A. Effect of Metformin on Different Non-Diabetes Related Conditions, a Special Focus on Malignant Conditions: Review of Literature. *J. Clin. Med. Res.* 9, 388–395 (2017).
91. Jia, Y. et al. Metformin prevents DMH-induced colorectal cancer in diabetic rats by reversing the warburg effect. *Cancer Med.* 4, 1730–1741 (2015).
92. Mudgal, J. et al. Possible involvement of metformin in downregulation of neuroinflammation and associated behavioural changes in mice. *Inflammopharmacology* 27, 941–948 (2019).
93. Liu, Y. et al. Metformin attenuates blood-brain barrier disruption in mice following middle cerebral artery occlusion. *J. Neuroinflammation* 11, 177 (2014).
94. Schwarz, N. et al. Long-term adult human brain slice cultures as a model system to study human CNS circuitry and disease. *Elife* 8, (2019).

95. Zhang, Y. et al. Reduced Neuronal cAMP in the Nucleus Accumbens Damages Blood-Brain Barrier Integrity and Promotes Stress Vulnerability. *Biol. Psychiatry* 87, 526–537 (2020).
96. Greene, C. et al. Dose-dependent expression of claudin-5 is a modifying factor in schizophrenia. *Mol. Psychiatry* 23, 2156–2166 (2018).
97. Kealy, J., Greene, C. & Campbell, M. Blood-brain barrier regulation in psychiatric disorders. *Neuroscience Letters* 726, 133664 (2020).
98. Schubert, K. O., Föcking, M., Prehn, J. H. M. & Cotter, D. R. Hypothesis review: Are clathrin-mediated endocytosis and clathrin-dependent membrane and protein trafficking core pathophysiological processes in schizophrenia and bipolar disorder. *Molecular Psychiatry* 17, 669–681 (2012).
99. Pimm, J. et al. The Epsin 4 gene on chromosome 5q, which encodes the clathrin-associated protein enthoprotin, is involved in the genetic susceptibility to schizophrenia. *Am. J. Hum. Genet.* 76, 902–907 (2005).
100. Kamintsky, L. et al. Response to: ‘Correspondence on “Blood- brain barrier leakage in systemic lupus erythematosus is associated with gray matter loss and cognitive impairment”’ by Pamuk and Hasni. *Ann. Rheum. Dis.* (2020). doi:[https:// doi. org/ 10. 1136/ annrheumdis- 2021- 220031](https://doi.org/10.1136/annrheumdis-2021-220031)
101. Kwon, Y. S. et al. Neuroprotective and antiepileptogenic effects of combination of anti-inflammatory drugs in the immature brain. *J. Neuroinflammation* 10, (2013)
102. Deoni, S. C. L., Rutt, B. K. & Peters, T. M. Rapid combined T1 and T2 mapping using gradient recalled acquisition in the steady state. *Magn. Reson. Med.* 49, 515–526 (2003).
103. Deoni, S. C. L., Peters, T. M. & Rutt, B. K. High-Resolution T 1 and T 2 Mapping of the Brain in a Clinically Acceptable Time with DESPOT1 and DESPOT2. 241, 237–241 (2005).
104. Chavez, S. & Stanisz, G. J. A novel method for simultaneous 3D B1 and T1 mapping: The method of slopes (MoS). *NMR Biomed.* 25, 1043–1055 (2012).
105. Wang, P. et al. Effects of flip angle uncertainty and noise on the accuracy of DCE-MRI metrics: Comparison between standard concentration-based and signal difference methods. *Magn. Reson. Imaging* 33, 166–173 (2015).
106. Wade, T., McKenzie, C. A. & Rutt, B. K. Flip angle mapping with the accelerated 3D look-locker sequence. *Magn. Reson. Med.* 71, 591–598 (2014).

Appendix I, Copyright Permissions

Manuscript title:

Blood-brain barrier imaging as a potential biomarker for bipolar disorder progression.

Kamintsky L, Cairns KA, Veksler R, Bowen C, Beyea SD, Friedman A, Calkin C.

Neuroimage Clin. 2019.

This paper is open access, and states that the authors have copyright ownership

© 2019 The Authors. Published by Elsevier Inc.

Manuscript title:

**Seizure-induced
microvascular injury
is associated with
impaired
neurovascular
coupling and blood-
brain barrier
dysfunction**

Prager O, Kamintsky L*
(*equal first co-authorship),
Hasam-Henderson LA,
Schoknecht K, Wuntke V,
Papageorgiou I, Swolinsky
J, Muoio V, Bar-Klein G,
Vazana U, Heinemann U,
Friedman A, Kovács R.*

Epilepsia, 2019

This Agreement between Mrs. Lyna Kamintsky ("You") and BMJ Publishing Group Ltd. ("BMJ Publishing Group Ltd.") consists of your license details and the terms and conditions provided by BMJ Publishing Group Ltd. and Copyright Clearance Center.

License Number	5016470831128
License date	Feb 26, 2021
Licensed Content Publisher	BMJ Publishing Group Ltd.
Licensed Content Publication	Annals of the Rheumatic Diseases
Licensed Content Title	Blood-brain barrier leakage in systemic lupus erythematosus is associated with gray matter loss and cognitive impairment
Licensed Content Author	Lyna Kamintsky, Steven D Beyea, John D Fisk, Javeria A Hashmi, Antonina Omissade, Cynthia Calkin, Tim Bardouille, Chris Bowen, Maher Quraan, Arnold Mitnitski, Kara Matheson, Alon Friedman, John G Hanly
Licensed Content Date	Dec 1, 2020
Licensed Content Volume	79
Licensed Content Issue	12
Type of Use	Dissertation/Thesis
Requestor type	Author of this BMJ article
Format	Electronic
Portion	Figure/table/extract
Number of figure/table/extracts	5
Description of figure/table/extracts	Tables 1,2 Figure 1,2,3
Will you be translating?	No
Circulation/distribution	500
Order reference number	1
Title	NEUROPSYCHIATRIC CORRELATES OF BLOOD-BRAIN BARRIER LEAKAGE
Institution name	Dalhousie University
Expected presentation date	Apr 2021

Manuscript title:

Blood-brain barrier leakage in systemic lupus erythematosus is associated with gray matter loss and cognitive impairment

Kamintsky L, Beyea SD, Fisk JD, Hashmi JA, Omisade A, Calkin C, Bardouille T, Bowen C, Quraan M, Mitnitsky A, Matheson K, Friedman A, Hanly JG

Annals of the Rheumatic Diseases, 2020

This Agreement between Mrs. Lyna Kamintsky ("You") and John Wiley and Sons ("John Wiley and Sons") consists of your license details and the terms and conditions provided by John Wiley and Sons and Copyright Clearance Center.

License Number 5016600655137

License date Feb 26, 2021

Licensed Content Publisher John Wiley and Sons

Licensed Content Publication Epilepsia

Licensed Content Title Seizure-induced microvascular injury is associated with impaired neurovascular coupling and blood-brain barrier dysfunction

Licensed Content Author Ofer Prager, Lyna Kamintsky, Luisa A. Hasam-Henderson, et al

Licensed Content Date Jan 4, 2019

Licensed Content Volume 60

Licensed Content Issue 2

Licensed Content Pages 15

Type of use Dissertation/Thesis

Requestor type Author of this Wiley article

Format Electronic

Portion Full article

Will you be translating? No

Title NEUROPSYCHIATRIC CORRELATES OF BLOOD-BRAIN BARRIER LEAKAGE

Institution name Dalhousie University

Expected presentation date Apr 2021